Silica Gel Encapsulated Cell Bioremediation System for Water Treatment

A DISSERTATION

SUBMITTED TO THE FACULTY OF THE GRADUATE SCHOOL

OF THE UNIVERSITY OF MINNESOTA

BY

Baris Ragip Mutlu

IN PARTIAL FULFILLMENT OF THE REQUIREMENTS

FOR THE DEGREE OF

DOCTOR OF PHILOSOPHY

Adviser: Alptekin Aksan

February 2016

TABLE OF CONTENTS

ACKNOWLEDGMENTS

I would like to thank my adviser, Professor Alptekin Aksan, for his guidance and support during my doctoral studies. I appreciate his patience, and his dedication to my research and my professional development as a scientist.

I would like to acknowledge all the present and past members of the Biostabilization and Bioencapsulation laboratory for their support and collaboration: Dr. Eduardo Reategui, Dr. Boris Tong, Lisa Kasinkas, Jonathan Sakkos, Molly Lefebvre, Goeun Heo, Joey Benson, Julian Preciado, Katie Hirschey and Benjamin Meyer. I would also like to thank Professor Lawrence Wackett and members of his lab: Sujin Yeom, Dr. Adi Radian, Dr. Kelly Aukema, and Dr. Tony Dodge. I am grateful to my doctoral committee, Professor Michael Sadowsky, Professor Victor Barocas, and Professor Sean Garrick. All have helped me through their valuable ideas, discussions, and criticisms.

I would like to acknowledge the funding sources that I had, specifically the MnDrive graduate student fellowship awarded by the Biotechnology Institute and the Doctoral Dissertation Fellowship awarded by the Graduate School.

Finally, I would like to thank my parents, Selma and Mehmet, for their support and encouragement. I am lucky to know that they will always be there for me.

ABSTRACT

In this dissertation research, a water bioremediation system which utilizes silica gel encapsulated biodegrading (biotransforming) bacteria was developed. Towards achieving this goal, both fundamental and practical scientific contributions were made. Novel silica gel compositions were developed for encapsulation of bacteria. The resulting bioreactive materials were characterized in terms of the cytocompatibility of the encapsulation process, and the physicochemical properties of the material. Feasibility of the process (*e.g.* material cost, temporal stability) was also evaluated to enable scale-up. An engineering model of a typical bioreactor utilizing the bioreactive material was developed for efficient utilization of the encapsulated bacteria. Design parameters such as material geometry, size and bacteria density encapsulated in the material were optimized using the developed biotransformation/transport model. Characterization experiments also revealed that alcohol treatment of *E. coli* cells expressing a catalytic enzyme (AtzA) can improve biotransformation activity up to a critical alcohol concentration, which was attributed to the enhanced membrane permeability of the cells. This was verified by comparing the biotransformation activities of bacteria with intact cell membranes and bacterial enzyme extract obtained via sonication. Long-term storage of the material at different temperatures, desiccation levels, and with various lyoprotectant solutions (sucrose, trehalose, glycerol) was studied to facilitate commercial use. By partial desiccation up to a critical water loss level, both the activity of the encapsulated cells and mechanical properties of the material were significantly improved. Large-scale synthesis methods were investigated to eliminate the diffusion barrier of substrates to cells and enable industry scale production of the material. Optimal operating conditions were determined to synthesize PVA/silica core-shell nanofibers with encapsulated bacteria via electrospinning. Based on the generated expertise in this research, a novel application was developed via encapsulation of synergistically working bacteria in an optically transparent silica gel matrix. In this system, heterotrophic bacteria performed aerobic biotransformation reactions while phototrophic cyanobacteria provided the required oxygen via photosynthesis. This self-sustaining system was shown to be more effective for oxygenation than external supplementation of

oxygen, which was attributed to the homogeneous and proximate distribution of the cells in the matrix.

LIST OF FIGURES

LIST OF TABLES

Chapter 1: Introduction

1.1 Motivation

Water supplies throughout the world are being contaminated by various organic and inorganic chemicals, which are byproducts of industrial and agricultural processes, posing a major environmental health risk [1]. As an example, atrazine is one of the most commonly used agricultural pesticides in the U.S. (and also in 70 other countries at an estimated annual rate of 111,000 tons [2]) and its concentration in drinking water is regulated by the Environmental Protection Agency (EPA). After heavy rains, runoff water from farmlands can cause increased levels of atrazine concentrations in drinking water that exceed these regulations. As the EPA pushes for stricter regulations on atrazine, the effective life-time of conventional activated carbon treatments is reduced [3]. Another potential risk for water pollution in the U.S. is caused by the use of the hydraulic fracturing (fracking) method for natural gas extraction. This technique uses millions of gallons of water, and several chemicals are added to water, including biocides, corrosion inhibitors, friction reducers, scale inhibitors and surfactants. Some of these chemicals, especially the polycyclic aromatic hydrocarbons (benzene, naphthalene, and *etc.*) carry potential health risks as known or suspected carcinogens [4].

In my dissertation research, a silica gel encapsulated cell bioremediation system was developed for water treatment. Many pollutants found in water can be biodegraded by naturally occurring microbes, which offers a green and sustainable solution to this problem. A powerful method to utilize microbes is bioencapsulation (*i.e.* physical entrapment of bacteria in a host structure), which provides a mechanical scaffold and protection to otherwise small and fragile cells, facilitating the integration of the technology into existing systems. Bioencapsulation requires that the cells are in a biocompatible, stable and mechanically strong encapsulation matrix. Silica is chemically inert, resistant to microbial attack, mechanically strong and thermally stable, which makes it an ideal material for this task. Bioencapsulation of cells has various other potential applications [5-8], thus the scientific output of this research can potentially benefit other areas of biomedicine and biotechnology.

1.2 Background

1.2.1 Silica precursors and sol-gel chemistry

Silicon alkoxides are popular precursors for silica gel synthesis because they react readily with water [9]. Hydrolysis of alkoxide precursors occur under acidic or basic conditions, followed by condensation of the hydroxylated units leading to the formation of a mesoporous gel. This process is called the sol-gel method [10]. In a typical procedure, the first step is to hydrolyze a low-molecular weight silicon alkoxide precursor molecule such as tetramethoxysilane (TMOS) or tetraethoxysilane (TEOS) in the presence of water, acid catalyst and a mutual solvent:

$$Si(OR)_4 + H_2O \rightarrow HO\text{-}Si(OR)_3 + ROH$$ (*Hydrolysis*)

Hydrolysis of silicon alkoxide precursor results in the formation of silanol groups (Si-OH). Through condensation, these silanol moieties react further and form siloxanes (-Si-O-Si-):

$$(OR)_3Si\text{-}OH + HO\text{-}Si(OR)_3 \rightarrow (OR)_3Si\text{-}O\text{-}Si(OR)_3 + H_2O$$ (*Water condensation*)

or

$$(OR)_3Si\text{-}OR + HO\text{-}Si(OR)_3 \rightarrow (OR)_3Si\text{-}O\text{-}Si(OR)_3 + ROH$$ (*Alcohol condensation*)

Finally, through polycondensation of silanol and siloxanes, SiO_2 matrices are formed (called "gelation"). The resulting gel is an interconnected rigid network with pores of sub-micrometer dimensions and polymeric chains whose average length is greater than a micrometer [10].

The major impact of the sol-gel method on cell viability is the alcohol (ROH molecule shown in the reaction) produced during hydrolysis and condensation. Depending on the precursor used, this alcohol is usually ethanol or methanol, for TEOS and TMOS respectively. Furthermore, in some gel making protocols in the literature, alcohol is added to the precursor mix, as a mutual solvent to eliminate phase separation between the silicon alkoxide and water. In the cases where no mutual solvent is used, phase separation is observed in the initial mixture but it will disappear as alcohol is produced through condensation reactions during gelation.

TEOS and TMOS are tetra-functional monomers because they can form 4 bonds after hydrolysis. In order to change the gel structure, it is also possible to use methyltriethoxysilane (*MTES*) and methyltrimethoxysilane (*MTMS*), which are trifunctional. Recently, another commercially available product tetrakis(2-hydroxyethyl) orthosilicate (THEOS) is also being used in literature. This is a tetrafunctional precursor which is highly soluble in water, which eliminates the addition of alcohol to avoid phase separation [11].

Hydrolysis and condensation reactions continue after gelation, causing strengthening, stiffening, and shrinkage of the matrix, in a process that is called "aging" [9]. The first stage is called syneresis, when the gel contracts and expels the pore liquid. The second stage is called drying, when the liquid evaporates and the gel is dehydrated. This characteristic shrinkage of aging process exhibits a compressive load on the cells and eventually may cause cell lysis [12]. Rooke *et al*. proposed immersing the gels in culture media, to avoid evaporation and thus subsequent shrinkage arising from aging [13]. This hydration method prolonged the life and activity of the cyanobacteria within the gel. Organic polymers have also been used as additives to form hybrid organic–inorganic gels in order to reduce shrinkage via a 'pore filling' effect [14]. Some successful examples include incorporation of sugars [6], glycerol [15] or polyethylene glycol (PEG) [16].

Aqueous silica gel precursors such as silica nanoparticles (SNPs) and sodium silicate are also appealing for gel synthesis due to their commercial availability at high volumes and low cost. Some studies have shown that silica gel encapsulation with aqueous silica precursors yield a more cytocompatible method [13, 17, 18]. Furthermore, SNPs are available in various sizes ranging from nanometers to micrometers, enabling the microstructure of a silica gel to be fine-tuned by using SNPs of different diameters.

1.2.2 Silica gel encapsulation of macromolecules and cells

Macromolecules and cells encapsulated in biocompatible matrices (*i.e.* bioencapsulation) with retained activity, viability and metabolic functionality have extensive applications in biotechnology (*e.g.* biosensing, biocatalysis, photobioreactors) and medicine (*e.g.* tissue engineering, recombinant protein production, and drug delivery) [19, 20]. Long-term sustained activity of the encapsulated cells still remains a challenge, because cells are more sensitive than biomolecules to the physical and chemical effects of encapsulation. The biocompatible host must be a noncyto- and geno-toxic material, including its degradation products. Numerous factors have to be thus considered in the choice of host material such as the chemical composition, the surface morphology and the mechanical and chemical stability (See Figure 1). In addition, the porosity/pore size of the material is vital to allow the diffusion of the required nutrients and the byproducts of cellular metabolism [21].

Different organic, inorganic and hybrid polymers can be used for cell encapsulation. Natural (collagen, alginate, chitosan and etc.) and synthetic (poly-lactic acid (PLA), polyethylene glycol (PEG), and etc.) polymers are attractive for cell encapsulation due to their abundance, biocompatibility and biodegradability. However, natural polymers have high purification cost. In the case of collagen, enzymatic degradability can be a problem. A potential limitation for alginate gel is its often uncontrollable and unpredictable dissolution, which occurs by a process involving the loss of divalent ions. Chitosan exhibits weak mechanical properties and lacks bioactivity, and it is usually combined with calcium phosphate to increase its mechanical strength [22]. For synthetic polymers, some of the limitations are the bulk degradation mechanisms, which typically results in a rapid loss of mechanical properties (*e.g.* in PLA gels), and the lack of biodegradation (*e.g.* in PEG).

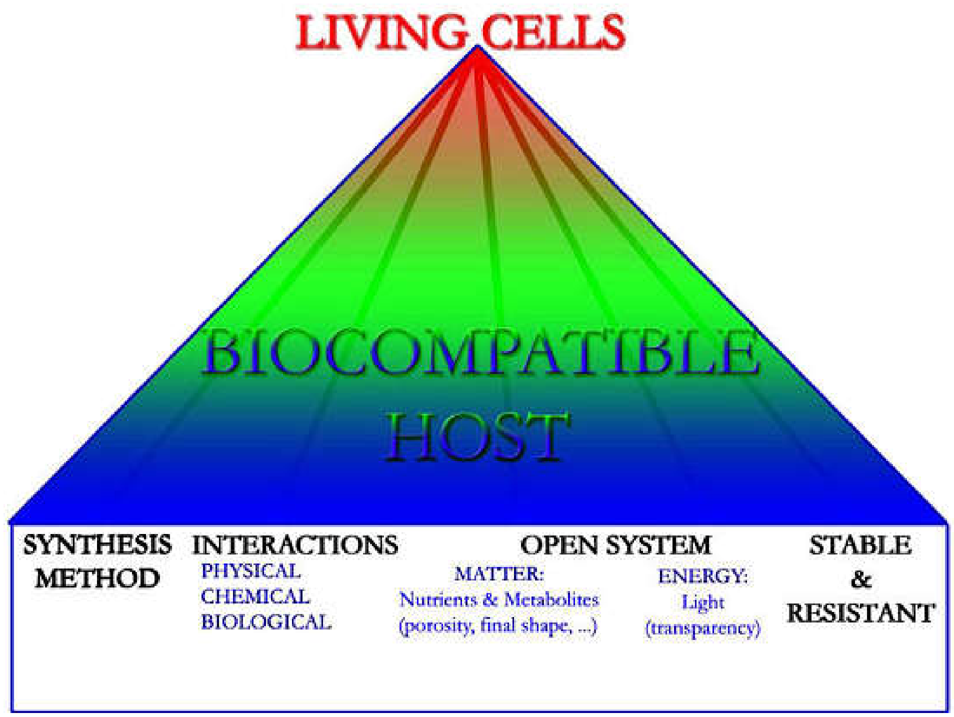

Figure 1 – Conditions required to design a biocompatible host for living cells (Adapted from [21])

Among the wide choice of materials, silica has appeared as a promising host for cell encapsulation. Silicon is the second most abundant element of the lithosphere [23]. Even if silicon is not abundant in the biota (0.03%), it plays a crucial role in all living organisms. Silicon, present in nature as silicates and silica, is required for the production of structural materials of many living species and even for major metabolic processes [24]. Therefore, being one of the most important and common chemical substances used in industry, silica is the most appropriate inorganic material for encapsulating cells and other biological species [14]. Furthermore, the porosity of the matrix can be adjusted within the mesoporous range to optimize encapsulation matrices for different cells. As a result, silica gels have been studied extensively in the last decade for encapsulation of whole prokaryotic or eukaryotic cells with promising results [25-28].

Cytocompatibility of the silica gel

The major effect of silica gel encapsulation process on cells is the alcohol produced during hydrolysis and condensation reactions. If the concentration of the alcohol is sufficiently high, it can disrupt the cell membrane and have a detrimental effect on the cells [29]. Furthermore, the osmotic stress induced by the high alcohol concentration in the extracellular space can cause cell lysis. If the degradation reaction is a metabolic pathway, the decrease in viability of the cells will decrease the performance of the system. To address this problem, evaporation of the alcohol by-product from the hydrolyzed solution before cell encapsulation is employed in literature, using methods such as roto-evaporation [30-32].

From a practical standpoint, the cell viability concern is limited to the cells being able to perform their biodegradation (remediation) tasks. Therefore, as long as cells can perform the degradation, viability or full metabolic activity of the cells is not essential. For instance, Reátegui *et al*. [33] have encapsulated AtzA expressing *E. coli* to clean Atrazine from drinking water. Since the degradation does not require cellular viability/activity, the cells are employed as micro-machines that produce the enzyme. Consequently, even though the cells are not viable, the bioreactive material has shown cleaning activity for up to 4 months after encapsulation. Furthermore, the activity of encapsulated cells was 30% higher than the cells in solution. For this particular case, this may be attributed to enhanced diffusion of the substrate through compromised cell membranes. However, there are also studies [34, 35] which have reported higher enzymatic activity in confinement than in solution.

Porosity/pore size of the silica gel

Confinement of cells and transport of chemicals through the encapsulation matrix depends on the porosity and pore size of the gel. A major advantage of silica based sol–gels for encapsulation is that they form a mesoporous (2 nm < pore range < 50 nm) matrix that allows for nutrient diffusion while firmly entrapping cells [32]. In particular, silicon alkoxide (TMOS, TEOS and etc.) derived sol–gels typically produce matrices with pore sizes in the range from 10 to 50 nm [36]. There are two methods to modify the porosity/pore size of the matrix: a) changing the gel composition, b) changing gelation conditions. In terms of gel composition, using an alkoxide precursor with higher functionality leads to a denser network, hence a lower porosity. This can be experimentally shown by replacing a gel formed by TEOS/TMOS (functionality=4) with MTES/MTMS (functionality=3).

Gel composition can also be changed by addition of silica nanoparticles (SNPs) to the precursor mixture. In mesoporous range, porosity is expected to increase with SNP size. As discussed before, there are also other additives that can be used in making of the gel to improve cell-matrix interactions, such as PEG. PEG interacts with the -SiOH surface of the gel and reduces the active hydroxyl (-OH) groups that can form further siloxane bonds. Therefore, any additive that interacts with the gel surface is expected to increase the porosity of the gel, and decrease shrinkage.

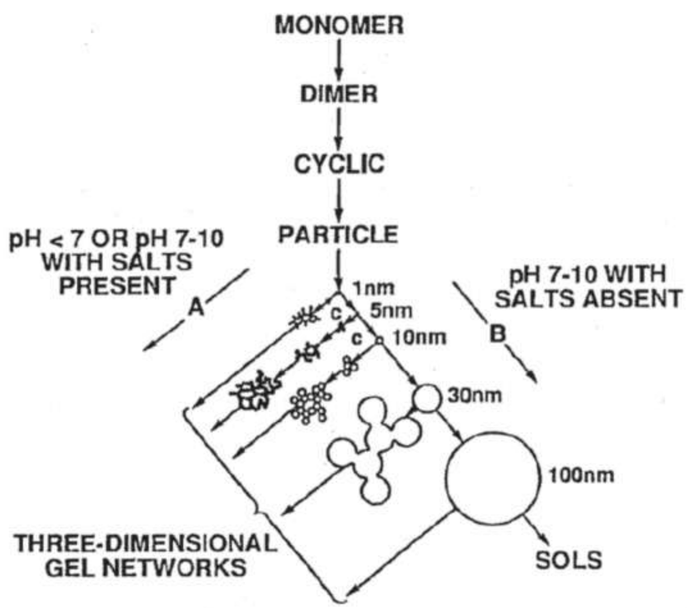

Figure 2 – Polymerization behavior of silica (Adapted from [37])

Gelation conditions also change the porosity of the gel structure, and the effect of pH is shown in Figure 2. It can be seen that to get a gel structure that is in mesoporous range, an acidic precursor mix is required, and as the acidity of the solution increases, the porosity decreases. It's been reported that the gelation temperature increases the particle size, therefore increases the porosity of the matrix [9].

Mechanical properties of the silica gel

The developed bioreactive material must yield some mechanical strength to be feasibly used in industrial applications. Otherwise, handling, transportation or utilization will be impractical. Furthermore, if the material cannot maintain its structural integrity, cells can also start leaking from the matrix, decreasing the performance of the system.

The mechanical properties of the material are primarily determined by the gel composition. Functionality of the precursors determines the extent of cross-linking in the gel. Chujo *et al*. [38] has reported a direct correlation between the increase in the Young's modulus and toughness of the gel and the multi-functionality of precursors. Generally, it can be said that higher the functionality of the precursors, the more rigid and stronger the gel is going to be. This can be experimented by using alkoxide precursors such as TEOS and TMOS (functionality=4) and MTES and MTMS (functionality=3). After gelation, condensation reactions keep occurring during aging, increasing the strength and stiffness of the gel. Brinker *et al*. reported that during aging, both moduli (Young's/Shear) increase by orders of magnitude [9]. Jang *et al* [35] has shown that for a gel comprised of only silica nanoparticles (SNPs) and PEG, strength is directly correlated to SNP concentration. However, if alkoxide precursors are also used, cross-linking might be hindered if SNP concentration is too high.

1.3 Objectives

Main objective of my dissertation research was to develop a bioremediation system which utilizes silica gel encapsulated bacteria for water treatment. The proposed system consists of a reactor packed with the developed bioreactive material, which comprises the encapsulated cells in a porous silica gel matrix. Components of the proposed system can be described as follows:

I. **Cells** perform the cleaning of the water by chemical degradation of the targeted chemicals into environmentally safe, non-hazardous products. This degradation process may be performed in multiple ways: I) A recombinant bacteria strain expressing an enzyme which degrades the target chemical can be used, so that the cell acts as a "bag of enzymes", II) A bacteria strain that metabolizes the target chemical can be used, so the cells use the chemical as a primary source of energy.

II. **Encapsulation matrix** is the material that acts as a porous barrier between the cells and the environment, confining the cells within but allowing the chemicals diffuse freely. Physical and chemical properties of this material should be such that the degradation activity of the bacteria is sustainable for long periods of time. This requires that the interactions between the material surface and the cells are not detrimental to the cells or do not hinder the cellular reactions. In addition, both chemicals and degradation products should be able to diffuse through the material without limiting the biochemical reaction rates required for degradation. ***Silica gel***, with its inert chemistry, porous structure and mechanical strength is an ideal candidate for this task.

III. **Reactor** is the vessel where the bioreactive material is contained in a flow-through system to clean the wastewater. In such a reactor, the chemicals need to transport (I) from the bulk flow to the bioreactive material, (II) within the material to the cells, (III) through the cell membrane to the cytoplasm for degradation reaction.

Figure 3 illustrates the bioremediation system in different length-scales, with silica gel microbeads as the bioreactive material utilized in a packed bed reactor. The noted length-scales on the figure are the characteristic lengths of the reactor, microbeads, average pore size of the gel and a typical bacteria cell respectively.

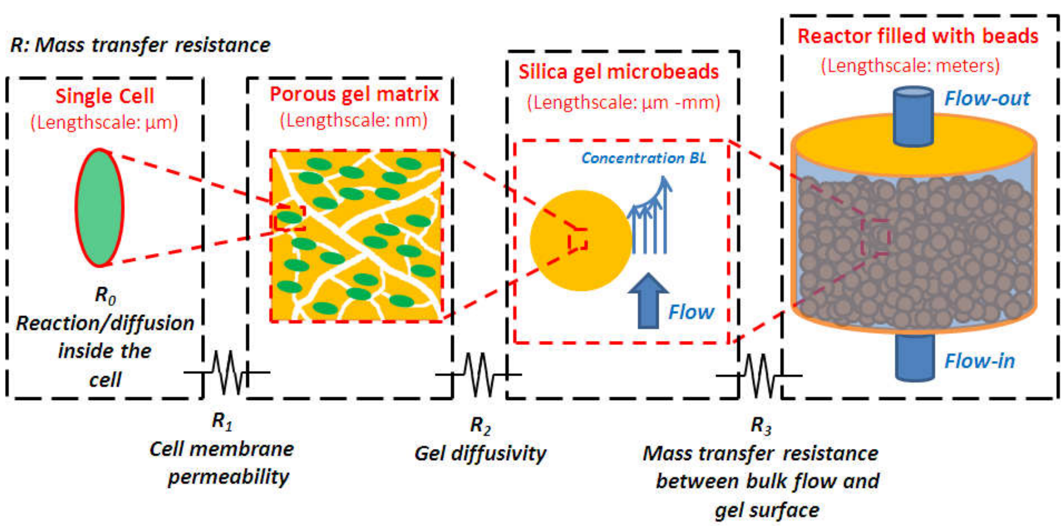

Figure 3 – Schematic of the proposed system in different length-scales

Margaritis *et al* [8] provided an excellent summary of the desirable characteristics of the encapsulation matrix for an immobilized cell bioreactor. Since my application here was water bioremediation, the list is slightly modified, as provided below.

A <u>cell encapsulation matrix</u> (for a bioremediation system) is required to:

1. Maintain the activity of the cells for long periods of time.
2. Not react with substrates or products.
3. Retain its physical integrity and be insoluble under the bioprocess conditions.
4. Be permeable to reactants and products.
5. Have large specific area per unit volume.
6. Have high diffusion coefficients for substrates and products (and possibly nutrients).
7. Be resistant to microbial degradation.
8. Have good mechanical strength.
9. Retain chemical and thermal stability under bioprocess and storage conditions.
10. Recognized as environmentally safe for water treatment applications.
11. Be available in adequate quantities with consistent quality and acceptable price.
12. Be feasible to produce efficiently for desired quantities.

1.4 Overview of dissertation

In order to accomplish the main objective of my dissertation project, the research was partitioned into four specific aims:

<u>SA 1:</u> Development of porous silica gels for bacteria encapsulation

<u>SA 2:</u> Biotransport/reaction modeling of a flow-through reactor with encapsulated bacteria

<u>SA 3:</u> Long terms storage of silica gel encapsulated bacteria

<u>SA 4:</u> Integration of developed silica gels with industry-scale manufacturing systems for scale-up

The outline of these specific aims are shown in Figure 4. These specific aims were addressed in Chapters 2, 3, 4 and 5 of this dissertation respectively. Building upon the developed material design, synthesis and modeling expertise, a novel co-encapsulation method for synergistically working bacteria is discussed in Chapter 6. A summary of the research is provided in Chapter 7.

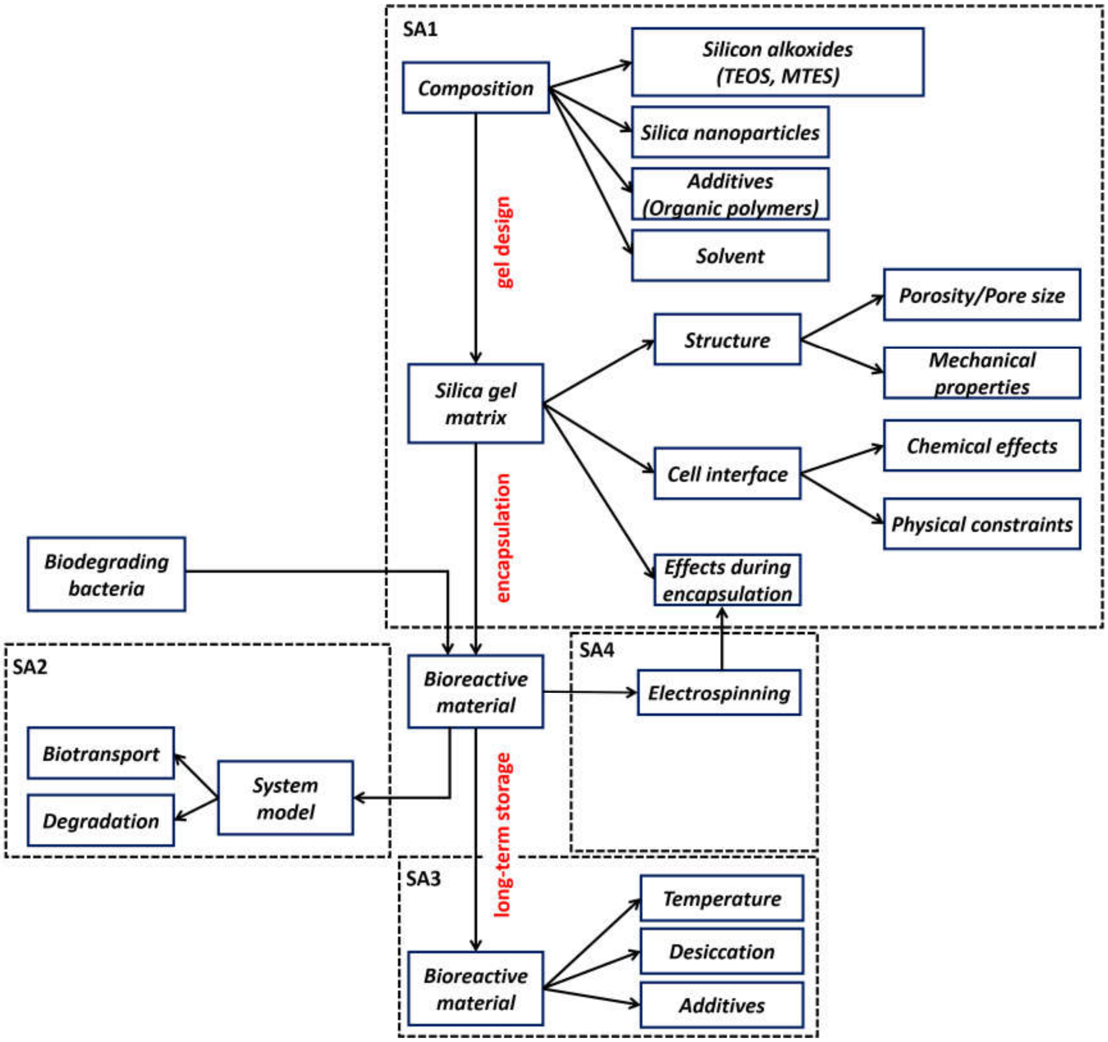

Figure 4 – Outline of the specific aims of the dissertation

Chapter 2: Silicon alkoxide cross-linked silica nanoparticle gels for encapsulation of bacterial biocatalysts[1]

2.1 Introduction

Silica gels have been extensively studied for encapsulation of whole cells for different applications in biotechnology and biomedical engineering [5, 25-28]. In most of these applications, ensuring biocompatibility (*i.e*. encapsulated cell viability) during the encapsulation process and in the resulting gel has been a major challenge. Many studies were conducted to increase the biocompatibility of the encapsulation processes [39] by removing the alcohol produced by the gelation process[30] or by incorporating additives (such as polyethylene glycol (PEG), glycerol) into the gel [15, 18]. However, recent studies reported that biocompatibility is not essential for biocatalysis applications where a thermodynamically favorable reaction is catalyzed by intracellular enzymes. For example, Fennouh *et al.* reported catalytic activity in silica gels that contained encapsulated *E. coli* cells with compromised cell membranes (observed by electron microscopy) [34], Nassif and Livage suggested that encapsulated bacteria can function as a "bag of enzymes" and suggested that the cells can still be enzymatically active even if they had compromised membrane integrity [40]. In two different studies [17, 41], it was shown that activity of the intracellular enzyme β-galactosidase increased significantly when encapsulated *E.coli* were treated with organic solvents to enhance the permeability of the cell membrane (and by potentially compromising it). These results showed that for biocatalysis applications that do not require cell viability, steps to increase biocompatibility (such as alcohol removal during encapsulation or incorporation of costly organic polymer additives to protect the cells) can be eliminated. In the present study, our aim was to sustain and potentially enhance biocatalytic activity while preventing leakage of intracellular enzymes from the bioreactive material. Moreover, we sought to keep the cost of the process and the materials low by bypassing the need to preserve cell viability.

Gel microstructure directly affects diffusivity of the chemicals through, and mechanical strength of, the porous silica material. Therefore, it is desirable to develop encapsulation methods that maintain catalytic activity of the encapsulated organisms, while simultaneously optimizing chemical and physical properties of the gels. The conventional silica gel encapsulation method is

[1] Reprinted from Mutlu, B. R.; Yeom, S.; Tong, H.-W.; Wackett, L. P.; Aksan, A., Silicon alkoxide cross-linked silica nanoparticle gels for encapsulation of bacterial biocatalysts. *Journal of Materials Chemistry A* **2013,** *1* (36), 11051-11060. DOI: 10.1039/C3TA12303K

the sol-gel transition of a silicon alkoxide [14]. In a typical process, a silicon alkoxide such as tetraethyl orthosilicate (TEOS) is hydrolyzed in the presence of water and an acidic catalyst. Depending on the pH and temperature of the solution, the reactive silanol (Si-OH) groups of the hydrolyzed silicon alkoxide go through condensation reactions to form siloxane (Si-O-Si) bonds, developing a 3D porous gel structure. The cells are added to the solution after the hydrolysis reaction is completed and they get entrapped within the gel during the condensation process (polymerization). One limitation of this method is realized when the cells are exposed to acid, which can hamper the activity of the intracellular enzymes or inactivate them irreversibly. To eliminate this problem, the common practice is to adjust the pH of the solution before adding cells. While neutralization of the pH can preserve enzyme activity, it may sacrifice gel microstructure control, resulting in gels of inadequate diffusion or inferior mechanical properties.

Silica nanoparticles (SNPs) are also appealing as precursors for silica encapsulation of bacteria due to their commercial availability at high volumes and low cost. SNPs are available in various sizes ranging from nanometers to micrometers, enabling the microstructure of a silica gel to be fine-tuned by using SNPs of different diameters. SNPs are commonly stabilized in highly alkaline solutions and by lowering the pH of the solution it is possible to obtain a gel. Finnie *et al.* have shown that sulfate-reducing bacteria can be encapsulated in such a gel obtained by lowering the pH of Ludox SM-30 SNP sol [42]. However, cell encapsulation by using SNPs exclusively enables limited control on the process and the properties of the formed gel. Therefore, SNPs are more commonly used in combination with other precursors such as sodium silicate [17]. However, it was reported that mechanical stability, as determined by Young's modulus of the gel, of sodium silicate + SNP gels decreases when the SNP concentration is increased [43]. Therefore, in this study, we opted to use a silicon alkoxide precursor (TEOS or MTES) to act as a crosslinker for the SNPs. After the pH of the SNP sol was neutralized, the bacteria were mixed with the aqueous sol and hydrolyzed silicon alkoxide was added to induce cross-linking and foster polymerization. Using this approach, it was possible to fine-tune the microstructure, and therefore the diffusivity of the gel, by altering the SNP size. A range of SNP to silicon alkoxide ratios were investigated to ensure formation of an SNP-governed microstructure and silicon alkoxide functionality was investigated for its potential effects on the process and gel structure.

We applied the methods described above to an important practical problem, using recombinant *E. coli* cells expressing the atrazine dechlorinating enzyme AtzA to transform atrazine to hydroxyatrazine. Atrazine (2-chloro-4-ethylamine-6-isopropylamino-*s*-triazine) is one of the most commonly used agricultural herbicides in the U.S. and its concentration in drinking water is regulated by Environmental Protection Agency (EPA). The World Health Organization (WHO) determined an acceptable daily intake limit of 0.1 mg/L (~100 ppb) for atrazine in drinking water [44]; whereas EPA determined an upper limit of 3 ppb as an annual average [45]. Currently, atrazine is removed from drinking water by filtration methods that rely on adsorption, most commonly activated carbon, that has to subsequently be disposed of or incinerated with some loss of the material. In this regard, a biocatalytic material that degrades atrazine is desirable for environmental sustainability provided that it is cost competitive. The overall challenges for a silica-based bioremediation system are that it needs to: (1) function well with trace levels of atrazine found in drinking water (< 10 ppb), (2) sustain function for weeks or months in a continuous, flow-through process, (3) be mechanically strong and stable under continuous flow conditions.

Successful applications of atrazine bioremediation at high concentrations (samples from farm run-off waters or buffer solutions fortified with atrazine), from 10 to 30 ppm, have been reported [46-49] but most laboratory studies have used much higher atrazine concentrations that do not mimic actual environmental situations. Galindez-Najera *et al.* reported complete removal (*i.e.* effluent concentration below detection limit of assay) of atrazine using a two-stage biofilm reactor with a binary culture of *Stenotrophomonas maltophilia* and *Arthrobacter* sp., at over 30,000 ppb influent atrazine concentration [47]. Liu *et al.* reported above 90% removal efficiency of atrazine from wastewater using a membrane bioreactor containing *Pseudomonas sp*. ADP, at ~15,000 ppb influent atrazine concentration [48]. While these approaches are suitable for removal of atrazine at high concentrations, effluent concentrations are still significantly higher than 3 ppb, despite the high removal efficiency. In a recent study, Buttiglieri *et al.* utilized a membrane bioreactor (MBR) with a denitrifying mixed culture atrazine treatment at low concentrations. [50] With a 10 ppb influent concentration, an average removal of 15% was obtained over a 3 month period. In addition to the low performance of the reactor at low atrazine concentrations, it is also not desirable to have living bacteria in a reactor for drinking water treatment. This requires further downstream processing to ensure that any bacteria that leach from the system are removed from water, increasing the overall cost of the system.

Our research group recently encapsulated recombinant *E. coli* cells expressing atrazine dechlorinating enzyme AtzA into silica gels and the cells were killed by a post-encapsulation heat treatment process. Batch activity tests were run with an ~30,000 ppb atrazine solution and biocatalytic activity of non-viable encapsulated cells (0.44-0.66 μmol/g cells-min) was comparable to free cell activity (0.61 μmol/g-min) but sustained for a much longer time,4 months, compared to free cells [51]. However, at low concentrations of atrazine (10 ppb), the biocatalytic activity of the cells was several orders of magnitude lower and the atrazine degradation of the encapsulated cells in a packed bed reactor gradually decreased to an immeasurable rate within 2 weeks. Mechanical integrity of the gels was also shown to degrade significantly during that time (data not shown).

To overcome the limitations of the previous studies, while also developing an economically feasible product, the present study sought to develop catalytic silica bioreactive materials that maintained high atrazine removal for long durations at a low influent concentration. Utilizing three of the developed formulations in a flow-through packed bed reactor system, effluent atrazine concentration was maintained at a level below 30% of the 10 ppb influent for 2 months. Additionally, as compared to our previous study [51], mechanical strength of the material was improved from a yield load of 0.2 N to a maximum of 3 N and cost of the product is significantly reduced by eliminating high cost silica precursors and organic polymer additives from the formulation. The design was conducted through a step-by-step evaluation/elimination process, based on bioreactive material characteristics such as gelation time, transient catalytic activity at high concentration and mechanical strength (Figure 5). Additional characterization studies (diffusivity and cell viability assays, SEM) were also performed for better interpretation of the results. Our results suggest that the developed catalytic bioreactive material(s) can be used for continuous treatment of water to remove environmentally-relevant concentrations of atrazine from drinking water. On a broader note, the proposed method can also be used to encapsulate different biocatalysts, aimed to treat other low concentration contaminants (pharmaceuticals, personal care products, endocrine disruptors, etc.) from drinking water supplies.

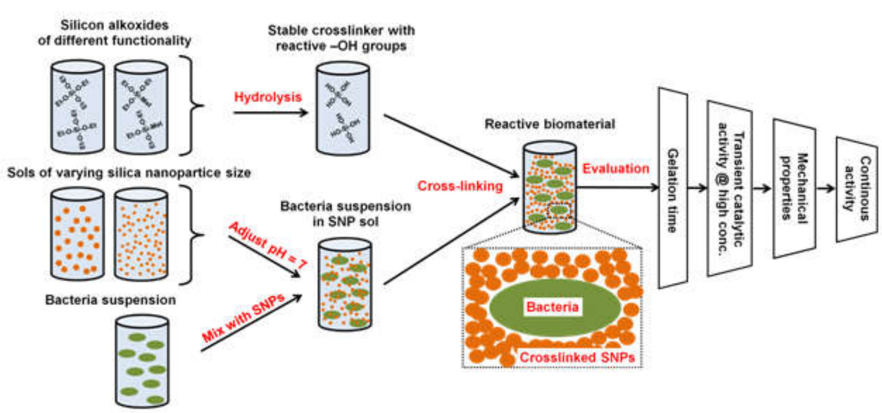

Figure 5 - Schematic of encapsulation and evaluation methods

2.2 Experimental

Materials

Tetraethoxysilane (TEOS: $Si(OC_2H_5)_4$) and triethoxymethylsilane (MTES: $CH_3Si(OC_2H_5)_3$) of reagent and technical grades, respectively were purchased from Sigma-Aldrich (Sigma-Aldrich Corp. St. Louis, MO, USA). Ludox HS40 and Ludox TM40 SNP sols were purchased from Sigma-Aldrich and NexSil 85-40 and NexSil 125-40 SNP sols were generously provided by Nyacol (Nyacol Nano Technologies Inc., Ashland, MA, USA). All the SNP sols had 40% SiO_2 content by mass and were stabilized by sodium ions. The only difference between different SNPs is the nanoparticle size and their initial pH, as shown in Table 1. Technical grade atrazine was provided by Syngenta (Syngenta Crop Protection, NC, USA). All the chemicals were used as received. Ultrapure water (UPW) was used in all the experiments. UPW was prepared by filtering deionized water through a Milli-Q water purification system (Millipore, Billerica, MA, USA) to a final electrical resistance of > 18.2 MΩ/cm.

Table 1 – Properties of the SNP sols used in this study

Commercial Name	**Abbreviation**	**Average particle diameter [nm]**	**Density [g/mL]**	**Initial pH**
Ludox HS40	HS40	12	1.3	9.7
Ludox TM40	TM40	22	1.3	9.0
Nexsil 85-40	NS85	50	1.2	9.5
Nexsil 125-40	NS125	85	1.2	9.5

Bacterial strains and growth conditions

The growth conditions were identical to those described previously, except for some minor modifications. [51] *E. coli* DH5 α (pMD4) [52] was grown at 37 °C in superbroth medium with vigorous aeration, supplemented with 30 μg/ml chloramphenicol. Intermediate cultures were grown by inoculation with 1% (v/v) starter culture and diluted 100-fold in production flasks containing the same medium. Cells were harvested by centrifugation at 6,000 x g for 20 min at 4 °C.

Catalytic bioreactive material synthesis and encapsulation

Hydrolysis and condensation reactions of silicon alkoxides were controlled by adjusting water to silicon alkoxide molar ratio (*r*) and pH of the solution. 1:5.3:0.0013 molar ratio of silicon alkoxide:water:HCl was used to obtain $r = 5.3$ and a pH of 4, which resulted in a fully-hydrolyzed silicon alkoxide solution with a slow condensation rate. The values for *r* and pH were selected based on previous literature reports. Brinker reported that, during hydrolysis with sub-stoichiometric amounts of water ($r < 4$), condensation starts before complete hydrolysis and alcohol-producing condensation reactions are favored. [53] However, increasing *r* excessively can promote depolymerization of the gel by siloxane bond cleavage reactions. Therefore, an *r* value that is slightly over 4 was selected. In the pH 3-8 range, hydrolysis rate of alkoxysilanes increases when acidity or alkalinity of the solution increases and condensation rate increases with increased alkalinity. [54] Therefore, the pH of the solution was adjusted to 4 to obtain fast hydrolysis and slow condensation reactions. This ensured that the silicon alkoxide did not polymerize by itself but cross-linked the SNPs. The hydrolyzed silicon alkoxides were kept in an ice bath until they were used to further slow down condensation reactions.

For verification of the desired (fully hydrolyzed, slow condensation) state of the silicon alkoxide, progress of the hydrolysis and condensation reactions were observed by IR spectroscopy. After the initial phase separation of the silicon alkoxide-water-HCl solution disappeared, 0.15 μL samples were extracted from the solution in 15 minute time intervals. Samples were placed between two BaF_2 windows. The windows were sealed with vacuum grease to prevent evaporation. The sealed sample was transferred to an infrared microscope attached to an FTIR spectrometer (Thermo-Nicolet Continuum equipped with a Mercury Cadmium Telluride detector, Thermo Electron, Waltham, MA, USA). The FTIR sampling resolution was 4 cm^{-1}, and 128 IR scans were averaged per spectrum in the 4000-740 cm^{-1} wavenumber range. The IR spectra were analyzed using OMNIC (Thermo-Nicolet) software. This experiment was run in duplicate. The state of hydrolysis and condensation reaction rates was determined by measuring the intensity of δ-OH bending peak of water at 1650 cm^{-1} and the CH_3 bending peak of silicon alkoxide (TEOS, MTES) and produced ethanol at 1384 cm^{-1}.

The pH of the SNP sol was adjusted to neutral pH by adding 1M hydrochloric acid to avoid inactivation of the enzyme and to eliminate initial pH variations between different SNP sols. After pH adjustment, bacteria were momentarily suspended in a 1 g/mL aqueous suspension and added to the SNP sol. The added amount was adjusted such that the final concentration of encapsulated bacteria in the gel was 0.125 grams/mL of silica precursor (SNPs and silicon alkoxide combined).

Silicon alkoxide was added to the bacteria + SNP solution by pipetting a few times to obtain a homogeneous sample. SNP sol to silicon alkoxide ratios were selected as 7:1, 3:1 and 1:1 (v/v). Mass contribution of silica precursors to the gel microstructure can be estimated using two assumptions: (1) Silicon alkoxide is fully hydrolyzed (2) All SNPs are cross-linked by silicon alkoxide. With these assumptions, Table 2 shows the estimated silica content contribution from different precursors of the gels.

The final product was either placed in molds or vials for gelation, depending upon the specifics of the experiment to be conducted. The gelation occurred within seconds to hours depending on the formula used. For molding of fast gelation time formulations, precursors were cooled by immersion in an ice bath to slow gelation. During gelation and storage, the vials were kept closed and molds were sealed with a PVDC film to prevent drying.

Table 2 – Total silica contribution ratio of SNP sol/crosslinker by mass based on volumetric ratio

Crosslinker	**TEOS**			**MTES**	
SNP sol/crosslinker (v/v)	**7:1**	**3:1**	**1:1**	**7:1**	**3:1**
Ludox HS40	8.45	3.62	1.20	7.54	3.23
Ludox TM40	8.45	3.62	1.20	7.54	3.23
Nexsil 85-40	7.80	3.34	1.11	6.96	2.98
Nexsil 125-40	7.80	3.34	1.11	6.96	2.98

Characterization

Gelation time

Bioreactive materials were synthesized in glass scintillation vials and gently shaken intermittently to determine the degree of crosslinking of the gel. The time intervals between observations were increased with increasing duration of the experiment. Gelation time was determined as the time when solution in the container no longer exhibited observable flow when agitated.

Biocatalytic activity assays

Catalytic activity of the bioreactive material is determined by transient and steady-flow activity assays. In transient activity assays, bioreactive materials were synthesized in glass scintillation vials as 2 mL cylindrical blocks (3.5 mm thickness and ~570 mm^2 surface area), in triplicate. Three mL of 150 µM (32.4 ppm) atrazine solution in 0.1 M potassium phosphate buffer (at pH 7.0) was added on top of each gel and vials were placed on a rotary shaker. Samples were collected after 60 min of incubation and immediately immersed in a 90°C water bath to stop their catalytic activity by denaturing the enzyme. After inactivation of the enzyme, samples were filtered through a 0.2-µm pore size PTFE syringe filter to remove any particulates that may be released from the material.

The concentrations of atrazine and its metabolite, hydroxyatrazine, were measured by using high performance liquid chromatography (HPLC) as described by de Souza *et al.* [52] Transient activity assays were performed right after encapsulation (day 0) and after 4 days of storage within scintillation vials at room temperature. The vials were kept tightly closed to prevent samples from drying.

For steady-flow activity measurements, bioreactive materials were synthesized in stainless steel molds as hemispherical beads of 1.5 mm diameter. 6.6 grams of beads were transferred into 15 mL glass bioreactors (Buchner funnels, coarse grade) that were connected to a peristaltic pump drive (Masterflex L/S variable speed modular drive, Cole-Parmer, Vernon Hills, IL, USA). Ten ppb atrazine solution in 0.1 M potassium phosphate buffer (at pH 7.0) was used as influent solution to the bioreactors and was replenished whenever required during experimentation. A slow flow rate of 0.05 mL/min was chosen to maximize residence time (5 hours) and minimize the produced effluent water. Collected samples were treated as previously described and concentration of atrazine in the effluent fluid was measured using the Atrazine Plate Kit (Beacon Analytical Systems Inc., USA) in accordance with the manufacturer's instructions.

Mechanical properties

Mechanical tests were performed on hemispherical beads (in triplicate) which were synthesized as previously described. A uniaxial testing machine was used with a 5 N load cell with 0.05 N resolution (Instron, Norwood, MA, USA). During testing, constant displacement rate was applied to the material until the material failed. Results were obtained in the form of a load-displacement curve.

Cell viability assay

Catalytic bioreactive materials were synthesized in scintillation vials, in triplicate. A 0.1 g aliquot of the material was pulverized using a mortar and pestle and the crushed material was suspended in 2 ml of sterile phosphate-buffered saline. The solution was serially diluted and spread-plated onto Luria-Bertani agar with 10 μg/ml chloramphenicol. Cell counts were determined based on the number of observed Colony Forming Units (CFUs) after overnight incubation.

Diffusivity assay

Trypan blue solution (0.4%) purchased from Sigma (Sigma-Aldrich Corp. St. Louis, MO, USA) was used to evaluate the diffusivity of the synthesized gels. Four hundred μL of gels without cells were synthesized in polystyrene cuvettes with 10x4 mm base dimensions. One hundred μL of Trypan blue solution was added on top of the gel and progress of the dye diffusion in the gel was recorded by taking a picture every hour for 6 hours.

The diffusivity of the dye in the gel was evaluated by using the error function solution of the 1D diffusion problem with constant concentration boundary condition [55]:

$$C(x,t) = C_{BC} \times \mathrm{erfc}\left(\frac{x}{2\sqrt{Dt}}\right)$$

In this equation C is concentration, x is distance from the boundary, C_{BC} is fixed boundary condition concentration, t is time and D is diffusivity. To solve for D, we have used a 4 step image processing technique: (1) The images were converted to grayscale, (2) The intensity values of the pixels were averaged along the horizontal axis, (3) $C(x)/C_{BC}$ was determined from the ratio of the averaged intensity along a given horizontal axis at distance x over the averaged intensity at x_0 – averaged intensity at x_∞ (far enough from the boundary such that boundary condition has no effect), (4) x values corresponding to $C(x)/C_{BC} = 0.1$, 0.2 and 0.3 were determined and obtained D values were averaged. All the image processing and computations were done using MATLAB.

Microstructure

Gel and encapsulated bacteria were examined by scanning electron microscopy (Hitachi S-4700). The encapsulated bacteria were fixed in 2% glutaraldehyde and then 1% osmium tetroxide in cacodylate buffer (0.1 M sodium cacodylate, pH 7.3). After fixation, the samples were gradually dehydrated in an up-grading series of ethanol (50, 70, 80, 95 and 100%). The samples were then dried in a Critical Point Dryer (Tousimis Model 780A) using liquid carbon dioxide as transitional fluid. Finally, the samples were sputter-coated with a thin layer of gold-palladium and examined under the SEM.

2.3 Results and Discussion

In reporting the results, different gel formulations are denoted as SNP – SNP to crosslinker ratio (v/v) – Crosslinker type (example: HS40 – 3:1 – TEOS).

2.3.1 State of hydrolysis and condensation reactions of silicon alkoxide crosslinkers

After 1 hour of stirring, it was visually observed that the mixture became miscible in both TEOS and MTES solutions. This is due to destruction of water and production of ethanol during hydrolysis reactions. Based on the TEOS-water-ethanol ternary phase diagram, it is expected that ~85% of the water was destroyed at this point. [9] Figure 6 shows the collected IR spectra from samples in terms of normalized ratio of δ-OH bending peak of water to CH_3 bending peak (actual spectra shown on inset) between 1 to 3 hours at 15 minute intervals. In both TEOS and MTES solutions, the ratio initially decreased for 15 to 30 minutes, indicating continuing hydrolysis. Then the water content in the solution started increasing with respect to the total amount of CH_3, contributed from both silicon alkoxide and produced ethanol during hydrolysis reactions. This shows that hydrolysis was completed and condensation reactions were taking place, as expected based on the selected *r* and pH of the solution. It can also be seen that the ratio increased very slowly, indicating that condensation rate was low and the hydrolyzed silicon alkoxide solution was stable over time. It should be noted that while samples were being transferred to the BaF_2 windows, it is possible that minute volumes of ethanol have evaporated. This would increase the H_2O to CH_3 amplitude ratio and explain the variation in the data points. Hence, it is possible that the increase is due to a combined effect of condensation reactions and ethanol evaporation, which means that silicon alkoxide solution is more stable than suggested by the data. Since we only seek to show temporal stability over the duration of encapsulation process, we have stopped FTIR analysis after 3 hours. Stability of the silicon alkoxide solution is also verified by leaving the hydrolyzed silicon alkoxide solution (both TEOS and MTES) in a scintillation vial without addition of SNPs. No gelation was observed within 2 days of storage at room temperature.

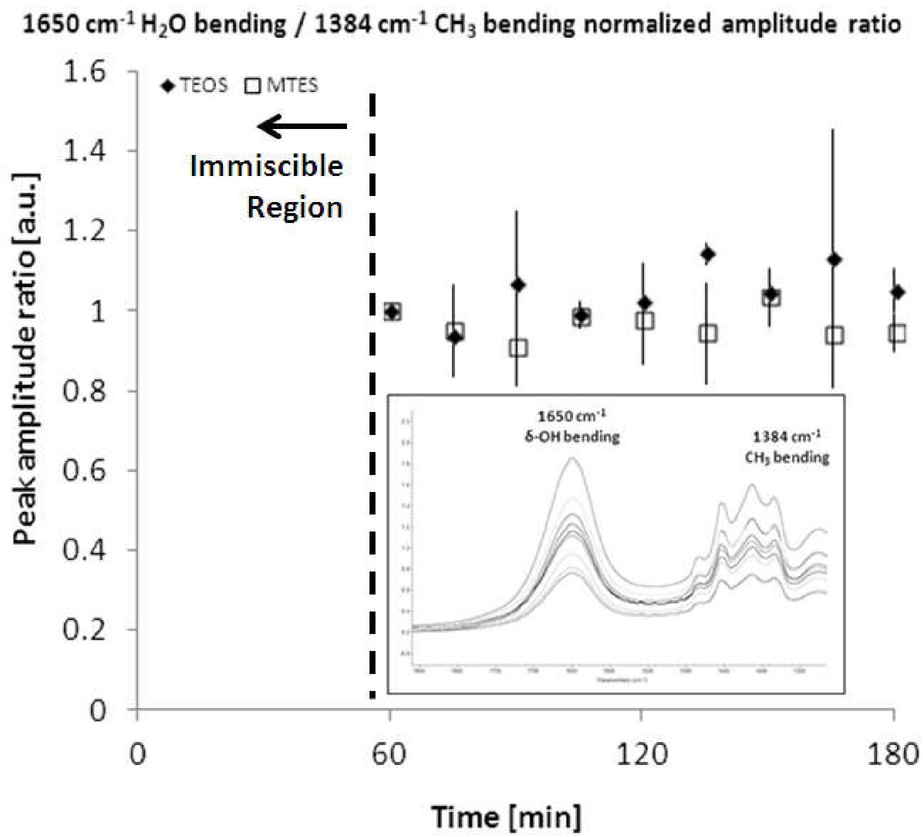

Figure 6 – Evaluation of the hydrolysis/condensation process by evolution of the peak amplitude ratio of δ-OH bending / CH_3 bending

2.3.2 Silica gel: Gelation time, diffusivity, mechanical properties and microstructure

Materials were initially characterized by their time to gel, as shown in Table 3. Gels cross-linked by MTES gelled in the time-scale of hours, whereas gels with TEOS crosslinker gelled within seconds to minutes. It was also observed that increasing SNP size and SNP to crosslinker ratio increased gelation time. In fast gelation time formulations, insertion in an ice bath was sufficient to slow down crosslinking for molding. In the range of our experiments, the most prominent factor that affected gelation time was the functionality of the silicon alkoxide crosslinker. This result can be attributed to trifunctional MTES having less reactive sites for siloxane bond formation compared to tetrafunctional TEOS. This result is in accordance with the observations of Innocenzi *et al.,* [56] who observed an increase in gelation time of TEOS/MTES gels with increasing MTES content. Another result was that gelation time increased when SNP to crosslinker ratio increased and larger

SNPs were used. This can be explained by the decrease in the total number of reactive sites per volume, as SNP content increases or nanoparticles get larger.

Table 3 – Gelation times for the catalytic bioreactive materials synthesized with selected parameters

SNP sol	Ludox HS40			Ludox TM40			Nexsil 85-40		Nexsil 125-40		
Crosslinker	TEOS		MTES	TEOS		MTES	TEOS	MTES	TEOS	MTES	
SNP to crosslinker ratio (v/v)	3:1 1:1	7:1	7:1 3:1 1:1	3:1 1:1	7:1	7:1 3:1 1:1	7:1 3:1 1:1	7:1 3:1 1:1	7:1 3:1 1:1	3:1 1:1	7:1
Approximate gelation time*	Sec	Min	Hr	Sec	Min	Hr	Min	Hr	Min	Hr	Hrs

*Gelation times are given as: Seconds (Sec): tgel < 1 min, Minutes (Min): 1 min < tgel < 10 min, Hour (Hr): 10 min < tgel < 2 hours and Hours (Hrs): tgel > 2 hours)

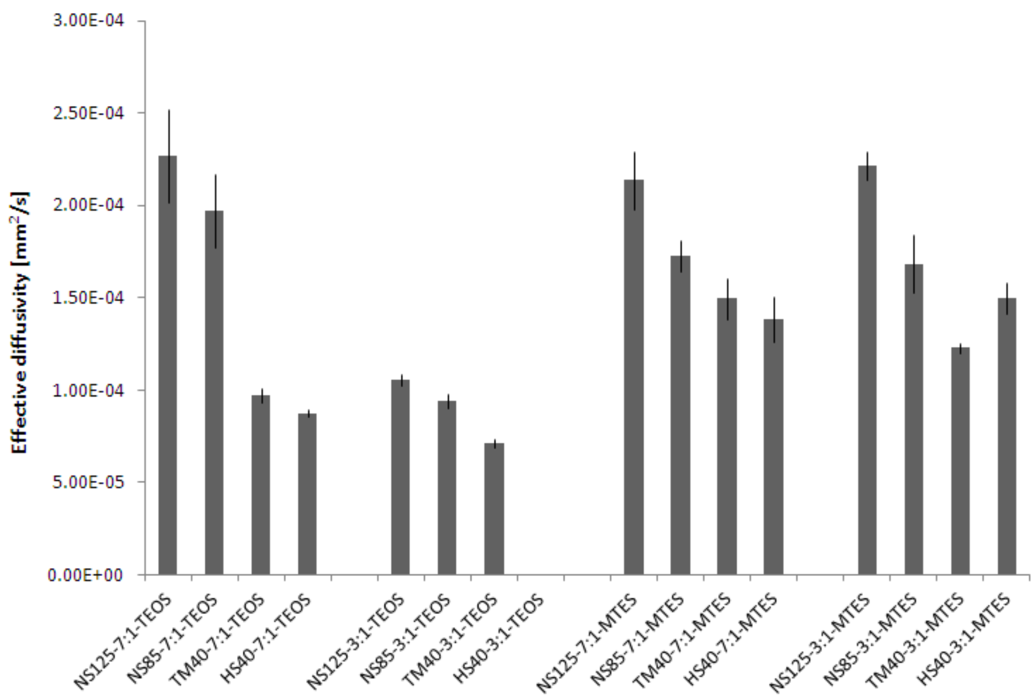

Figure 7 – Effective diffusivity of the selected gels

Effective diffusivity of the Trypan blue dye in the selected gels is shown in Figure 7. It can be observed that the highest diffusivities were around 2.25 x 10^{-4} mm^2/s and were obtained with largest size (NS125 ~85 nm) nanoparticles. In all gels, diffusivity decreased with decreasing SNP size, except for HS40-3:1-MTES gel. Data from the 1:1-TEOS gels and HS40-3:1-TEOS gel are not shown due to observed rapid propagation of the dye through cracks within the gel due to gravitational force instead of diffusion. Dye diffusivity experiments show that the diffusivity of the gel can be controlled by varying the SNP size. It was also observed that the effect of SNP size on diffusivity is the most significant in 7:1-TEOS gels and least significant in 3:1-TEOS gels. This can be explained by SNP size having more effect on the microstructure in 7:1 SNP to crosslinker ratio gels as compared to 3:1 gels. This can also be observed in Figure 8. In 12 nm SNPs (HS40), when SNP to crosslinker ratio was 7:1, SNPs were linked to each other with no observable crosslinker. However, when the ratio decreased to 1:1 (*i.e*. crosslinker content increased), SNPs were linked together with observable crosslinker. Note that the particles in 1:1 ratio appear slightly larger, because of crosslinker deposition on the surface before crosslinking. Similar effect of SNP to crosslinker ratio was observed for 50 nm SNPs (NS85). In 7:1 SNP to crosslinker ratio, particles were linked together with small area of contact. In 1:1 ratio, smaller aggregates of silica were observed along with the SNPs, formed by condensation reactions of the crosslinker. Note that even though the silicon alkoxide is stable in low pH conditions of the hydrolysis, when SNPs are introduced the pH of the solution rises and condensation reactions are unavoidable. Perullini *et al.* reported the effect of SNP content on diffusivity in sodium silicate + SNP gels, where diffusivity of cationic dye Crystal Violet was used as a model. They reported that transport was faster when the gel was richer in SNPs. [43] We observed a similar trend only in TEOS cross-linked NS125-7:1 and NS85-7:1 gels. For MTES cross-linked gels, the effect of SNP to crosslinker ratio did not have a significant effect on gel diffusivity. The decreasing effect of larger SNP size on gel diffusivity was observed in all MTES gels, except for TM40 to HS40 transition in 3:1 gels. Encapsulated cells in silica gel are shown in Figure 9.

It should be noted that, a macroporous structure was observed in SEM micrographs of the NS85-3:1-TEOS gel. This was caused by excessive crosslinker deposition on the SNP surface and large SNP size. However, it is interesting that this macroporous structure was not conserved when SNP to crosslinker ratio was increased to 7:1 or SNP size was increased to ~85 nm (NS125 SNPs). One would expect to see increased diffusion rates of NS85-3:1-TEOS gel, with increased porosity seen in SEM images, however this was not the case as shown in Figure 7. Therefore, microstructures of the gels (especially the conditions leading to the observed macroporous structure of NS85-3:1-TEOS gel) needs to be further investigated in future studies.

Mechanical properties of different samples were evaluated on the basis of load at compressive yield (Figure 10). In both TEOS and MTES cross-linked gels, best mechanical properties were obtained with the smallest size SNPs (HS40 and TM40 respectively) and there was a decreasing trend in load at compressive yield when SNP size was increased. When 12 nm size HS40 SNPs were used, decreasing the SNP to crosslinker ratio decreased the load at compressive yield of the gel. On the contrary, when 85 nm size NS125 SNPs were used, the effect was reversed. Independent from the crosslinker functionality, we observed a decreasing trend in load at compressive yield of 7:1 gels with increasing particle size. As seen in Figure 8, for 7:1 gels, number of SNPs per volume increases when SNP size is decreased. Therefore, the number of crosslinking sites increased per volume which can explain the increase in compressive strength. MTES cross-linked gels had higher compressive strength than TEOS in TM40-7:1 and NS125-7:1 formulations. However, a wider range of gel formulations need to be tested to evaluate the effect of crosslinker functionality on mechanical strength of the gels. We selected hemispherical beads for mechanical testing since they were utilized in the flow-through biocatalytic activity assays. However we suspect that the geometry of the samples has contributed to variation in the results, due to non-perfect curvature of the samples.

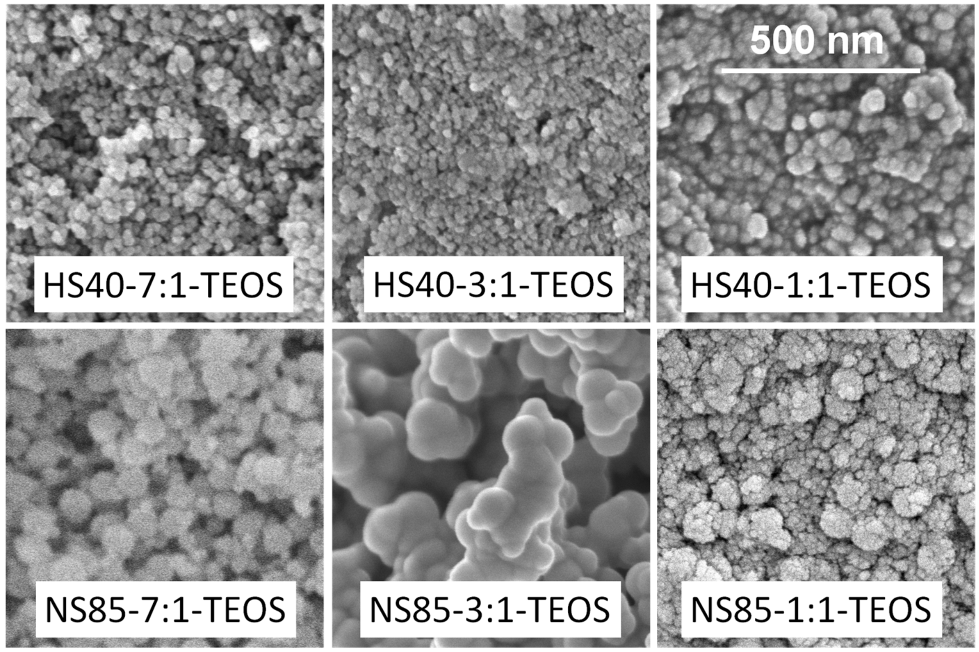

Figure 8 – Particle-scale SEM micrographs of TEOS cross-linked gels with different SNP sizes (HS40 ~12nm and NS85 ~50nm) and SNP to crosslinker ratios (the scale-bar is the same for all images)

In summary, it was observed that during gelation, silicon alkoxide crosslinkers can react with surface silanol groups of SNPs and deposit on the particles and/or form aggregates by condensation reactions. Note that even though the silicon alkoxide crosslinkers are stable after hydrolysis in low pH conditions, introduction of the SNPs in neutral pH catalyzes the condensation reactions. Therefore, it is unavoidable to obtain small aggregates of silica formed by silicon alkoxides. Higher SNP to crosslinker ratios favor microstructures dictated by SNP size as shown in Figure 8, which also increases the diffusivity of the gel. However, the gels with higher diffusivity values (such as NS125-7:1-TEOS, NS125-7:1-MTES and NS125-3:1-MTES) have lower mechanical strength under compressive loading as can be seen in Figure 10.

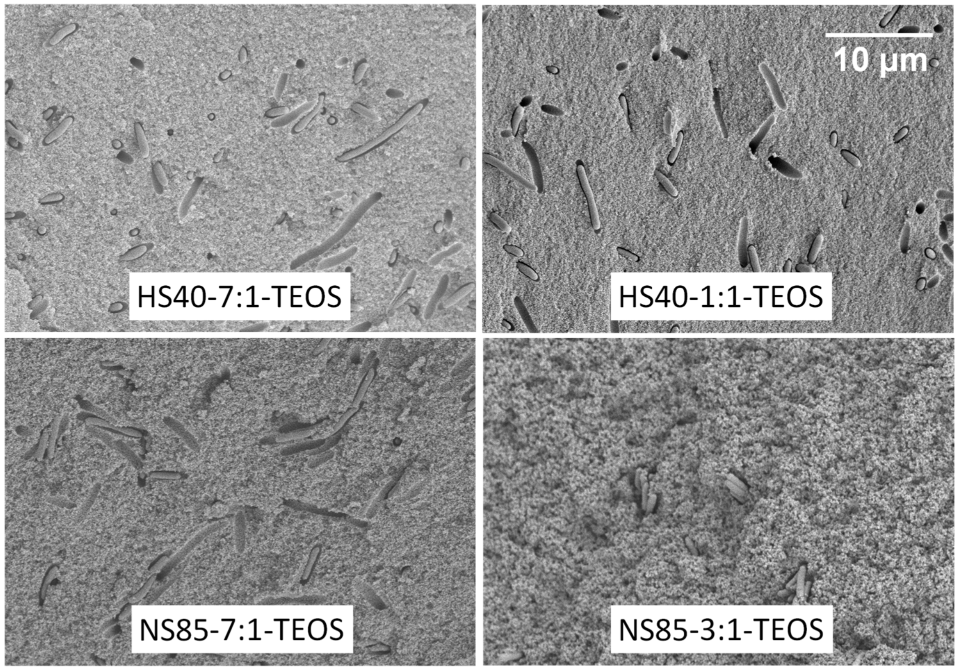

Figure 9 – Cell-scale SEM micrographs of TEOS cross-linked gels with different SNP sizes (HS40 ~12nm and NS85 ~50nm) and SNP to crosslinker ratios (scale-bar is the same for all images)

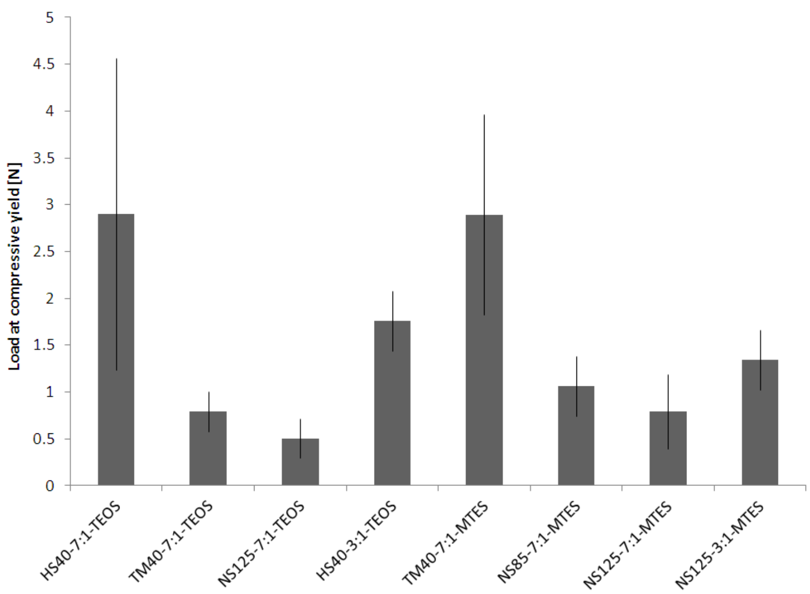

Figure 10 – Mechanical properties of the selected silica gels

2.3.3 Bacterial biocatalyst: Cell viability and catalytic activity

Cell viability assay results are shown in Figure 11 (Gel formulations with no viable cells on day 0 are not shown). On day 0, TEOS cross-linked samples with 7:1 and 3:1 SNP to crosslinker ratio had viable cells with comparable CFU counts, whereas 1:1 SNP to crosslinker ratio samples had no viable cells. MTES cross-linked samples had viable cells with 7:1 SNP to crosslinker ratio, but not with 3:1 SNP to crosslinker ratio. On day 4, only one of the TEOS cross-linked samples (HS40-7:1-TEOS) had viable cells. MTES-7:1 gels, however, had viable cells even though the CFU count has decreased 1-2 orders of magnitude on average. It is well known that ethanol is detrimental to the bacteria and time-scale of alcohol's detrimental effects is very rapid. Therefore, we expect that all the viability loss in day 0 is due to alcohol. However, alcohol does not explain the decrease in viability after 4 day storage period. One possible explanation is the aging of the material and stiffening of the gel inducing increased mechanical stress on the cells. Another possible explanation is the desiccation of the bacteria due to lack of water. For either theory, we were unable to find evidence based on micrographs obtained after 4 days of storage (data not shown).

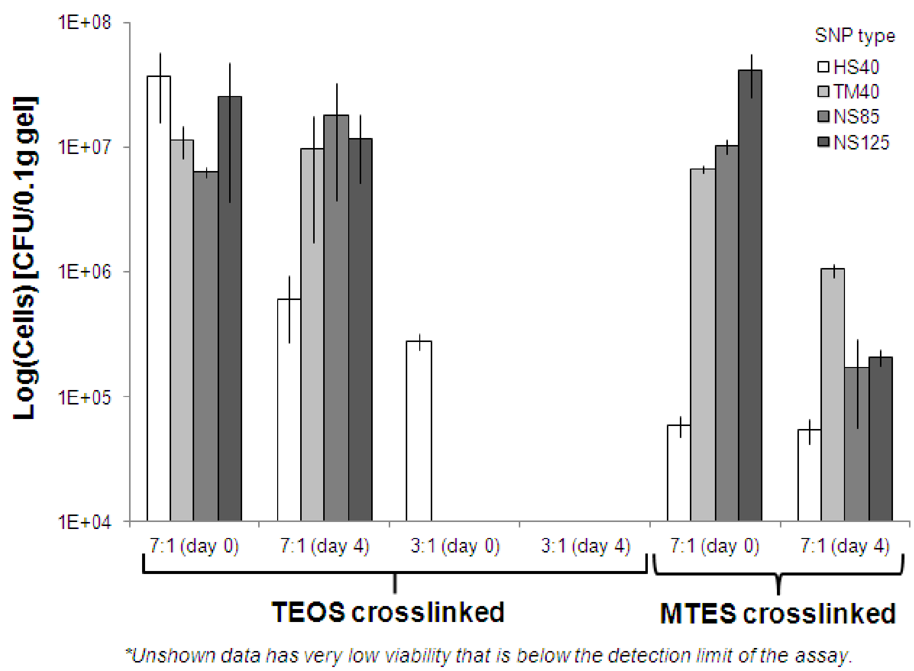

Figure 11 – *E. coli* viability in TEOS and MTES cross-linked bioreactive materials after encapsulation (day 0 and day 4)

Transient biocatalytic activity results show hydroxyatrazine (degradation product of atrazine by the encapsulated AtzA biocatalyst) concentration in the initially 150 µM (~32.4 ppm) aqueous atrazine buffer solution after an hour of incubation with the catalytic bioreactive material. Results for TEOS and MTES cross-linked gels are shown in Figure 12 (a) and (b). For TEOS cross-linked gels, the most prominent factor affecting biocatalytic activity was SNP to crosslinker ratio. On day 0, 7:1 and 3:1 samples had comparable biocatalytic activity for all SNP sizes; whereas 1:1 samples had significantly lower activity. On day 4, 7:1 samples retained 50 to 90% of their activity (except NS85) while 3:1 samples lost more than 50% activity. We did not observe a trend based on the SNP size. Based on these observations, we did not proceed with the 1:1 ratio for the MTES cross-linked gels. For MTES cross-linked gels, 7:1 and 3:1 samples had comparable biocatalytic activity for all SNP sizes on day 0, similar to the TEOS case. Likewise on day 4, 7:1 samples retained 60 to 90% of their activity (except HS40) while most of the 3:1 samples lost more than 90% of activity (except NS125). Unlike the previous case, we could observe an apparent trend based on the SNP size where activity increased slightly with increasing SNP size. MTES cross-linked gels had higher activity than TEOS gels on day 0 for all SNP sizes and SNP to crosslinker ratios. On day 4, most of the 7:1 gels with MTES crosslinker had higher activity (except HS40) and 3:1 gels with both TEOS and MTES had comparably low activity, except for NS125-3:1-MTES. We selected 8 gels out of 20 to proceed with the mechanical tests, based on their activity on day 4.

It was shown in a previous study that biocatalytic activity does not require cell viability [51] and MTES-3:1 results in Figure 12 confirms this result. Based on the day 0 results in Figure 11, three conclusions can be drawn:

(1) In most cases, SNP size did not significantly affect viability of the cells.

(2) When SNP to crosslinker ratio was decreased to 1:1, cell viability decreased to zero. Note that crosslinker content of the gel increases from 12.5% (7:1 ratio) to 25% (3:1 ratio) and 50% (1:1 ratio) as SNP to crosslinker ratio changes. Since hydrolyzed crosslinker solution also contains produced ethanol during hydrolysis reactions, ethanol content also doubles and quadruples respectively; which would explain the loss of viability.

(3) When the crosslinker with lower functionality was used (MTES), the cell viability diminished in 3:1 ratio, even though the alcohol content contribution from MTES is lower (assuming full hydrolysis, hydrolyzed MTES solution contains 25% less alcohol than TEOS) due to its lower functionality. Since MTES gels have longer gelation times, bacterial cell membranes are fully exposed to alcohol for longer durations, which can

increase the detrimental effect of alcohol. Day 4 results show that all MTES cross-linked gels with 7:1 ratio had viability, whereas only HS40-7:1 gel had viable cells within TEOS cross-linked gels.

The transient activity results show that biocatalytic activity is affected significantly by SNP to crosslinker ratio and crosslinker functionality, but not SNP size. The loss of activity with decreasing SNP to crosslinker ratio can be explained by chemical composition within the gel. When SNP to crosslinker ratio decreases, water content decreases and alcohol concentration increases and both parameters can hamper enzymatic activity. We have shown that by increasing SNP size, diffusivity of the gel increases. Therefore, we would expect SNP size to have an effect on activity if the overall reaction rate was limited by species transport in the gel. However, no correlation was observed between the catalytic activity rate of the bioreactive material and its diffusivity. This result suggests that the reaction rate is either limited by the enzymatic reaction rate of AtzA or a larger transport resistance that occurs at the cell membrane or material/solution interface. It was previously reported that there is about 7% variation in the catalytic activity of free *E. coli* cells expressing AtzA [51]. Consequently, we believe that the variation in the activity of free biocatalyst contributes to the variation of activity results in encapsulated cells. In future studies, reaction kinetics studies should be conducted in both high and low concentrations of atrazine with free *E. coli* cells expressing AtzA to better understand the reaction/diffusion rate limitations on the overall catalytic activity rate. The effects of pH and alcohol content on the catalytic activity rate of the free cells should also be investigated.

Three formulations (HS40-7:1-TEOS, TM40-7:1-MTES, NS125-7:1-MTES) were selected for flow-through biocatalytic activity experiments based on the results of transient activity assays and mechanical testing. We selected HS40-7:1-TEOS and TM40-7:1-MTES based on their sustained activity during storage (Figure 7) and superior mechanical strength (Figure 10), and NS125-7:1-MTES based on its superior biocatalytic activity on day 4 (Figure 7). As a negative control, we used TM40-7:1-MTES gel without encapsulated cells. Long-term steady-flow biocatalytic activity assay results (Figure 13) show that for all the selected gels, the effluent atrazine concentration was sustained below 30% of the influent concentration of 10 ppb for 2 months. It can be observed that effluent concentration of the reactor with the no-cell control gradually reached the influent concentration only after ~7 weeks, suggesting that some portion of atrazine was still being adsorbed by silica gel within that time frame. The difference in effluent concentrations between no cell material and encapsulated cells over the duration of the experiment shows that the removal of atrazine was mostly due to degradation rather than adsorption. Within the reported duration of the experiment, no significant variation in atrazine removal efficiency was observed amongst different gel formulations. Therefore steady-flow performance of different formulations could not be evaluated. This is primarily due to the long residence time of atrazine solution within the bioreactors, concealing any performance difference between the gels. Higher flow rates need to be investigated in future studies to fully assess the limitations of the developed materials both in terms of their mechanical integrity and degradation activity.

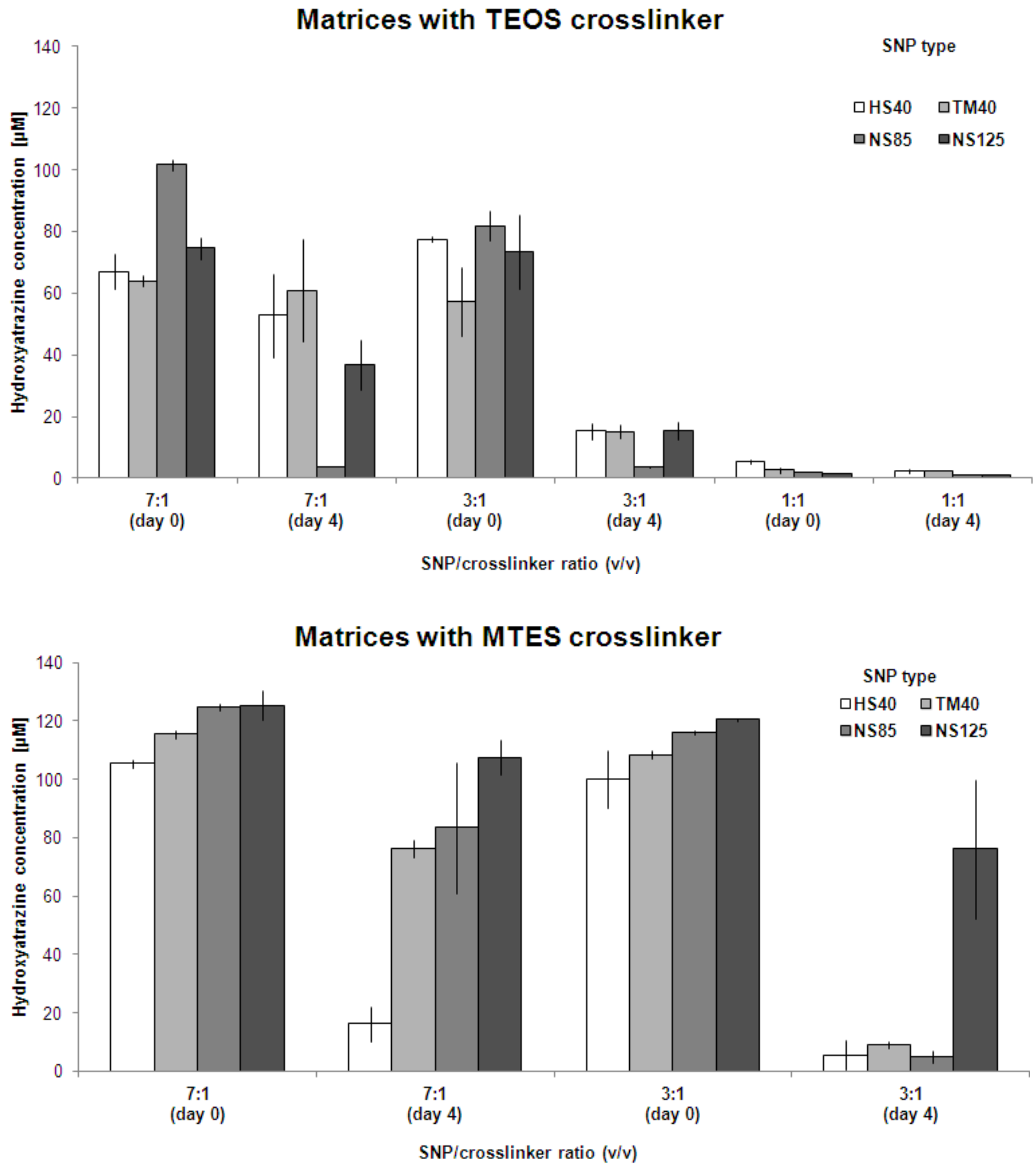

Figure 12 – Catalytic activity of TEOS (a) and MTES (b) cross-linked bioreactive materials measured by hydroxyatrazine (metabolite) concentration in solution after an hour of incubation with atrazine (day 0 and day 4)

2.4 Conclusion

Sol-gel encapsulation of bacterial biocatalysts in silica gel requires a fine balance between obtaining good material properties (mechanical strength, structural integrity, permeability, etc.) and preserving biocatalytic activity of the cells. These constraints cause limitations on the design process, oftentimes leading to insufficient material properties or biocatalytic performance. Solving these problems usually involves incorporation of additives, which in turn increases the cost of the material. In this study, we show that by using silicon alkoxide cross-linked silica nanoparticle gels for encapsulation of bacterial biocatalysts, silica gel microstructure can be fine-tuned while preserving good biocatalytic activity. Use of SNPs as the major silica precursor and elimination of the additives significantly reduces the cost of the material, making it a suitable alternative for large scale water treatment applications.

Besides pesticides, other low concentration contaminants in drinking water supplies (pharmaceuticals, personal care products, endocrine disruptors, etc.) is also an increasing concern, and studies suggest that water treatment plants cannot completely remove these pollutants by conventional treatment methods [57]. Our results show that the developed catalytic bioreactive materials can be used to remove trace levels of atrazine in a flow-through packed bed reactor system with high removal efficiency for at least 2 months. Therefore, the developed encapsulation method in this study holds potential to be applied to different bacterial biocatalysts, and can be used for removal of other pollutants from drinking water supplies.

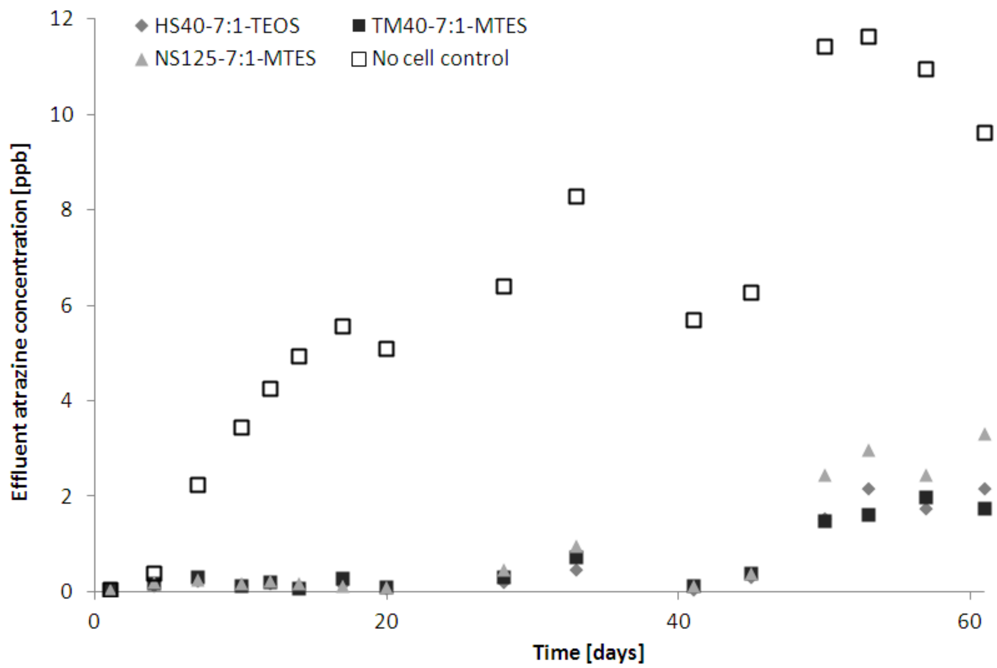

Figure 13 – Long term steady-flow biocatalytic activity of selected bioreactive materials as demonstrated by measuring effluent concentration of atrazine. The influent concentration was 10 ppb.

Chapter 3: Modelling and optimization of a bioremediation system utilizing silica encapsulated whole-cell biocatalyst[2]

3.1 Introduction

Silica gel encapsulation of biocatalysts (*i.e.* bioencapsulation) have been extensively studied in the last decade [14]. Silica gel bioencapsulation provides a robust mechanical structure and protection to otherwise fragile biocatalysts (enzymes or whole cells), which makes the technology more applicable to a wider range of engineering applications. In addition, many studies report long-term stabilization and possible enhancement to catalytic activity after encapsulation [58]. A major focus of these studies has been material and process design: Investigating biocompatible sol-gel routes [30, 39], incorporating biocompatible polymers [15, 18] and improving the encapsulation process to preserve and enhance biocatalytic activity. The possibility of using biocatalytic materials synthesized by silica gel bioencapsulation for water bioremediation applications have also been investigated [59-61].

In order to utilize a biocatalytic material (*i.e.* synthesized by bioencapsulation) in a water bioremediation application, specific constraints of the system need to be considered. These constraints include performance (such as the desired effluent concentration), material/operation costs (*e.g.* cost of material, biocatalyst, pumping costs) and mechanical properties (*e.g.* strength, stiffness) of the biocatalytic material. These parameters not only depend on the material, the design and the encapsulation method, but also depend significantly on the independent design parameters such as biocatalyst loading density (**ρ**) and characteristic length (*i.e.* size and geometry) of the material (L_c). Therefore, determining the optimal values for these design parameters are essential for successful utilization of the biocatalytic material in a large scale industrial bioremediation application.

In this study, we proposed an optimization method to determine the design parameters: **ρ** and L_c, for a bioremediation system. This system is comprised of a flow through packed bed bioreactor, filled with biocatalytic material (silica gel encapsulated AtzA biocatalyst). The proposed method consists of three steps (Figure 14). First step is the experimental characterization of the catalytic activity of the free cell biocatalyst and the permeability/mechanical properties of silica gel. For

[2] Reprinted from Mutlu, B. R.; Yeom, S.; Wackett, L. P.; Aksan, A., Modelling and optimization of a bioremediation system utilizing silica gel encapsulated whole-cell biocatalyst. Chemical Engineering Journal 2014. DOI: http://dx.doi.org/10.1016/j.cej.2014.07.130

encapsulation of a free cell biocatalyst, these properties of the gel need to be investigated as a function of **ρ**. This necessity arises from the micron scale size of the free cell biocatalyst, significantly affecting the microstructure of the mesoporous silica network. Second step is the development of a steady-state reaction/diffusion model for the encapsulated cells and experimental verification of this model. Last step is the optimization of the design parameters for the bioremediation system, using constraints on performance, mechanical properties and cost. There have been previous studies where the dependence of Thiele modulus (Φ) and the effectiveness factor (η) of encapsulated cells in alginate matrices have been investigated by varying ρ [62] or L_c [63-65]. However a method to use this information in a bioreactor setting, while satisfying biocatalytic performance, mechanical properties of the material and cost constraints to optimize ρ and L_c has not been established. Furthermore, silica gel encapsulation provides some unique differences such as production of ethanol during encapsulation (which affects cell membrane permeability) and strict inhibition of cell proliferation.

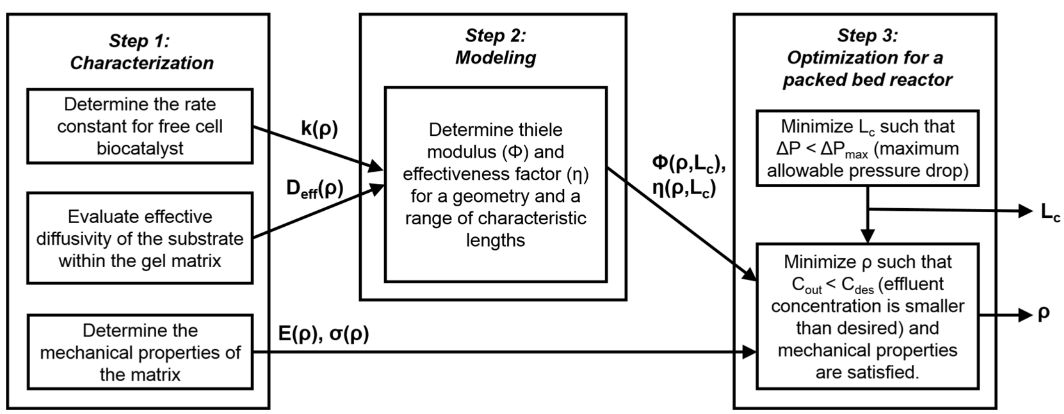

Figure 14 - **Design algorithm for determining optimal cell loading density (ρ) and characteristic length (L_c) for silica gel encapsulated biocatalyst**

Atrazine (2-chloro-4-ethylamine-6-isopropylamino-*s*-triazine) is a widely used herbicide in the U.S, up to 36,000 tons annually, along with other parts of the world such as Canada, Africa and the Asia-Pacific region [66]. Its concentration is regulated by the U.S. Environmental Protection Agency (EPA) to 3 ppb in drinking water [45], and thus, bioremediation is of great practical importance. Currently, atrazine is removed from the drinking water by adsorptive filtration methods, most commonly using activated carbon that has to be disposed of or recharged by incineration with some loss of the material, added cost and CO_2 release. The biocatalyst used in this study is a recombinant

Escherichia coli (*E.coli)* strain overexpressing the atrazine dechlorinating enzyme AtzA that transforms atrazine to hydroxyatrazine.

Our research group has previously shown that silica gel encapsulated AtzA biocatalyst can sustain its atrazine degradation activity over four months [51]. We have also shown that AtzA biocatalyst can be encapsulated in different geometries including slabs, spherical beads or electrospun PVA/silica nanofibers [67]. When utilized in a spherical bead form in a flow through packed bed reactor bioremediation system, continuous degradation activity at low ppb concentrations of atrazine was achieved [68]. In this study, we propose an optimal design for the biocatalytic material to satisfy specific performance constraints, such as reaching the desired 3 ppb limit in the effluent with a sustained influent AtzA concentration of 10 ppb, while ensuring high mechanical integrity of the system at a low cost.

3.2 Experimental

Materials

Reagent grade tetraethoxysilane (TEOS: $Si(OC_2H_5)_4$) was purchased from Sigma-Aldrich (Sigma-Aldrich Corp. St. Louis, MO, USA). NexSil 125-40 silica nanoparticle (SNP) sol was purchased from Nyacol (Nyacol Nano Technologies Inc., Ashland, MA, USA). Technical grade atrazine was provided by Syngenta (Syngenta Crop Protection, NC, USA). All chemicals were used without further purification. Ultrapure water (UPW) was used in all the experiments, which was prepared by filtering deionized water through a Milli-Q water purification system (Millipore, Billerica, MA, USA) to a final electrical resistance of > 18.2 MΩ/cm.

Bacterial strains and growth conditions

The growth conditions were identical to those described previously [51], except for some minor modifications as described below. *E. coli* strain DH5α (pMD4) [52] was grown at 37 °C in superbroth medium with vigorous aeration. The medium was supplemented with 30 µg/ml chloramphenicol. Intermediate cultures were grown by inoculation with 1% (v/v) starter culture and diluted 100-fold in production flasks containing the same medium. Cells were harvested by centrifugation at 6,000 g for 20 min at 4 °C.

Silica gel synthesis and encapsulation of cells

A previously reported silica gel matrix (NS125-7:1-TEOS) and encapsulation method was used in this study [68], where the cells are well-entrapped in the silica matrix and are not able to proliferate. Briefly, TEOS was hydrolyzed by stirring (2 hours) at a 1:5.3:0.0013 molar ratio of TEOS:water:HCl. The pH of the Nexsil 125-40 SNP sol was adjusted to neutrality by adding 1M hydrochloric acid. After pH adjustment, bacteria were suspended in phosphate buffered saline (1 g cells/mL PBS) and added to the SNP sol. Hydrolyzed TEOS was added to the bacteria and SNP solution by pipetting a few times to obtain a homogeneous sample. The final product was either placed in silicone molds (for mechanical testing) or in 20 mL scintillation vials (for activity testing) for gelation.

Characterization of free cell AtzA catalyst reaction kinetics

It was previously reported that free AtzA enzyme obeys Michaelis-Menten (MM) kinetics and its K_m and V_{max} values were determined [52]. To apply these values for kinetic modeling of an intact cell containing AtzA, one would need to have good estimates of parameters such as: enzyme concentration in the cell, cell membrane permeability and diffusivity of atrazine/hydroxyatrazine in the cell. Instead, we used a more convenient approach by developing a free cell model that does not require explicit knowledge of these parameters. We also investigated the effect of ethanol (a by-product of silica gel synthesis), on cell membrane permeability and free cell kinetics.

A 0.003 g aliquot of cells suspended in PBS was added to five mL ($\boldsymbol{\rho}$ = 6 x 10^{-4} g cells/mL) of an atrazine solution (concentration of atrazine ranged from 30 to 150 μM) prepared with 0.1 M potassium phosphate buffer (at pH 7.0) in a 20 mL scintillation vial. Scintillation vials were placed on a rotary shaker and incubated for 20 minutes. After incubation, samples were collected and immediately immersed in a 90°C water bath to stop the catalytic activity by denaturing the enzyme. After inactivation of the enzyme, samples were filtered through a 0.2-μm pore size PTFE syringe filter to remove the cells. The concentrations of atrazine and its metabolite, hydroxyatrazine, were measured by using high performance liquid chromatography (HPLC) as described by de Souza *et al* [52]. HPLC results were converted to concentrations using calibration curves for atrazine (0 to 150 μM, 30 μM increments, R^2 = 0.9986) and hydroxyatrazine (0 to 80 μM, 20 μM increments, R^2 = 0.9999).

In order to evaluate the effects of ethanol concentration, a similar procedure was followed with minor changes. Three mL buffer solutions were prepared with ethanol concentrations ranging from

1% to 50% (v/v). Sonicated cell suspension was obtained by immersing a sonicator tip into the free cell suspension and operating it at 30% power, 5s on-off intervals for 90 seconds. After sonication, sonicated cell suspension was centrifuged to separate the supernatant with cytoplasmic proteins from the cell membrane fragments. Then, 0.03 g of non-sonicated free cells and 50 µL of supernatant solution (0.005 g cell extract) from sonicated cells were added to the buffer solutions with ethanol and were incubated for an hour. After incubation, 2 mL of 150 µM atrazine solution was added ($\boldsymbol{\rho}_{\mathbf{free}}$ = 6 x 10^{-3} g cells/mL and $\boldsymbol{\rho}_{\mathbf{sonicated}}$ = 1 x 10^{-4} g cell extract/mL) to a final concentration of 90 µM and vials were incubated for 20 minutes. The remainder of the assay procedure was identical.

Determination of atrazine transport in silica gel matrix

The silica gel matrix was synthesized as a thin cylindrical disk (diameter = 7.5 mm, thickness = 3 mm). One side of the disk was exposed to a reservoir filled with 150 µM atrazine solution in 0.1 M potassium phosphate buffer, and the other side was exposed to water. After 24 hours of exposure, samples were collected to determine the amount of atrazine that permeated through the membrane from the atrazine reservoir to the water reservoir. In order to investigate the possible effect of cell loading on the matrix permeability, silica gel disks with wild-type cells (that do not express AtzA) were synthesized as a control. Cell loading density ($\boldsymbol{\rho}$) values of 0.11, 0.20, 0.33, 0.43 and 0.5 g cells/mL gel were tested. Rest of the experimental procedure was identical to the cell-free disk case.

Evaluation of the mechanical properties

Cylindrical test pieces of silica gel matrix with a thickness of 12 mm and a diameter of 12 mm were synthesized using a silicone mold. After 24 hours of aging in the mold, the samples were air dried for another 24 hours for easy removal from the molds. It was observed that the sample diameter decreased from 12 mm to 11.4 ± 0.1 mm during this process. After removal from the mold, samples were rehydrated by immersion in PBS before the mechanical testing on an MTS QTest 10 machine (MTS Systems, Eden Prairie, MN, USA). Compressive strength (σ) and elastic modulus for compression (E) of the material were evaluated by compression tests conducted on the hydrated samples at 1%/min strain rate. Cell-free samples and samples with cells ($\boldsymbol{\rho}$ = 0.059, 0.11, 0.20, 0.33 g cells/mL gel) were tested in quadruplicate. Samples were determined to be too weak for practical purposes beyond $\boldsymbol{\rho}$ = 0.33 g cells/mL for mechanical testing and therefore not tested.

Experimental verification of reaction/diffusion model

Silica gel matrix with encapsulated cells was synthesized as a cylindrical slab (gel thickness = 7 ± 0.1 mm) at the bottom of a 20 mL scintillation vial. The experiments were conducted immediately after gelation and no changes in dimensions were observed due to shrinkage or swelling of the gel. Five different cell loading density (**ρ**) values were tested (0.03, 0.059, 0.11, 0.20, 0.33 g cells/mL gel) in triplicate. Three mL atrazine solutions (in 0.1 M potassium phosphate buffer) at 150 μM concentration were added to the scintillation vials. Vials were placed on a rotary shaker and incubated for 20 minutes. After incubation, solution was removed, replaced with fresh atrazine solution and incubated for another 20 minutes. This "re-spiking" procedure was repeated 5 times, until further atrazine adsorption to the silica gel matrix has stopped (as verified by mass balance) so that steady state degradation was achieved. In preliminary studies (data not shown), it was observed that atrazine adsorption to silica gel matrix reduced the observed activity rates. This is because the atrazine transport within the matrix is hindered by adsorption of atrazine to silica gel. Therefore, minimizing adsorption by re-spiking yielded an accurate estimation of the steady-state activity rates. Note that this re-spiking procedure also removes any cells, which may have been leaked from the gels during gelation. The experimental measurements of activity were then compared to the predictions of the reaction/diffusion model developed.

The aim of the developed model is to successfully estimate the steady-state biocatalytic activity of encapsulated cells, based on cell loading density (**ρ**), characteristic length (L_c), and geometry of the material. Two dimensionless numbers can be used to estimate the steady-state performance of encapsulated catalysts: Thiele modulus (**Φ**) and the effectiveness factor (**η**) [69]. **Φ** is the ratio of characteristic reaction rate to characteristic diffusion rate. Small values of **Φ** (**Φ** << 1) correspond to reaction-limited catalysis while large values of **Φ** (**Φ** >> 1) correspond to diffusion-limited catalysis. **η** is the ratio of observed reaction rate ($\mathbf{r_{obs}}$) to maximum reaction rate ($\mathbf{r_{max}}$), which would only be achieved in the absence of internal diffusion limitations. Mathematically, these two dimensionless numbers are expressed as follows:

$$\boldsymbol{\Phi} \equiv L_c\sqrt{\frac{k'_{free} * \boldsymbol{\rho}}{D_{eff}}} \text{ (1.a) and } \boldsymbol{\eta} \equiv \frac{r_{obs}}{r_{max}} \text{ (1.b)}$$

Note that $\mathbf{k'_{free}}$ (or $\mathbf{k'_{enc}}$ which can also be used in Eqn. (1.a)) and $\mathbf{D_{eff}}$ need to be determined in characterization studies. **η** can also be analytically derived as a function of **Φ**, for different encapsulation geometries. For slab and spherical geometries, **η** can be written in terms of **Φ** as [69]:

$$\boldsymbol{\eta} = \frac{\tanh(\boldsymbol{\Phi})}{\boldsymbol{\Phi}} \text{ (for slab) (2.a) and } \boldsymbol{\eta} = \frac{3}{\boldsymbol{\Phi}}\left[\frac{1}{\tanh(\boldsymbol{\Phi})} - \frac{1}{\boldsymbol{\Phi}}\right] \text{ (for sphere) (2.b)}$$

Using Eqn. 2.a or 2.b, $\boldsymbol{\eta}$ can be determined and inserted in Eqn. 1.b to get an estimation for the observed degradation rate. For verification of this model, we compared this expected degradation rate to the experimentally observed degradation rates. For modeling results, we have used two different rate constants ($\mathbf{k'_{free}}$ and $\mathbf{k'_{enc}}$), to demonstrate the effect of ethanol concentration on free cell activity.

Table 4 – Parameters used in the packed bed reactor case study

Influent atrazine concentration (C_{in})	50 ppb	**Reactor volume (V)**	10 L (400 cm^2 x 25 cm)
Desired output concentration (C_{out})	< 3 ppb	**Packing density (ε)**	0.6
Flow-rate (Q)	1 L/min	**Fluid properties (μ, ρ_f)**	Water properties at 20°C
Cost of cells	0.1 $/g cells		

Optimization of ρ and L_c

For a bioremediation system, maximizing $\boldsymbol{\eta}$ (or minimizing $\boldsymbol{\Phi}$) is not sufficient for optimization of **ρ** and L_c because other constraints such as performance, material/operating cost and mechanical properties of the material need to be satisfied. In order to demonstrate this, a case study is considered where atrazine contaminated water is treated using a bioreactor packed with spherical biocatalysts in a flow-through setup. Table 4 shows the parameters and performance criteria used in the case study. For simplicity, external mass transfer resistances within the reactor are assumed negligible such that $C_{surface}$ (L) = C_{bulk} (L), where $C_{surface}$ is the atrazine concentration at the bead surface and C_{bulk} is the concentration of the bulk flow, at a distance L from the inlet of the reactor.

3.3 Results and Discussion

3.3.1 Characterization: Reaction kinetics, diffusivity and mechanical properties

Free cell AtzA catalyst reaction kinetics and effect of ethanol concentration on activity

Figure 15.a shows that up to the solubility limit of atrazine in water (in the 30 - 150 μM range) the enzymatic reaction transforming atrazine into hydroxyatrazine is of first order. Therefore, the free cell model takes the following form:

$$r = k_{free}(\boldsymbol{\rho})C_{Atrazine} = k'_{free}\boldsymbol{\rho}C_{Atrazine} \quad (3)$$

where $\mathbf{C_{Atrazine}}$ is the atrazine concentration in [μM], $\mathbf{k_{free}(\rho)}$ is the degradation rate constant for free cells at a given cell loading density [s^{-1}], $\mathbf{k'_{free}}$ is the degradation rate constant for free cells per cell loading density [s^{-1}/(g cells/mL)] and **r** is the reaction rate in [μmole/L-s].

Using the experimental parameters ($\boldsymbol{\rho}$ = 6 x 10^{-4}) and a least-squares-regression analysis, we determined that $\mathbf{k_{free}}$ = 4.43x 10^{-5} s^{-1} and incorporating $\boldsymbol{\rho}$, we get $\mathbf{k'_{free}}$ = 7.38 x 10^{-2} s^{-1}/(g cells/mL). For verification of these results, we obtained an activity value per cell mass using experimental parameters (5 mL solution, 0.003g cells) and an initial atrazine concentration of 150 μM. This leads to an activity rate of 0.66 μmoles/(g cells - min), which is in accord with our previously reported free cell activity of 0.61 ± 0.04 μmoles/(g cells - min) measured at 150 μM atrazine concentration [51].

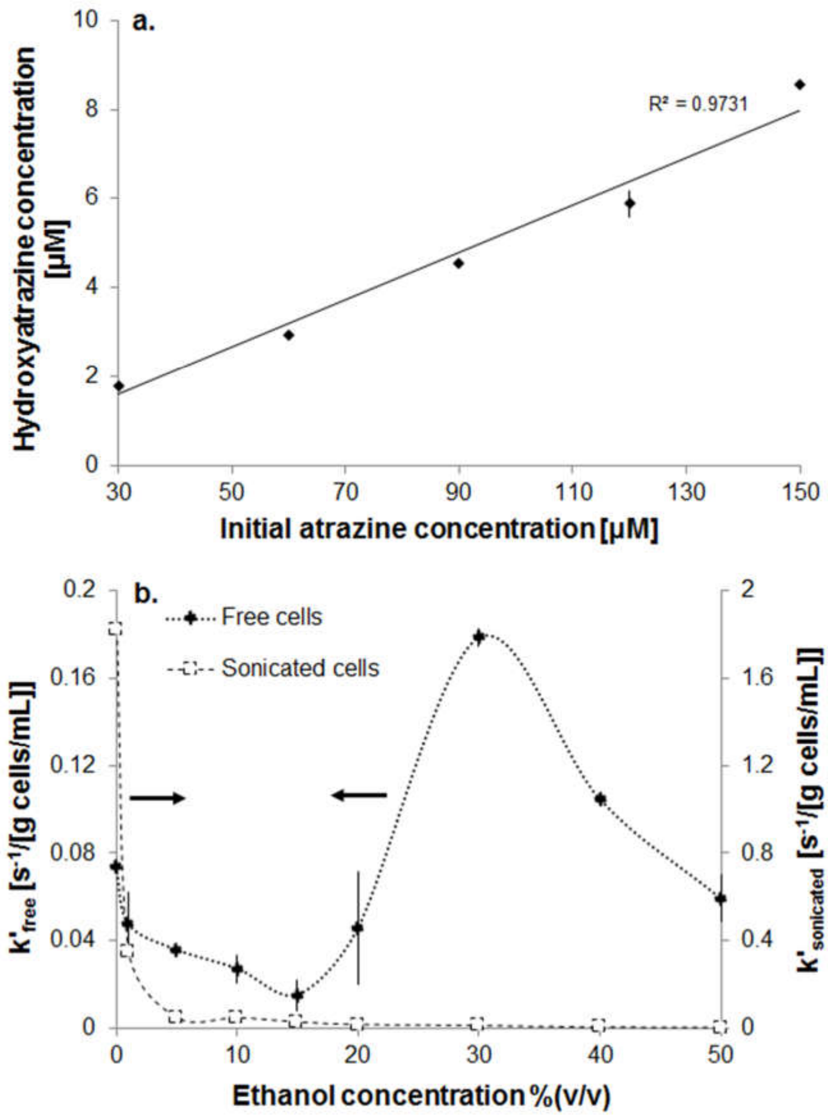

Figure 15 – a) Free cell AtzA biocatalyst activity (at ρ = 6 x 10^{-4} g cells/mL solution, 20 minute incubation time) b) Effect of ethanol concentration on biocatalyst activity rate constant (k'_{free})

Figure 15.b shows that both $\mathbf{k'_{free}}$ (free cells) and $\mathbf{k'_{sonicated}}$ (sonicated cells) change significantly with changing ethanol concentration (C_{EtOH}). It can be immediately observed that $\mathbf{k'_{sonicated}}$ is an order of magnitude higher than $\mathbf{k'_{free}}$ when C_{EtOH} = 0%, which shows the effect of transport limitations caused by the cellular membrane and intracellular transport. It can also be observed that the activity loss with increasing C_{EtOH} is more significant with sonicated cells compared to free cells, since there is no protection offered to the free enzyme by the intracellular environment. A

peak can be observed around C_{EtOH} = 30% for free cells, which can be attributed to increased permeability of the cell membrane due to ethanol damage.

Assuming full hydrolysis and condensation, we can estimate the ethanol concentration in the synthesized gel to be approximately 5% (v/v). Then, using Figure 15.b, a new rate constant for encapsulated cells as $\mathbf{k'_{free@5\%\ EtOH} = k'_{enc}}$ = 3.58 x 10^{-2} s^{-1}/(g cells/mL) can be obtained to be used in the reaction/diffusion model.

Atrazine diffusivity in silica gel matrix

Figure 16 shows that atrazine has a diffusivity of D_{eff} = 3.51 x 10^{-4} mm^2/s within the silica gel matrix (an order of magnitude lower than that of water in water [70]: 2.3 x 10^{-3} mm^2/s) without encapsulated cells. In contrast, Trypan blue dye (MW: 873 Da) has a diffusivity of D_{eff} = 2.25x 10^{-4} mm^2/s in the same silica gel matrix [68], therefore it was expected that atrazine (MW: 218 Da) had a higher diffusivity due to its smaller molecular size. It was observed that increasing cell loading density (**ρ**) increased the permeability of the gel to atrazine. To incorporate this into the model, the following correlation, derived from the data presented in Figure 16 was used to estimate the diffusivity of the matrix for a given **ρ** as follows:

$$D_{eff} = (7.23 \times 10^{-4})\ \boldsymbol{\rho} + (3.46 \times 10^{-4})\ mm^2/s \quad (4)$$

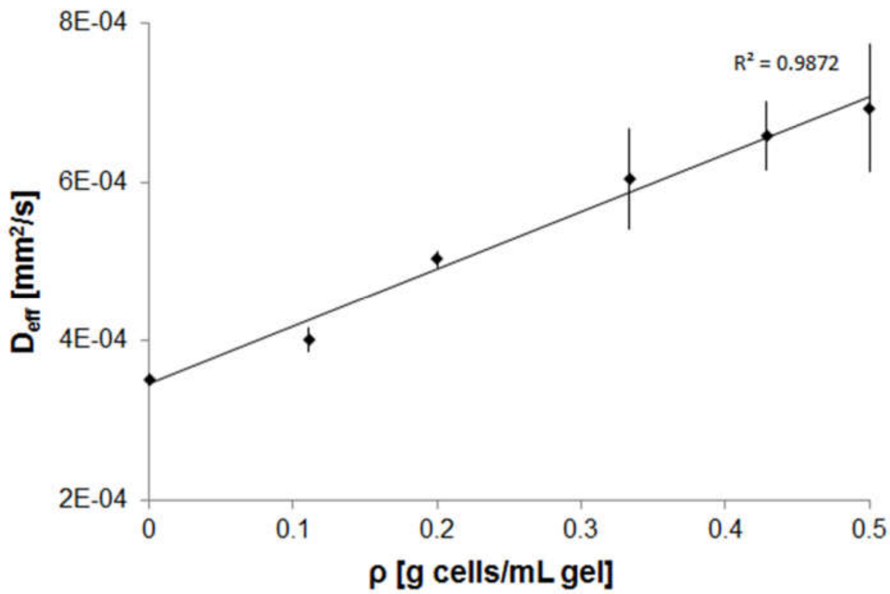

Figure 16 - Change in gel diffusivity to atrazine (D_{eff}) as a function of cell loading density (ρ)

Based on (4), it can be seen that diffusivity of atrazine in the gel increased with increased cell loading density (**ρ**), from 3.51 x 10^{-4} mm^2/s up to 6.93 x 10^{-4} mm^2/s. We suspect that this phenomenon could be due to increased transport of atrazine through: a) Cell-silica interface within the matrix, b) The cells themselves. Due to this effect, **ρ** not only affects the biocatalytic activity rate constant, but also the transport of atrazine in the matrix.

Compressive strength (σ) and elastic modulus (E)

Figure 17 shows that cell free silica gels have **σ** ≈ 1.75 MPa, **E** ≈ 160 MPa. It can also be seen that both σ and E of the material deteriorate with increased **ρ**, down to **σ** ≈ 0.28 MPa, **E** ≈ 23 MPa at the maximum tested **ρ** (0.33 g cells/mL gel). Both **σ** and **E** showed an exponential decreasing trend with the following least-square fit correlations:

$$\boldsymbol{\sigma} = 1736.5e^{-5.5\rho} \text{ [kPa] (5.a)}, \ \mathbf{E} = 182.19e^{-5.966\rho} \text{ [MPa] (5.b)}$$

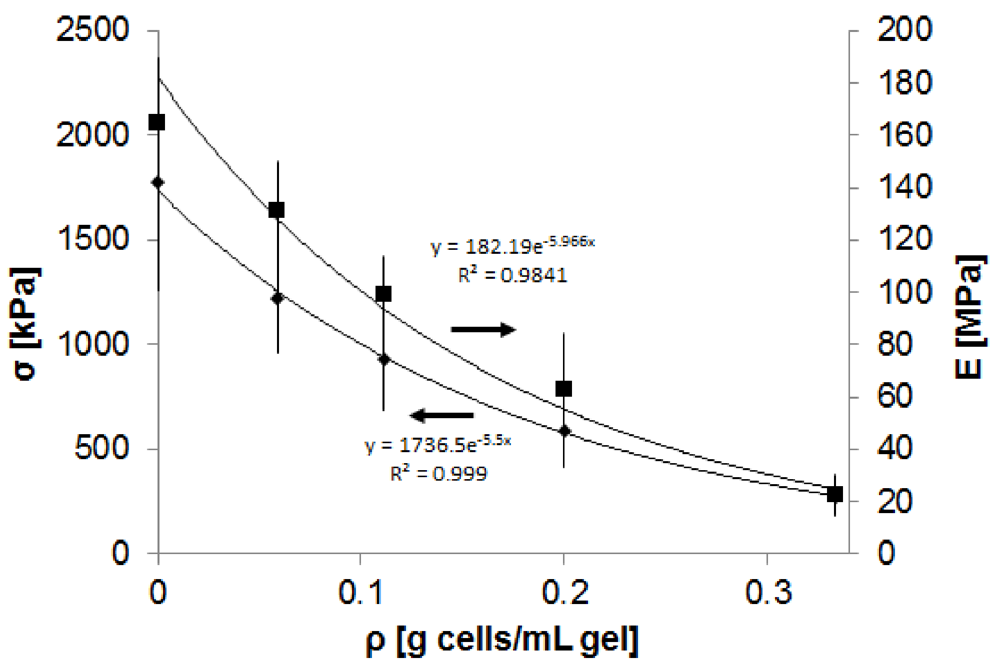

Figure 17 - Mechanical properties of the gel (Maximum yield strength (σ) and Elastic modulus (E)) as a function of cell loading density (ρ)

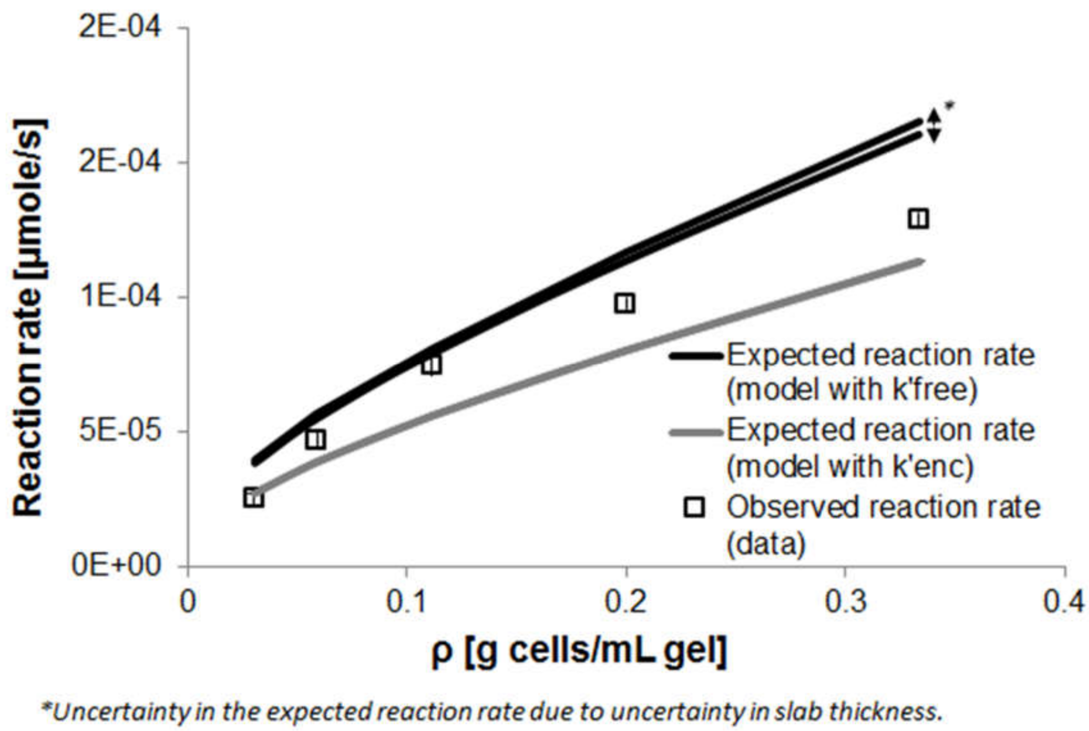

Figure 18 - Steady-state model verification

3.3.2 Biodegradation/transport model verification

Figure 18 shows that the experimentally observed activity was lower than the expected activity of the model when ethanol-free rate constant (**k'**$_{\mathbf{free}}$) is used. This result suggests that 19.7% ± 10.2% of cell degradation activity was lost during encapsulation. When 5% ethanol medium rate constant (**k'**$_{\mathbf{enc}}$) is used, the observed activity was higher than the expected activity (116.7% ± 14.7%). This result suggests that the alcohol content of the gel is overestimated or some alcohol evaporated during gelation. Even though expected activity with **k'**$_{\mathbf{enc}}$ was slightly lower than the experimentally observed activity, it was still used for optimization purposes, to ensure that the performance constraints of the system is met.

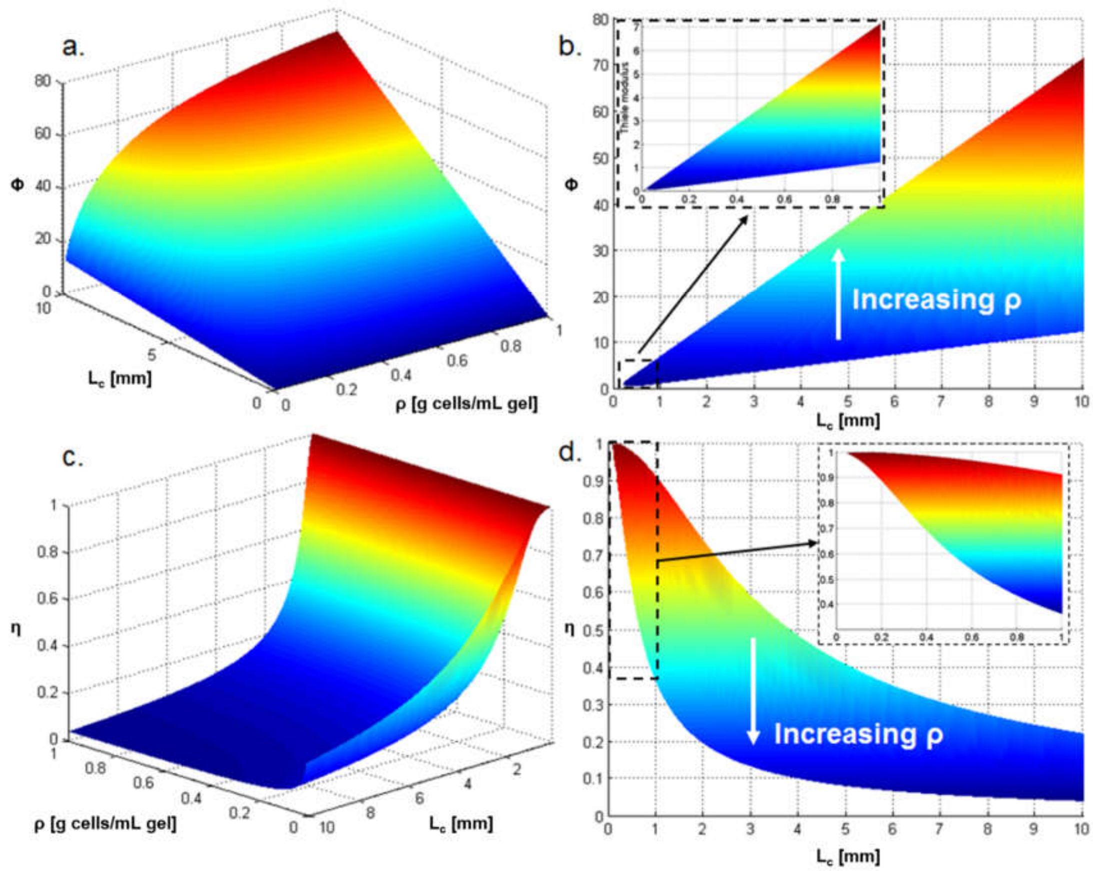

Figure 19 - Variation of dimensionless numbers: Φ and η, based on design parameters: ρ and L_c

3.3.3 Optimization of design parameters ρ and L_c

Figure 19 shows the range of attainable operating conditions for a spherical biocatalyst in terms of **Φ** and **η**, for $0.01 < \boldsymbol{\rho} < 1$ g cells/mL gel and $0.1 < L_c < 10$ mm. Figure 6.a shows that as L_c increases, **Φ** also increases, indicating that diffusion limitations become more severe as material gets larger, as expected. As **ρ** increases, **Φ** also increases, and the effect is more significant at large values of L_c. Figure 19.c shows that the increasing trend in **Φ** reflects a decrease in **η**, which can also be seen from Eqn. (2.b). Two-dimensional projections of Figure 19.a and 6.c are shown in 6.b and 6.d for ease of visualization. The inset in Figure 19.b shows that diffusion limitations become significant (**Φ** > 1) when L_c of the material (sphere radius) exceeds 0.1-0.3 mm, depending on **ρ**. Figure 19.d shows that for a typical bead radius of 1 mm, AtzA biocatalyst reaction is severely diffusion limited and only 35% (at **ρ** = 1 g cells/mL gel) to 90% (at **ρ** = 0.01 g cells/mL gel) of the material can be utilized.

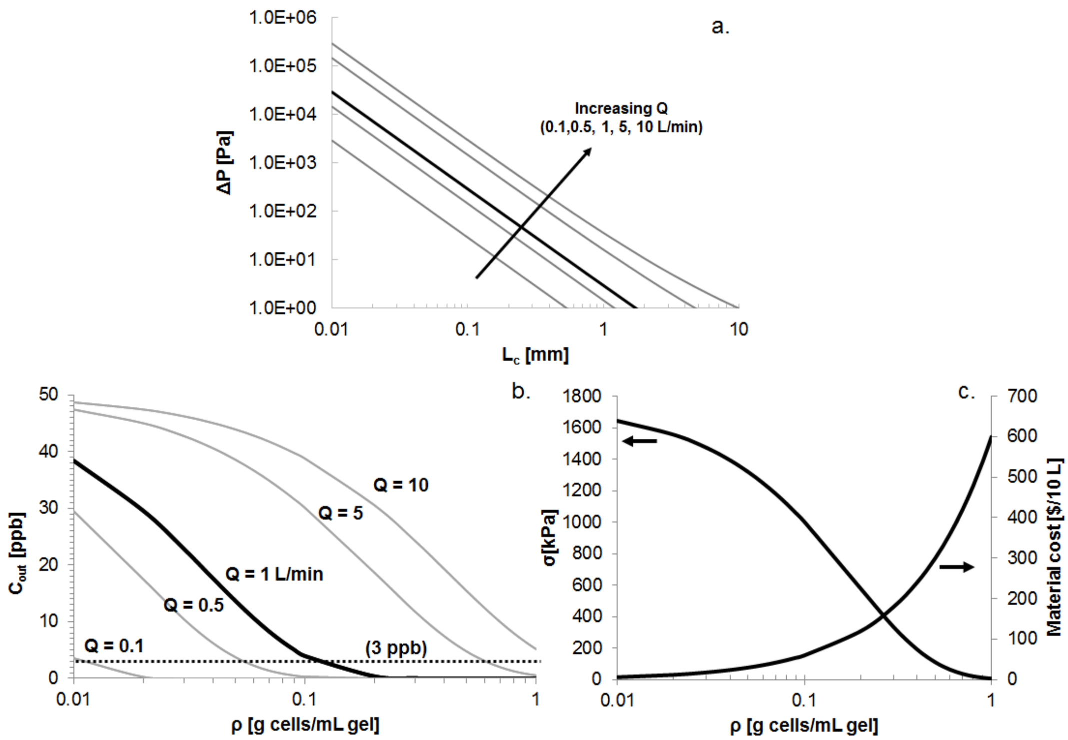

Figure 20 - a) Pressure drop (ΔP) across the packed bed reactor based on L_c, b) Effluent concentration (C_{out}) of the packed bed reactor based on ρ and flow-rate (Q), c) Maximum yield strength (σ) and total material cost based on ρ

Optimization of L_c

It is apparent from Figure 20 that L_c should be minimized to decrease the diffusion limitations, regardless the material geometry or reactor type. However, in a packed bed setup, minimizing L_c is not desirable due to increased pressure drop, which would increase initial cost (high pressure pump, high pressure reactor design) and operating costs (pumping cost) of the system. Figure 20.a shows the pressure drop vs. catalyst size for a range of volumetric flow-rates, based on Ergun equation [71]:

$$\frac{\Delta P}{L} = \frac{150\mu(1-\varepsilon)^2 u_0}{\varepsilon^3 (2L_c)^2} + \frac{1.75(1-\varepsilon)\rho_f {u_0}^2}{\varepsilon^3(2L_c)} \quad (6)$$

where **μ** is the fluid viscosity, **ρ_f** is fluid density, **u_0** is superficial velocity of the fluid and **L** is the length of the reactor. Due to this pressure drop, instead of minimizing L_c, it is more practical to set a lower bound on **η** and pick the corresponding catalyst size. **η** = 0.9 is a reasonable selection that ensures 90% utilization of the material. The inset of Figure 6.d shows that if a minimum of **η** = 0.9 is selected, the optimal value for catalyst radius is L_c = 0.2 mm, regardless of **ρ**.

Optimization of ρ

Minimizing **ρ** is desirable to increase effectiveness factor, obtain enhanced mechanical properties and decrease material cost; whereas it should still be large enough such that performance constraints of the system are satisfied. For a packed bed reactor operating at steady-state, the output concentration is given by [72]:

$$C_{out} = C_{in} e^{\frac{-\varepsilon V \eta(\rho) k_{enc}(\rho)}{Q}} \quad (7)$$

Note that both **η** and **k_{enc}** changes with **ρ**. Figure 7.b shows the change in output concentration of the packed bed reactor as a function of **ρ**, for the selected optimal catalyst size L_c = 0.2 mm and a range of volumetric flow-rate values (Q = 0.1 – 10 L/min). It can be seen that to obtain the desired output concentration lower than 3 ppb, **ρ** must be greater than 0.11 g cells/mL gel (for Q = 1 L/min). Figure 20.c shows that to minimize the cost and maximize mechanical strength of the material, minimum **ρ** value that satisfies the performance constraint should be selected. Then, for this case study, **ρ** = 0.11 g cells/mL gel is the optimal cell loading density, which yields **σ** = 578 kPa and a material cost of $120 to fill up a 10 L reactor.

In this case study, optimal design parameters (L_c = 0.2 mm and **ρ** = 0.11 g cells/mL gel) were selected to minimize material cost and pressure drop, maximize material strength while satisfying a performance constraint for a given reactor size and flow-rate (**Q**). Selection criteria of these parameters are summarized in Table 5. It can be seen that if any of these constraints are relaxed and other constraints are imposed on the system, Figures 7.a-c can still be used to determine values for L_c and **ρ**, which satisfy these requirements. Otherwise, they can also be used to determine that all the constraints cannot be satisfied at once and one or more of the requirements need to be relaxed.

3.4 Conclusion

In this study, we proposed a 3-step (1. Characterization, 2. Modeling, 3. Optimization) design approach for determining cell loading density (**ρ**) and characteristic length (L_c) of silica gel encapsulated AtzA biocatalyst used in a packed bed bioremediation system. The approach was to maximize mechanical properties and minimize material/operation cost, while satisfying performance requirements of the bioremediation system. This 3-step approach is demonstrated for a case study, whose parameters are described in Table 4. The proposed method to choose minimum, maximum and optimal values of these design parameters are summarized in Table 5. Note that Table 5 is not specific to silica gel encapsulated AtzA biocatalyst, and can be used for other biocatalytic materials. However, this requires a corresponding characterization and modeling step, as described in this study.

Table 5 – Minimum, maximum and optimal values of ρ and L_c

	Minimum value	**Maximum value**		**Optimal value**
L_c	Imposed by **ΔP** across the reactor (Figure 7.a)	Imposed by **η** (Figure 6.d)		Minimum value satisfying $\Delta P < \Delta P_{max}$ (Maximum allowable pressure drop)
ρ	Imposed by performance constraint of the system (Figure 7.b)	Imposed by material properties and cost of the material (Figure 7.c)		Minimum value satisfying $C_{out} < C_{des}$ (Desired effluent concentration)

Chapter 4: Long-term preservation of silica gel encapsulated bacterial biocatalysts by desiccation[3]

4.1 Introduction

Silica gel encapsulation of whole-cells (i.e. bioencapsulation) has extensively been studied in the literature and summarized in recent reviews [14, 21, 73]. Silica gel bioencapsulation provides a mechanical scaffold and protection to otherwise small and fragile bacteria, which makes the technology applicable to a wide-range of engineering applications. These applications include water bioremediation [59, 60], where the encapsulated bacteria biodegrade chemicals that diffuse through the porous silica gel. A typical water treatment scheme with encapsulated bacteria consists of a flow-through reactor, packed with the biocatalytic silica gel synthesized as small spherical beads. In such a configuration, a small bead size is desirable to decrease the internal diffusion length of the chemicals (thereby increasing the efficiency of the material). However, this increases the pressure drop in the system due to increased packing density of the beads, requiring a strong and stiff gel material (typical compressive strength in the range of 1 to 10 MPa [74, 75]) that can withstand high pressures in such a reactor.

Drying the silica hydrogel is a desirable post-gelation step for improving gel mechanical properties. After initially forming to encapsulate bacteria, the silica hydrogel structure continues to polymerize; strengthening, stiffening and shrinking the matrix, a process called aging [9]. Drying the material during/after this process further improves the mechanical properties [76, 77], also making the material lighter for ease of transportation and storage. However, preserving activity of biological materials in a desiccated state is a challenge. Some bacterial species have evolved mechanisms to survive desiccation by utilizing non-reducing disaccharides such as trehalose and sucrose [78, 79]. It is suggested that these disaccharides replace the surface-bound water to protect the integrity of the cell membrane and proteins during desiccation. Therefore, we hypothesized that introduction of these lyoprotectants or glycerol (a widely used osmolyte and cryoprotectant [80, 81]) can potentially protect and preserve the biocatalytic activity of the encapsulated bacteria during drying.

[3] Reprinted from Mutlu, B. R.; Hirschey, K.; Wackett, L. P.; Aksan, A., Long-term preservation of silica gel-encapsulated bacterial biocatalysts by desiccation. *Journal of Sol-Gel Science and Technology* **2015,** *74* (3), 823-833. DOI: 10.1007/s10971-015-3690-8.

Long-term retention of biological activity (growth, metabolic activity, and enzymatic activity) of bacteria encapsulated in silica gels is a challenge, even without dehydration of the material. For instance, with an aqueous silica encapsulation method and glycerol as an additive, Nassif *et al*. reported that the percentage of culturable bacteria in silica gels diminished to 40% while the percentage of bacteria that can incorporate glucose declined to 55% in 4 weeks [28]. In a more recent study, Perullini *et al*. reported a similar encapsulation method by replacing glycerol with glycine betaine, where after 15 days, viability of encapsulated *E. coli* reduced to 40% [43]. Klein *et al*. investigated atrazine bioremediation by encapsulating *Pseudomonas sp*. ADP in silica/polymer fibers and reported that after 15 days the atrazine removal rate reduced to 35% under non-growth conditions [49]. These results were obtained right after encapsulation however, the effect of storage on activity has not been investigated. The most promising technique to date for long-term storage was reported by Pannier *et al*., where phenol degrading Rhodococcus ruber was encapsulated in silica gels by freeze-gelation, followed by freeze-drying for 24 hours [61]. With this technique, they obtained degradation activity comparable to pre-storage values after 6 months of storage at 4°C. The downside of this approach is the cost associated with the scale-up of the process for manufacturing at large scales for industrial use.

We have previously reported a silica gel encapsulation method for an atrazine biodegrading *Escherichia coli* (*E.coli*) strain and demonstrated that the material sustained long-term biocatalytic activity (> 2 months) in a flow-through, packed bed bioreactor [68]. We used low flow-rates in that study, emphasizing material design and retention of long-term activity under continuous use in the reactor. In this study, we are focusing on drying and storage conditions for the same material, in order to improve its mechanical properties while sustaining biocatalytic activity until use. In both studies, we used a recombinant *E.coli* strain overexpressing the atrazine dechlorinating enzyme AtzA that transforms atrazine to hydroxyatrazine. This transformation within the bacterium is a thermodynamically favorable hydrolytic reaction that does not require viability. Atrazine (2-chloro-4-ethylamine-6-isopropylamino-s-triazine) is a widely used herbicide in the U.S, up to 36,000 tons annually, and is also deployed in Canada, Africa and the Asia-Pacific region [66]. Its concentration is regulated by the U.S. Environmental Protection Agency (EPA) at 3 ppb in drinking water, and thus, bioremediation of atrazine in surface or groundwaters is of great practical importance.

In the first part of this study, we investigated how aging/drying parameters affected the mechanical properties and biocatalytic activity of the material (Figure 21). Later, we tested the biocatalytic activity of the encapsulated AtzA bacteria in the presence of lyoprotectants with and without drying. To better understand the results, we tested the effect of these lyoprotectants on non-encapsulated bacteria and bacterial protein extracts (cell extracts obtained by sonication, see methods for details) in solution. In the second part of the study, we selected the most effective parameters from the first part and measured the activity of the material after long-term storage (three months). Additionally, we investigated the effect of storage temperature on the activity of the bacterial biocatalyst. We determined that without using any lyoprotectants, partially dried gels preserved the activity of the encapsulated bacteria for three months when stored at 4°C.

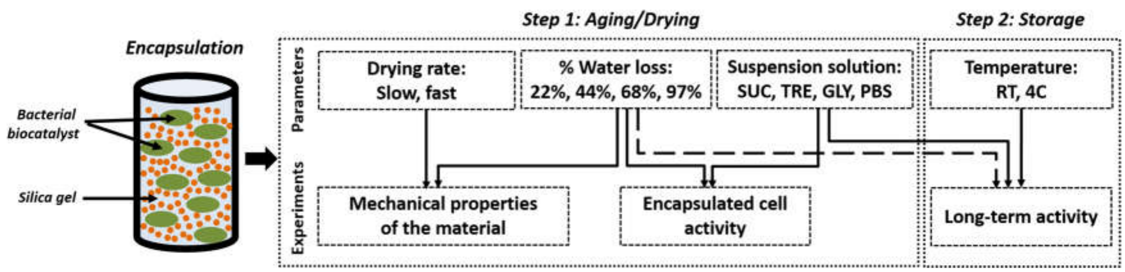

Figure 21– Outline of the study

4.2 Experimental

Materials

Reagent grade tetraethyl orthosilicate (TEOS: Si(OC2H5)4) was purchased from Sigma-Aldrich (Sigma-Aldrich Corp. St. Louis, MO, USA). NexSil 125-40 colloidal silica nanoparticle (SNP) solution was purchased from Nyacol (Nyacol Nano Technologies Inc., Ashland, MA, USA). Reagent grade atrazine was provided by Syngenta (Syngenta Crop Protection, NC, USA). All chemicals were used without further purification. Ultrapure water (UPW) was used in all the experiments, which was prepared by filtering deionized water through a Milli-Q water purification system (Millipore, Billerica, MA, USA) to a final electrical resistance of > 18.2 MΩ/cm.

Bacteria strains and growth conditions

The growth conditions were identical to those described previously [51], except for some minor modifications as described below. *E. coli* strain DH5α (pMD4) [52] was grown at 37 °C in superbroth medium with vigorous aeration. The medium was supplemented with 30 μg/ml chloramphenicol. Intermediate cultures were grown by inoculation with 1% (v/v) starter culture and diluted 100-fold in production flasks containing the same medium. Bacteria were harvested by centrifugation at 6,000 g for 20 min at 4 °C.

Silica gel synthesis and encapsulation of bacteria

A previously reported silica gel matrix (NS125-7:1-TEOS) and encapsulation method was used in this study [68]. Briefly, TEOS was hydrolyzed by stirring 2 h at a 1:5.3:0.0013 molar ratio of TEOS:water:HCl. The pH of the Nexsil 125-40 SNP sol was adjusted to neutrality by adding 1M hydrochloric acid. After pH adjustment, hydrolyzed TEOS was added to the SNP solution by pipetting a few times to obtain a homogeneous sample. The final product was either placed in silicone molds for mechanical testing (cylinder with thickness = 12.5 mm and diameter = 12.5 mm) or in 20 mL borosilicate glass scintillation vials (cylindrical slab with thickness = 7 ± 0.1 mm) for gelation. To produce samples for activity testing that contained encapsulated bacteria, bacteria were suspended in different experimental solutions (PBS, 0.4M sucrose, 0.4M trehalose or 30% (wt/wt) glycerol) at a density of 1 gbacteria/mL and added to the SNP sol after pH adjustment. The final bacterial loading density in the gels was 59 mgbacteria/mLgel. Mechanical testing samples did not have encapsulated bacteria.

Evaluation of mechanical properties after aging and drying

For the aging study, after gel synthesis in the silicone molds, samples were extracted and stored in a PBS solution until they were tested. For the drying study, samples were kept in the molds and placed either in a sealed container with drierite (for fast drying) or in a ~85% relative humidity chamber where humidity was kept constant by a saturated potassium chloride solution (for slow drying). After removal from the molds, samples were rehydrated by immersion in PBS before the mechanical testing. Testing was performed on an MTS QTest 10 mechanical testing machine (MTS Systems, Eden Prairie, MN, USA). Compressive stress at failure (σ) and elastic modulus for compression (E) of the material were evaluated by compression tests conducted on the hydrated samples at 1%/min strain rate.

Evaluation of biocatalytic activity

Non-encapsulated bacteria and bacterial protein extracts

Bacteria were suspended in PBS, 0.4M sucrose, 0.4M trehalose or 30% (wt/wt) glycerol solutions (at a density of 1 gbacteria/mL) and incubated from one hour to one day. Then, 30 µL of bacteria solution was added to 3 mL (bacteria loading density = 1 x 10-2 gbacteria/mL) of an atrazine solution at 150 µM prepared with 0.1 M potassium phosphate buffer (at pH 7.0) in a 20 mL scintillation vial. Scintillation vials were placed on a rotary shaker (at 125 rpm) and incubated for 20 minutes. After incubation, samples were immediately immersed in a 90°C water bath to stop the catalytic activity by denaturing the enzyme. After inactivation of the enzyme, samples were filtered through a 0.2-µm pore size PTFE syringe filter to remove the bacteria. The concentrations of atrazine and its metabolite, hydroxyatrazine, were measured using a Hewlett-Packard HP 1090 Liquid Chromatograph system equipped with a photodiode array detector. The detection method used an analytical C18 reverse-phase Agilent column at a wavelength of 220 nm, a H2O/methanol solvent ratio of 35%/65% and a flow rate of 1.0 mL/min.

To assay bacterial protein extracts, bacteria were suspended in PBS at a density of 0.1 gbacteria/mL. A sonicator tip was immersed into this solution and operated at 30%, 5 seconds on/off, for 30 seconds, three times. Then, bacteria debris was removed from the solution by centrifugation at 10,000 rpm for 5 minutes. 200 µL of the supernatant solution with the bacterial protein extract was added to 2 mL of PBS, 0.4M sucrose, 0.4M trehalose or 30% (wt/wt) glycerol solutions and incubated until the time point for the activity measurement. Atrazine solution was added to the bacterial protein extract solution, to reach a final concentration of 90 µM. The rest of the procedure was identical to the activity measurements for non-encapsulated bacteria.

Encapsulated bacteria

Two methods were tested for the introduction of the lyoprotectants to the encapsulated bacteria:

<u>Incubation (post-encapsulation) method:</u> Bacteria were suspended in PBS before encapsulation. After encapsulation, gels containing the encapsulated bacteria were incubated with lyoprotectant solutions.

<u>Suspension (pre-encapsulation) method:</u> Bacteria were suspended in lyoprotectant solutions before encapsulation. No solution was added after encapsulation. Dry gels were also obtained with this method, with a drying step following the encapsulation process.

We will refer to these three different cases as: I) Wet-I gels (incubation method), II) Wet-S gels (suspension method) and III) Dry gels.

Based on these methods, bacteria were either suspended in PBS, 0.4M sucrose, 0.4M trehalose or 30% (wt/wt) glycerol solution (1 $g_{bacteria}$/mL of solution), and encapsulated as described in silica gel synthesis section. After gel synthesis, samples were washed with PBS to remove any bacteria that may have escaped encapsulation. For Wet-I gels, ten mL of 0.4M sucrose, 0.4M trehalose, 30% (wt/wt) glycerol or PBS solutions were added, and incubated until the time point for activity measurement. For Wet-S gels and Dry gels, no solution was added after encapsulation and Wet-S gels were PTFE sealed and capped to prevent further drying. For Dry gels, samples were air dried until they lost 22% (40 h), 44% (110 h), 68% (170 h) or 97% (300 h) of their total water (initial water content = 65% wt/wt). Then, samples were PTFE sealed and capped. Gel weights were measured at corresponding time points to ensure that they have not dried further. All the samples were stored at room temperature, except for the long-term storage study where storage at 4°C was also investigated. At corresponding time points, activity was measured by adding 3 mL atrazine solution (in 0.1 M potassium phosphate buffer) at 150 µM concentration to the scintillation vials (for Wet-I gels, the incubation solution was removed first). Then, vials were placed on a rotary shaker and incubated for 60 minutes. The rest of the procedure was identical to the activity measurements for non-encapsulated bacteria.

4.3 Results and Discussion

4.3.1 Mechanical properties of the gel after desiccation

The two different drying methods applied resulted in approximately 0.45% water loss per hour for fast drying, and 0.09% water loss per hour for slow drying, respectively (determined by the initial slope with the first four time points, Figure 22 a). The gel shrunk to 44% of its initial volume at 68% water loss but did not shrink with further drying (fast drying method, Figure 22 b). We observed that the mechanical properties of the gel - elastic modulus (E) and compressive stress at failure (σ) - improved only slightly during aging in PBS (without drying). When the material was aged in these conditions, the highest mechanical properties were achieved after 5 days, where σ increased from 46 ± 20 kPa to 126 ± 22 kPa and E improved from 1.15 ± 0.61 MPa to 3.51 ± 1.05 MPa. However, the improvement in mechanical properties were significant (two orders of magnitude) when the samples were dried. σ improved to 5.4 ± 0.63 MPa, and E improved to 1104 ± 109 MPa at ~97% water loss (Figure 22 c and d). Note that in Figure 22 c and d, the mechanical properties are reported with respect to water content (not drying time). It can be observed that the water content had a significant impact on the mechanical properties of the gel while the drying rate did not. Therefore, we have proceeded with the fast drying rate for the remainder of the study.

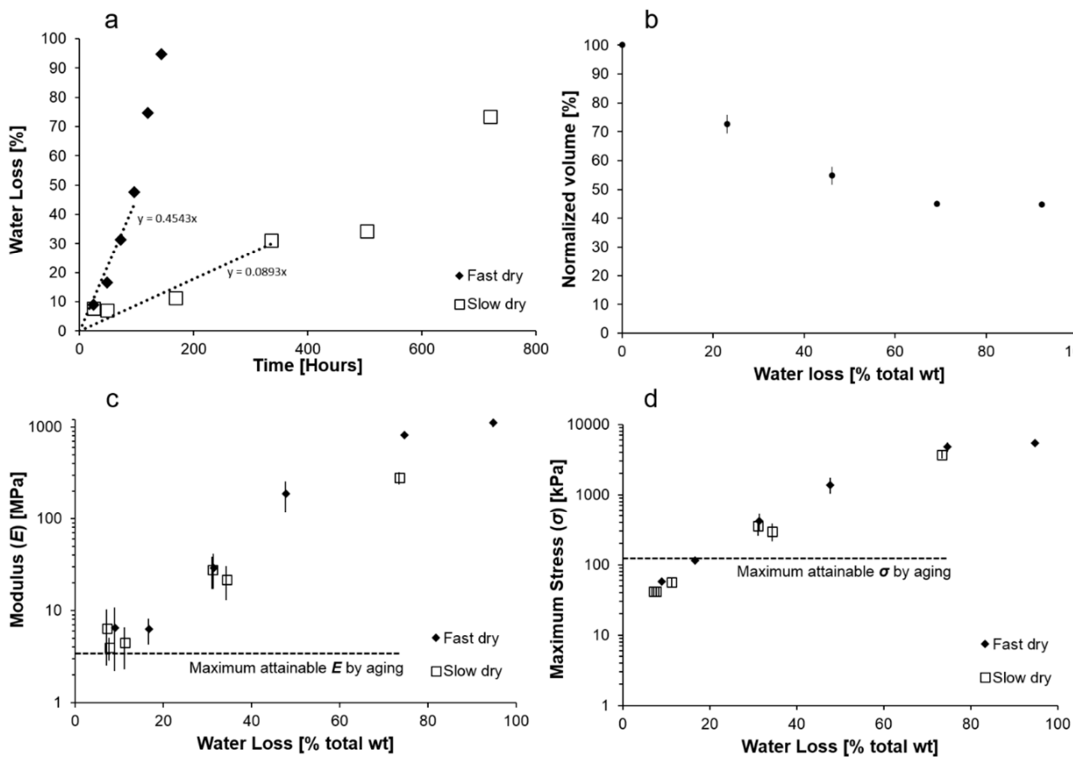

Figure 22 - Mechanical properties of the gels after aging and drying: a) Rate of water loss, b) Shrinkage, c) Elastic modulus (*E*), d) Stress at failure (*σ*)

It has been reported that drying silica gels at high temperatures increases the mechanical properties of the material significantly: For instance, Rabinovich *et al*. reported colloidal silica gels with σ = 6 MPa, after drying for a week at 150°C [76]. Similarly, Mackenzie *et al*. reported that TEOS derived silica gels with E = 5 GPa [77] were obtained by drying for three weeks at 200°C. The drying temperatures used in these studies would destroy the biocatalytic activities of even the most stable thermophilic enzymes. Therefore, it is not feasible to dry the gels that contain encapsulated bacteria at high temperatures. In this study, we reached mechanical property values of (σ = 46-126 kPa) and (E = 1.15-3.51 MPa) without any drying. These values were very similar to the values (σ = 50-100 kPa and E = 90-400 kPa) reported by Krupa *et al*. for TEOS derived silica hydrogels that are synthesized and aged in physiological conditions [82]. Nevertheless, the mechanical properties achieved here are significantly lower than those that could be achieved with high temperature drying. Therefore, we have opted to dry the gels to improve the mechanical properties, but did it at room temperature to sustain biocatalytic activity. The results showed that removal of 68% of the initial water content in the gel resulted in significantly improved mechanical properties ($\sigma = 4.8 \pm 0.7$ MPa and $E = 814 \pm 53$ MPa), while the biocatalytic activity was maintained (Figure 22 c and d). Note that these values are well within the range of typical catalysts used in packed bed reactors [74, 75]. Even though further drying continued to improve the mechanical properties, the biocatalytic activity started to decrease, rendering additional drying of the gel unfeasible (see biocatalytic activity section for further discussion).

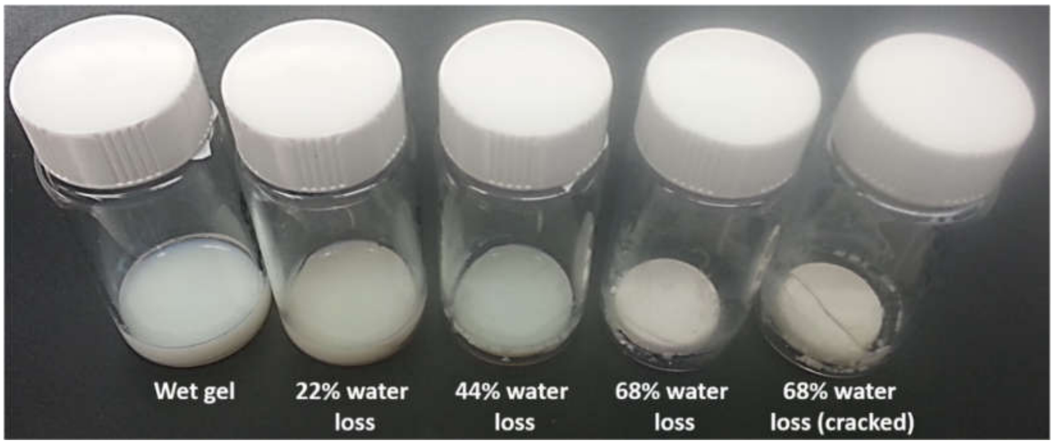

Figure 23 – Images of gels for activity testing

Note that cracks may form in the gel during drying and shrinking, depending on the surface energy of the mold material and the interactions between the mold and the gel. Cracking was observed in some of the samples used for biocatalytic activity testing where the sample gels were synthesized in borosilicate glass (high surface energy) scintillation vials (Figure 23). The effect of these cracks on activity results is discussed later in the manuscript. It is reasonable to assume that cracks would affect the mechanical testing results very significantly. To avoid cracking of the gel samples to be used in mechanical testing, gels were cast in hydrophobic silicone molds. No cracks were observed in any of the mechanical testing samples. The significant increase in the mechanical properties also suggested that crack free samples could be obtained when the gels were synthesized in hydrophobic molds.

4.3.2 Biocatalytic activity

Encapsulated bacteria activity experiments were conducted to determine the effects of the processing parameters (drying level and lyoprotectant type) and the explicit effect of time on long-term storage stability. Three cases were tested: Wet-I gels, Wet-S gels and Dry gels. Wet-S gel with

PBS is neither dried nor have lyoprotectants, thus form the baseline for activity measurements. Therefore, for easier assessment of the effects of drying and lyoprotectants, all the encapsulated bacteria activity results (Figure 24) are reported with respect to the atrazine degradation activity of Wet-S gel with PBS immediately after encapsulation (r = 1.23 ± 0.23 µmoles/min, shown as 100% normalized activity at t0 in Figure 24.b). Activity of this gel had a decaying trend over time, eventually going down to 42 ± 22% of the initial activity after 300 hours. Activity of the Wet-I gel with PBS decreased over time as well (Figure 24.a), decaying from 207 ± 30% (at t = 40h) to 146 ± 8% (at t = 300h). Thus, it was concluded that without drying or the addition of lyoprotectants, encapsulated bacteria lost activity over time when stored at room temperature.

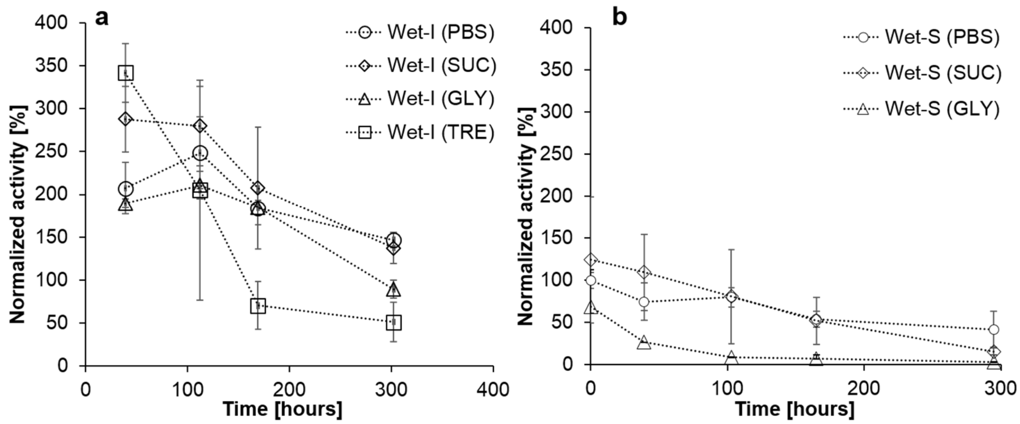

Figure 24 – Effect of the tested lyoprotectant solutions on the biodegradation activity of wet gels: a) Wet-I gels (incubation method) b) Wet-S gels (suspension method)

All Wet-I gels had significantly high biocatalytic activity (ranging from 200% to 350%) after 40 hours of incubation. Note that no activity measurement was taken at t0 for Wet-I gels to provide time for the diffusion of lyoprotectants into the gel. Wet-I gels with 0.4M sucrose and PBS solution had higher than 100% activity, even after 300 hours of storage (137 ± 17% and 146 ± 12%, respectively). Wet-I gel with 0.4M trehalose showed a steep decline after 40 hours, and had the worst activity amongst the lyoprotectants after 300 hours of incubation. Therefore we did not proceed with trehalose in the rest of the encapsulated bacteria activity measurements; however we still investigated the reason for this inhibitive effect (see effect of lyoprotectants section for details). Even though all the wet gels (Wet-I and Wet-S) lost activity over time, Wet-I gels (Figure 24.a) had higher activity throughout the experiment compared to the Wet-S gels (Figure 24.b). The loss in activity of Wet-S gel with PBS was comparable to Wet-S gel with 0.4M sucrose (Figure 24.b), whereas Wet-S gel with 30% (wt/wt) glycerol lost activity very rapidly.

These results show that when the gels were stored (wet) at room temperature, they lost activity over time. One possible explanation for the decrease in encapsulated bacteria activity over time is the gradually increasing concentration of alcohol in the gel due to alcohol-generating condensation reactions that can continue during aging of the gel. We observed that the mechanical properties reached a maximum after 5 days of aging (data not shown), which showed that the aging process continued for at least 120 hours. This explains why the Wet-I gels had higher activity than Wet-S gels (compare data in Figure 24 a and b). The excess water in the incubation solution effectively reduced the concentration of produced alcohol within the gel, and thus its effects on activity. To better understand the effects of lyoprotectants (e.g. the unexpected difference between sucrose and trehalose, despite their similar chemical structure), we also investigated their effects separately on non-encapsulated bacteria and bacterial protein extracts.

Effect of the lyoprotectants

We observed that the activity of the bacterial protein extracts was affected significantly when incubated with lyoprotectant solutions (Figure 25.a). After one hour of incubation of the bacterial protein extracts in the 0.4M sucrose, 0.4M trehalose and PBS solutions, full biodegradation of atrazine to hydroxyatrazine was observed in the 20-minute activity assay, except for 30% (wt/wt) glycerol suspended bacterial protein extracts which achieved only 55% conversion. However, after one day of incubation in the lyoprotectant solution, only 10% of the original biodegradation activity was observed in 0.4M sucrose and 0.4M trehalose suspended bacterial protein extracts and 5% biodegradation was observed with the 30% (wt/wt) glycerol group. These values were significantly lower than the activity of the bacterial protein extracts incubated in PBS, where 60% of the original biodegradation activity was remained.

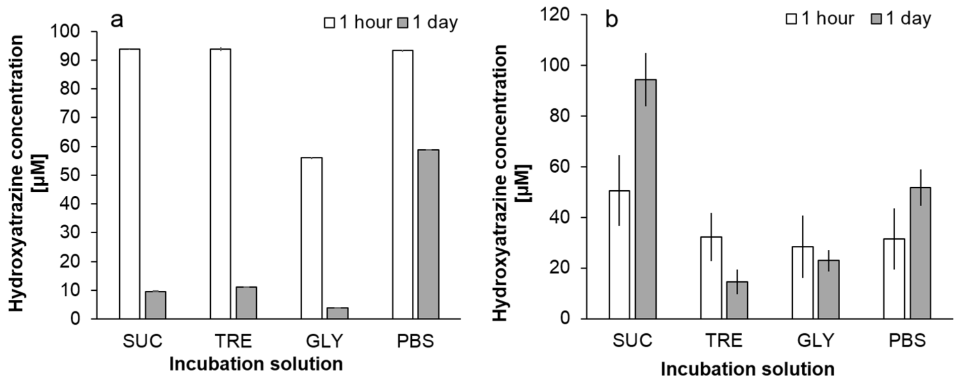

Figure 25 – Activity of: a) bacterial protein extracts* and b) non-encapsulated bacteria in different lyoprotectant solutions. (Error bars are too small to show on graph*)**

Incubation in different lyoprotectant solutions had a different effect on non-encapsulated bacteria, as compared to bacterial protein extracts (Figure 25.b). Incubation in sucrose increased the activity of the bacteria significantly (~300% w.r.t. PBS at 1 hour), whereas PBS increased the activity slightly after a day of incubation (~164% w.r.t. PBS at 1 hour). In addition, the detrimental effect of trehalose or glycerol was not as severe with the non-encapsulated bacteria, as compared to the bacterial protein extracts. Activity of bacteria suspended in trehalose decreased to 46 ± 15% and glycerol decreased to 73 ± 13% after a day of incubation, with respect to PBS at 1 hour while the activity of the sucrose suspended bacteria remained high.

Trehalose had the worst effect on activity (amongst other lyoprotectants) when it was present in the incubation solution (Wet-I gels, Figure 24.a). Trehalose also had a negative effect on the biocatalytic activity of the non-encapsulated bacteria, as well as the bacterial protein extracts (Figure 25). The effect was most prominent in the bacterial protein extracts, potentially due to lack of protection from the cell membrane, and was naturally delayed in Wet-I gels due to diffusion limitations in the gel. It was reported that trehalose can decrease enzymatic activity by increasing the solution viscosity [83]. The viscosity of a 0.4M trehalose solution at 20°C is 1.29 cP [84], which is 29% higher than to that of water. To examine this possibility, we investigated the *E. coli* strain DH5α expressing a different enzyme: cyanuric acid hydrolase (CAH). This is also a thermodynamically favorable enzymatic reaction within the bacterium, so its activity should be affected similarly by the trehalose solution. However, we did not observe an inhibitive effect of trehalose on CAH (results not shown). Thus, it was concluded that the reduction in activity was caused by some specific interactions between trehalose and the AtzA biocatalyst.

Sucrose did not cause an additional difference in activity in comparison to PBS, when it was introduced by either method (Wet-I or Wet-S gels), even after 300 hours of incubation (Figure 24 a and b). Sucrose did not reduce the activity of the non-encapsulated bacteria (Figure 25.b), but significantly decreased the activity of the bacterial protein extracts, in a fashion similar to trehalose (Figure 25.a). This was an interesting result because trehalose and sucrose have very similar chemical structures (and molecular weight) and properties are also known to be very similar in terms of the protection that they offer against desiccation and freezing. Therefore, this result suggested that unlike trehalose, sucrose was not immediately transported inside the bacterium. Luckey *et al*. and Wang *et al*. reported that permeation of sucrose through maltoporins (porins responsible for diffusion of maltodextrins across the outer membrane of *E. coli*) is significantly slower (by a factor of 40), as compared to trehalose [85, 86]. Therefore, even though sucrose has the same inhibitive effect on the enzyme activity as trehalose (as evidenced by Figure 25.a), this effect was not immediately observed in encapsulated and non-encapsulated bacteria in the time period of experimentation. An additional finding was that the activity of the non-encapsulated bacteria in sucrose was higher than that in PBS. This suggests that besides its inhibitive effect, sucrose also has a facilitative effect when it is not transported inside the bacterium. This may be due to the osmotic stress, inducing crowding effects inside the bacterium and increasing the effective concentration of atrazine. However, we have not observed an increase in encapsulated bacteria activity with sucrose. Diffusion can be an activity rate limiting step for silica gel encapsulated bacterial biocatalysts [87]. The fact that the increase observed in non-encapsulated bacteria activity is not observed in encapsulated bacteria suggests that the biocatalytic activity rate in the gel is limited by the diffusion rate of atrazine.

Glycerol is a hygroscopic cryoprotectant, which has also been used in the literature as a biocompatible agent in silica gel encapsulation [15]. When encapsulated bacteria were suspended in (prior to encapsulation) or incubated with glycerol, they performed worse than PBS and sucrose (Figure 24 a and b). As expected, the activity of the bacterial protein extracts decreased significantly when incubated with glycerol (Figure 25.a). In the time scale of the experiment, we observed a small effect of glycerol on the activity of non-encapsulated bacteria (Figure 25.b).

In conclusion, all of the lyoprotectants tested had an inhibitive effect on the activity of the AtzA biocatalyst at the enzyme (bacterial protein extract) level, which was an unexpected finding. To our knowledge, such specific inhibitive effect of these well-established lyoprotectants to an enzymatic reaction has not been reported. Since trehalose, sucrose and glycerol are widely used in the biopreservation field, it is worth exploring the nature of these interactions to identify other potential enzymes that they can affect.

Effect of drying

A drying profile with an initial slope of 0.39% water loss/h was obtained when the gels were dried (Figure 26.a). The activity of Dry gel with PBS (no lyoprotectant) and 0.4M sucrose increased up until 68% water loss (after 170 hours of drying), up to 300-350% activity (Figure 26.b). This is an interesting result because wet gels at this time point (170 h) had significantly lower activity: Wet-I gels with PBS or SUC had less than 250% activity and Wet-S gels with PBS or SUC had less than 100% activity (Figure 24). Activity of Dry gels with PBS and SUC decreased sharply at 97% water loss, after 300 hours of drying. Unlike PBS and 0.4M sucrose, Dry gel with 30% (wt/wt) glycerol lost activity when it was dried. Based on these results, we proceeded with the long-term storage experiments with Dry gels that contained bacteria encapsulated in the presence of 0.4M sucrose or PBS.

It was an unexpected finding that the activity of encapsulated bacteria was sustained and even increased with drying, without using any lyoprotectant additives (Figure 26.b). We believe that the retention of the encapsulated bacteria activity is due to presence and availability of water on the pore surface, despite the significant water loss from the gel. The highly hydrophilic nature of the mesoporous silica gel used in this study facilitates strong water-silica surface interactions. It has been hypothesized that at low water contents, all the nano-confined water is adsorbed to the surface of the hydrophilic silica pores (surface water) and a liquid bulk phase (bulk water) exists only above a certain level of water content [88]. During the initial phases of drying, the bulk water is lost which does not affect the hydration level of the encapsulated bacteria that interact with surface water. Therefore, while no loss in activity is observed at 68% water loss (where only bulk water was lost and surface water was retained), a significant loss is observed at 97% water loss. Even though activity was not measured with slow dried gels, it would be reasonable to expect that the confined water would also be retained during slow drying. However, it would take longer to dry the gels at a slow drying rate (see Figure 22.a). The explicit effect of time on activity is further discussed in the long-term storage results.

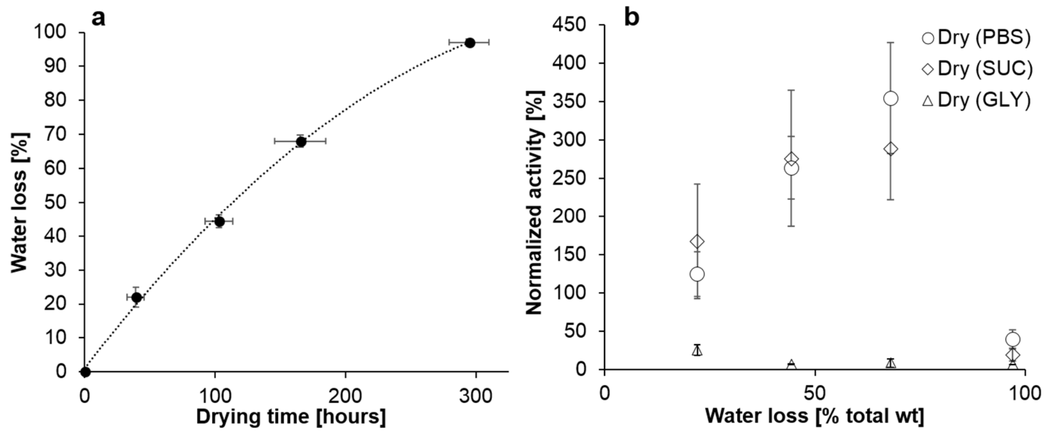

Figure 26 – Effect of drying on the biodegradation activity of the gels: a) Drying profile and time points b) Activity results of Dry gels

The increase in the encapsulated bacteria activity with drying can be explained by two phenomena. It was observed that the material shrank down to 45% of its initial volume when it lost 68% of its initial water content (Figure 22.b), which decreased the dimensions of the gel in each direction down to approximately to 75% of their initial value. In a diffusion limited system, this much reduction in size would translate up to a 25% increase in activity (see Mutlu *et al*. [87] for additional details). Since the observed increase in activity is higher, we believe that another factor is in play as well. We hypothesize that a contribution to activity comes from formation of cracks in the gel during drying in scintillation vials (see "Mechanical properties" section for additional discussion on shrinkage and crack formation), which increases the surface area of the material and facilitates the transport of chemicals to the encapsulated bacteria.

4.3.3 Long-term storage of the encapsulated bacteria

It has been reported that storage in 4°C as compared to room temperature improves viability of the silica encapsulated bacteria after four months of storage [51, 89]. Since we observed a decrease in activity when the gels are stored in room temperature (Figure 24), we decided to investigate storage at 4°C as well. Storage results show a significant difference between cold stored (4°C) and room temperature stored gels (Figure 27). Regardless of the level of drying or the choice of suspension solution, encapsulated bacteria stored at 4°C had significantly (an order of magnitude) higher activity than room temperature stored bacteria after storage. On average, wet gels lost approximately 80% activity after three months of storage at room temperature. However, when stored at 4°C, the activity of the wet gels was sustained.

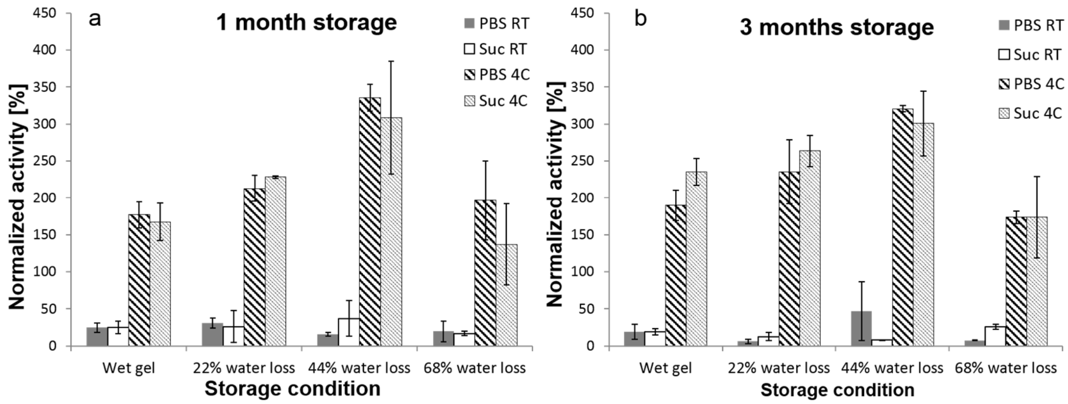

Figure 27 – Activity of gels after a) one month, b) three months of storage normalized w.r.t encapsulated bacteria suspended with PBS immediately after encapsulation (t_0 = 100%)

"Our research group has previously reported a similar difference in the biocatalytic activity of Silica-PEG encapsulated AtzA bacteria stored at room temperature vs. 4°C [21]. In the same study, it was also reported that non-encapsulated AtzA bacteria can retain biocatalytic activity only up to 21 days when stored at room temperature or 4°C, before activity was lost. In order to determine whether this storage temperature difference is effective in the cellular or enzymatic level, we also stored bacterial protein extracts (prepared from AtzA bacteria) at room temperature and at 4°C. The results (Figure 28) show that bacterial protein extracts lost around 90% activity within one week when stored at room temperature, and lost the same amount of activity within four weeks when stored at 4°C. Thus, based on these non-encapsulated bacteria and bacterial protein extract results, we can conclude that silica gel encapsulation is also beneficial for long-term storage (> 4 weeks) of AtzA bacteria while retaining biocatalytic activity."

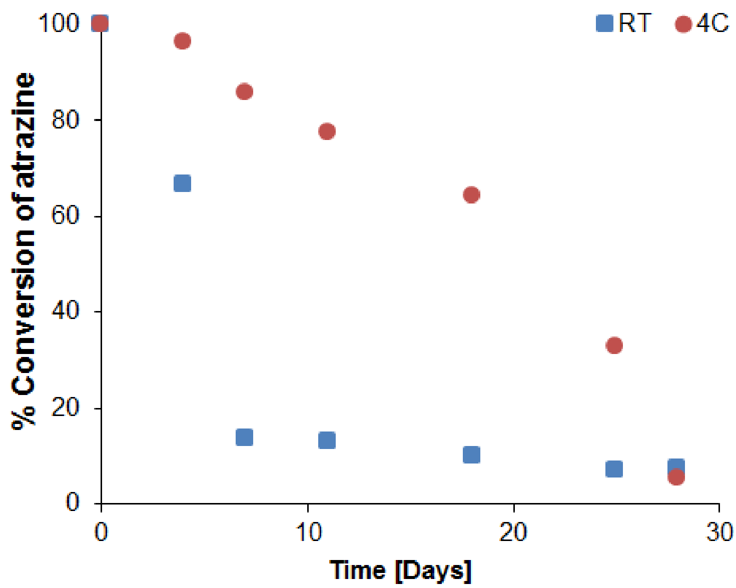

Figure 28 – *In vitro* stability of bacterial protein extract stored at room temperature and 4°C* (Error bars are too small to show on graph*)**

Drying level (water loss) did not have a significant effect on the activity of the Dry gels stored at room temperature since a significant portion of the activity was already lost. Dry gels stored at 4°C had the highest activity (300-350%) when the samples were dried up to 44% water loss before storage. We have observed that the activity of Dry gels (PBS or SUC) at 68% water loss reduced to 150-200% activity after a month of storage, as compared to 300-350% activity right after drying (Figure 26.b). Nonetheless, 68% water loss gels still had comparable activity with the wet gels. After three months of storage at 4°C, there was no change in the activity of the gels, indicating that no more chemical or structural changes were happening in the gels and the biocatalytic activity was stabilized. Since the enzymatic transformation in this study does not require viable bacteria, bacteria viability after storage was not measured.

Similar to the activity results immediately after drying (Figure 26.b), encapsulated bacteria suspended with PBS and 0.4M sucrose had comparable activity after one and three months of storage. Therefore, we concluded that none of the additives that we investigated improved the activity of the gels (when compared to PBS only) in the long-term, and thus use of lyoprotectants is unnecessary during drying and long-term storage of silica gel encapsulated bacterial biocatalysts.

4.4 Conclusion

In this study, we have shown that the mechanical properties (σ and E) of a biocatalytic silica gel can be improved up to two orders of magnitude by drying at room temperature. Drying is also shown to preserve and enhance the activity of the material. Furthermore, this enhanced activity was sustained without loss during long-term storage if the gels were stored at 4°C. After 3 months of storage, the highest activity was achieved in gels with 44% of their initial water removed prior to storage, while the highest mechanical properties (with sustained activity) was achieved in gels with 68% of their initial water removed. It was observed that all three lyoprotectant additives considered in this study; 0.4M sucrose, 0.4M trehalose and 30% (wt/wt) glycerol inhibited activity of the AtzA biocatalyst. Consequently, lyoprotectants did not improve the activity of encapsulated bacteria during storage.

In conclusion, a biocatalytic silica gel material with enhanced mechanical properties and preserved long-term biocatalytic activity was obtained by optimizing the post-encapsulation drying and storage conditions. This is an important result widening the potential engineering applications of silica gel encapsulated biocatalysts. It was shown that for silica gel encapsulated AtzA bacteria, the optimal post-encapsulation procedure is to remove 44% (for highest activity) to 68% (for highest mechanical properties) of the initial water, followed by storage at 4°C to achieve improved mechanical properties and sustained biocatalytic activity. We expect that similar results could be achieved with other bacterial biocatalysts, which utilize a thermodynamically favorable enzymatic reaction within the bacterium and do not require viability for activity. However, further investigation is required for biocatalysts that utilize a metabolic pathway and thus require viability.

Chapter 5: Manufacturing of Bioreactive Nanofibers for Bioremediation[4]

5.1 Introduction

More than one-third of the accessible freshwater throughout the world is used for agricultural, industrial, and domestic purposes, leading to worldwide contamination of freshwater systems with myriads of chemicals such as pesticides (e.g., DDT, acetochlor, and atrazine) or heavy metals (e.g., lead, mercury, and cadmium) as well as various synthetic chemicals, unmetabolized drugs, hydrocarbons and radioactive wastes affecting the health of billions of people. In this context, contamination of waters has become one of the major problems facing humanity and this issue has received considerable attention over the past two decades ([90, 91]).

Electrospun membranes has been widely used in traditional filtration, and manufacturing of biosensors, protective clothing, energy conversion systems, cosmetics, tissue engineering products, drug delivery systems, electronic and optical devices, food items, and advanced composite materials ([92-95]). Thanks to their high permeability, small pore size, high specific surface area, good interconnectivity of pores and ability to be functionalized chemically at the nanoscale electrospun nanofibrous membranes have been used in environmental remediation applications for the removal of different contaminants from wastewaters such as adsorption of heavy metal ions ([96-101]). Apart from their adsorbtive capability (e.g. of heavy metal ions) electrospun nanofibrous membranes are also suitable candidates for biodegradation of various contaminants because of their potential to incorporate immobilized enzymes [102] or encapsulate cells within [103]. Dai *et al*. and Niu *et al*. made laccase-containing fibrous mats by emulsion electrospinning and have reported rapid adsorption and degradation of polycyclic aromatic hydrocarbons [104, 105]. Similarly, horseradish peroxidase (HRP)-containing fibrous mats were made by emulsion electrospinning and the adsorption and degradation of pentachlorophenol (PCP) was measured [106]. The PCP adsorption values reached were as high as 44.69 mg/g while the removal efficiencies were 83% and 47% for the immobilized and the free HRP, respectively. Singh *et al*. used electrospun ZnO nanofibrous mats and

---

[4] Reprinted from Tong, H.-W.; Mutlu, B. R.; Wackett, L. P.; Aksan, A., Manufacturing of Bioreactive Nanofibers for Bioremediation. *Biotechnology and Bioengineering* **2014,** *111* (8), 1483-1493. DOI: 10.1002/bit.25208. Research presented in this chapter was conducted in collaboration with Dr. Ho-Wang Tong, who had significant contributions to this work.

demonstrated the efficacy of these mats in complete degradation of naphthalene and anthracene dyes in waters [107]. In a recent study, Klein *et al*. encapsulated *Pseudomonas sp*. ADP cells into electrospun microfibers and demonstrated their atrazine degradation ability [49].

There are significant advantages offered by reactive filtration systems and biosensors that utilize bioreactive organisms encapsulated in electrospun microfibers. There is also the potential for wide-spread industrial use due to very high surface area to volume ratio achieved, ease in scale up and the cost-effectiveness of the technology. However, development of a water insoluble, solvent-free and multilayered coaxial encapsulation technology that ensures long-term reactivity of the encapsulated microorganisms remains to be a challenge. Figure 29 summarizes the critical requirements for wide-spread adoption of encapsulated cell-based electrospun systems in bioremediation industry. In previous studies to date, cells have been encapsulated into electrospun nanofibers made of materials that slowly degrade, such as polycaprolactone (PCL) [108], or are not biodegradable, such as Pluronic F127 dimethacrylate (FDMA) [109]. However, these fabrication processes required extensive use of organic solvents, which are known to reduce the reactivity and longevity of the encapsulated cells. Electrospinning techniques that do not require the use of organic solvents were also developed and live cells have successfully been encapsulated by electrospinning [110-113]. However, the resultant materials were water-soluble, making them unsuitable for use in aqueous environments that are encountered in all water bioremediation applications.

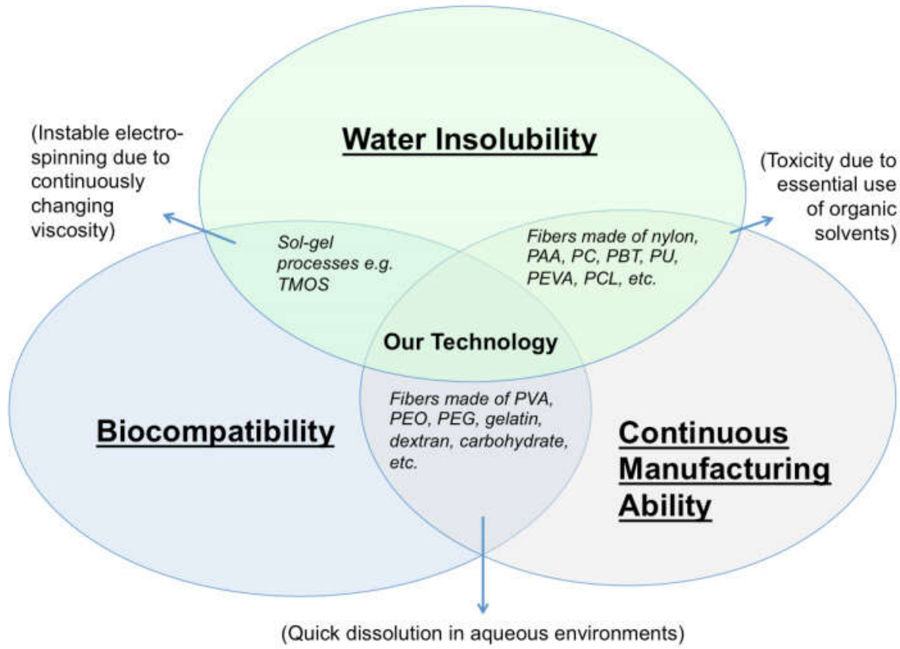

Figure 29 - Critical requirements for electrospinning reactive bacteria for bioremediation applications.

Silica nanofibers can be made by sol-gel electrospinning without using organic solvents, and the produced electrospun nanofibers are water-insoluble [5, 114]. This makes silica an appealing material for electrospin encapsulation biological materials, but the electrospinning process is not stable due to continuously changing viscosity of the silica precursor solution during gelation [115]. In the present study, we developed an electrospinning system that utilizes a microfluidic timer coupled with a coaxial electrospinning setup. We utilized coaxial electrospinning that combines a silica precursor solution (that formed a hard shell around the nanofibers) and a bacteria suspension medium (that formed the biocompatible core for the nanofibers, encapsulating reactive bacteria). This enabled us to continuously produce water insoluble, high bioreactivity nanofibers thus satisfying the critical design requirements for successful bioremediation applications (Figure 29).

5.2 Experimental

Materials

Tetramethyl orthosilicate (TMOS), hydrochloric acid (HCl), and polyvinyl alcohol (PVA) were obtained from Sigma (Sigma-Aldrich Corp. St. Louis, MO, USA). 8-28% w/v PVA was dissolved in water to make the core solution. Silica was used as the shell solution by hydrolyzing TMOS in the presence of HCl. The molar ratio of TMOS:water:HCl was 1:2.8:0.00024. *E. coli* expressing green fluorescent protein (GFP) were encapsulated for confocal microscopy imaging while the *E. coli* expressing Atrazine Chlorohydrolase (AtzA) were encapsulated to be used for atrazine bioremediation activity assays [116].

Preparation of reactive membranes

Figure 30 shows the schematic of the designed electrospinning setup capable of forming reactive membranes comprised of nanofibers that have PVA-based biocompatible cores that contain the encapsulated bacteria and porous silica shells surrounding the core. To prepare the core solution, *E. coli* pellets were mixed with the PVA solution at a cell loading density of 0.5 g/ml and the mixture was loaded into syringe A. Three different PVA solution concentrations [8, 18, 28% (w/v)] were investigated. The hydrolyzed TMOS solution was loaded into syringe B, which was connected to one of the inlets of a microfluidic timer. The 18% (w/v) PVA solution, which had the optimum viscosity for electrospinning when mixed with the TMOS solution, was loaded into syringe C, which was connected to the other inlet of the microfluidic timer. The microfluidic timer precisely controlled the reaction of the hydrolyzed TMOS solution and the 18%(w/v) PVA solution. The reaction time was set to 9 min to ensure that the optimum viscosity of the mixture is reached during gelation before electrospinning. The viscosities of the shell solution and the core solutions at different PVA concentrations were measured by a digital viscometer (NDJ-8S, Shanghai Nirun Intelligent Technology Co Ltd). The flow rates of the shell TMOS solution extruded from syringe B and the PVA solution fed from syringe C were 0.7 mL/h and 0.5 mL/h, respectively. This was done to reach an optimum viscosity value for the mixture. A voltage of 15 kV was applied to the outer needle by a high voltage power supply so that the shell solution was drawn by the electric force while the core solution was drawn by the shear force at the interface of the core solution and the shell solution, as illustrated in Figure 30c. Core/shell structured nanofibers were collected by a grounded conductive plate. As a control, core/shell nanofibers that do not contain any bacteria were manufactured.

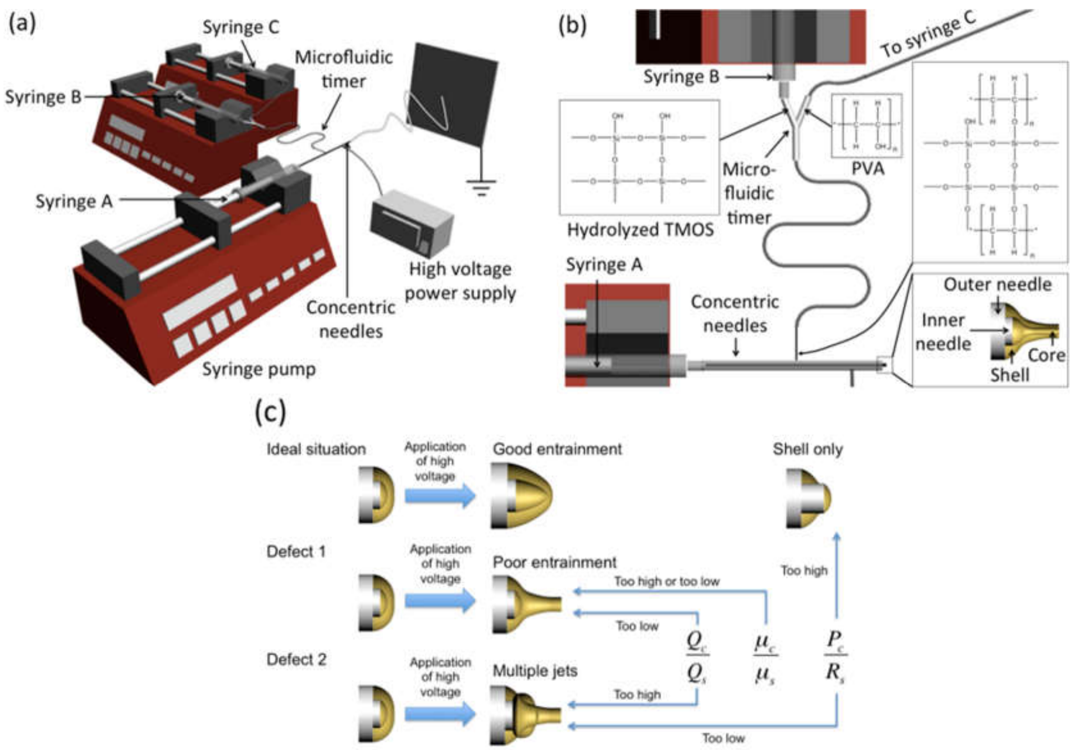

Figure 30 - Electrospinning setup for core/shell nanofibers having a bacterium-containing core and a silica-based shell surrounding the core: (a) the coaxial electrospinning system coupled with a microfluidic timer; (b) reaction between the hydroxide groups of PVA and the silanol groups of silica during the electrospinning process; (c) effects of the three critical parameters: the ratio of the flow rate of the core solution to the flow rate of the shell solution (Qc/Qs), the ratio of the core needle protrusion length to the shell needle radius (Pc/Rs), and the ratio of the viscosity of the core solution to the viscosity of the shell solution (μc/μs) on the success of the coaxial electrospinning process.

Optimization of parameters

The quality of the electrospinning manufacturing system is defined by cell encapsulation efficiency (g cells encapsulated per g material produced), and the production homogeneity (minimization of defects such as droplets intermixed with the fibers as well as ensuring a uniform diameter distribution of the nanofibers). Therefore, the quality of the product is affected by the physical and chemical properties of the solutions used to make the core and the shell as well as the processing parameters. To achieve the highest quality for production, a factorial design method was employed to optimize the solution properties and the processing parameters.

Selection of the manufacturing parameters

Continuous manufacturing of core/shell nanofibers via coaxial electrospinning relies on the formation of a jet of the shell solution and the entrainment of the core solution. For successful entrainment of the core solution, certain parameters should be optimized: (1) ratio of the flow rate of the core solution to the flow rate of the shell solution (Qc/Qs), (2) ratio of the core needle protrusion to the outer needle radius (Pc/Rs), and (3) ratio of the viscosity of the core solution to the viscosity of the shell solution (μc/μs) [117]. The effect of these parameters on coaxial electrospinning is illustrated in Figure 30c. Extreme values of these ratios generally lead to poor entrainment of the core material into the jet or formation of multiple jets rather than a stable core/shell jet [118]. The values/levels for the parameters investigated in the present study are listed in Table 6. Level 0, level 1 and level 2 corresponded to the low, medium and high levels, respectively. A complete factorial design with three parameters and three levels was constructed to estimate the resultant effects and the interactions between these parameters to determine the best conditions to continuously produce core/shell nanofibers (Table 7).

Table 6 - Parameters and levels investigated in the factorial design

Parameter	Level		
	0	1	2
A. Core solution flow rate [mL/h]	0.6	1.2	1.8
B. Core needle protrusion length [mm]	0.2	0.4	0.6
C. Core solution concentration [% (w/v)]	8	18	28

Product quality estimation

To determine the quality of the reactive membranes, three aspects should be considered: cell encapsulation efficiency (y1), droplet (defect) formation (y2), and fiber diameter (y3). An ideal reactive membrane should have a large density of encapsulated cells to enhance its specific degradation rate per volume of the material produced. The defects (i.e. droplets) should be minimized so that additional processes/steps for the removal of the defects from the final product are not needed. Uniform fibers with smaller diameters are preferred because they not only decrease diffusion length when the fiber diameter is larger than the bacteria size but also result in a higher surface area-to-volume ratio and permeability. \

Table 7 - Effects of the three parameters on the quality (*y*) of the electrospun fibers.

Exp.	Parameter and its level			Response y_1	Response y_2	Response y_3	Overall response y
	A	B	C				
1	0	0	0	0.7810	0.3088	0.6026	0.5641
2	0	0	1	0.5429	0.1324	0.6485	0.4412
3	0	0	2	0	0	0.8603	0.2868
4	0	1	0	0.6571	0.3235	0.5993	0.5267
5	0	1	1	0.3048	0.2353	0.6648	0.4016
6	0	1	2	0.3048	0	0.6714	0.3254
7	0	2	0	0.9714	0	0.6616	0.5443
8	0	2	1	0.9810	0	0.7194	0.5668
9	0	2	2	0.9905	0	0.7194	0.5700
10	1	0	0	0.6381	0.5735	0.5819	0.5978
11	1	0	1	0.4857	0.3676	0.7784	0.5439
12	1	0	2	0.2667	0	1	0.4222
13	1	1	0	0.6476	0.5735	0.5742	0.5985
14	1	1	1	0.5143	0.4265	0.7707	0.5705
15	1	1	2	0.3048	0	0.9662	0.4236
16	1	2	0	0.9905	0	0.6572	0.5492
17	1	2	1	0.9810	0	0.7151	0.5653
18	1	2	2	0.9810	0	0.7271	0.5693
19	2	0	0	0.5524	1	0.5448	0.6990
20	2	0	1	0.2952	0.7353	0.6343	0.5549
21	2	0	2	0.1714	0	0.9651	0.3788
22	2	1	0	0.2952	0.4853	0.5699	0.4501
23	2	1	1	0.2476	0.1471	0.6288	0.3412
24	2	1	2	0.0762	0	0.9727	0.3496
25	2	2	0	0.9714	0	0.6703	0.5472
26	2	2	1	0.9905	0	0.7205	0.5703
27	2	2	2	0.9905	0	0.7194	0.5700

To determine the cell encapsulation efficiency, *E. coli* expressing GFP were encapsulated in electrospun reactive membranes. The membranes were then washed with ultrapure water three times to get rid of the loosely-bound, surface-attached cells to ensure that only fully-encapsulated cells are visualized in the subsequent confocal microscopy images (Olympus FluoView FV1000, USA). For each membrane, confocal microscopy images were obtained at three different regions (the area of each region was 0.01 mm2). The number of cells in each region was counted (using green fluorescence imaging). The average value (Nc), which reflected the number of cells within an area of 0.01 mm2, was used as a measure of cell encapsulation efficiency. The cell encapsulation efficiency of each sample was given a value (y1), normalized with respect to the maximum number of cells (Ncmax) measured among all samples so that y1 values were kept in a range between 0 and 1 (Eqn. 1). As the number of cells in Exp. 3 was the maximum among all samples, Nc was taken to be equal to Ncmax in Exp. 3. Therefore, y1 = 0 in Exp. 3, as can be seen in Table 7.

$$y_1 = \frac{N_{c\max} - N_c}{N_{c\max}} \quad (1)$$

To determine defect formation, each reactive membrane sample was examined by Scanning Electron Microscopy (SEM) (Hitachi S-4700, Japan). In each sample, SEM micrographs were obtained at three different regions measuring approximately 256 μm2. The number of droplets (that are not connected to fibers) in each region was counted and the values determined at the three regions were averaged (Nd). The defect formation in each sample was given a value (y2) and normalized with respect to the maximum number of droplets (Ndmax) measured among all samples so that y2 fell within a range between 0 and 1 (Eqn. 2). As the number of droplets in Exp. 19 was the maximum among all samples, Nd was equated to Ndmax in Exp. 19. Therefore, y2 = 1 in Exp. 19, as can be seen in Table 7.

$$y_2 = \frac{N_d}{N_{d\max}} \quad (2)$$

To determine the fiber diameter uniformity in the produced filters, each SEM micrograph was analyzed using ImageJ. The fiber diameters were measured at 50 different locations and the average fiber diameter (D) was obtained. The response reflecting the fiber diameter of each sample was given a value (y3) and normalized with respect to the maximum fiber diameter (Dmax) to ensure that y3 fell within a range between 0 and 1 (Eqn. 3). As the fiber diameter in Exp. 12 was the maximum among all samples, D was taken as Dmax in Exp. 12. Therefore, y3 = 1 in Exp. 12, as can be seen in Table 7.

$$y_3 = \frac{D}{D_{\max}} \quad (3)$$

The overall response (y) that corresponds to the overall quality of the manufactured filter (Eqn. 4) is calculated as the weighted average of all of the parameters measured above.

$$y = \frac{y_1 + y_2 + y_3}{3} \quad (4)$$

The weight for each outcome (yi) can be adjusted according to the desired application. If a very high atrazine degradation efficiency is desired at the expense of increased defects (i.e. a high number of droplets with respect to the number of fibers) in the finished product, one may assign a higher weight for cell encapsulation efficiency and a lower weight for tendency of droplet formation. On the contrary, if a moderately high atrazine degradation efficiency is sufficient but the homogeneity of the finished product is of utmost concern, one may assign a higher weight for the defect formation and a lower weight for the cell encapsulation efficiency. In this manuscript, we assigned equal weights to each of the three outcomes (yi) used in this study.

The value of overall response (y) was between 0 and 1 for each reactive membrane manufactured in this study. A quality response value of 0 indicated that the reactive membrane had a high amount of encapsulated cells, had minimum defects, and the smallest fiber diameter among all reactive membranes investigated, whereas a value of 1 meant the opposite. A reactive membrane with the minimum overall response was regarded as the optimized membrane. The 27 experimental conditions conducted in the three-parameter, three-level factorial design and the corresponding overall responses were analyzed by a statistical analysis software (Statgraphics®) and optimum values for operational parameters were determined.

Characterization

Fourier Transform Infrared Spectroscopy (FTIR) analysis was conducted with the reactive membranes manufactured using the optimized parameters, silica/PVA nanofibrous membranes that did not contain any bacteria, and silica/PVA mixtures with known *E. coli* content (for calibration) using a Nicolet Continuμm FTIR microscope. IR spectra in the range of 400-4000 cm-1 were recorded at a resolution of 4 cm-1. Each sample was scanned at five different regions on the sample using an aperture size of 100x100 μm. The amount of the encapsulated *E. coli* in the electrospun membrane sample was calculated using the ratio of the intensity of the Amide II peak (corresponding to cellular proteins) to the intensity of the methylene peak (originating from silica and PVA) (Figure 31). For SEM and Transmission Electron Microscopy (TEM, FEI Tecnai G2 F30, USA) imaging, reactive membranes containing *E. coli* cells expressing AtzA were manufactured using the optimized values for the parameters examined. Reactive membranes comprised of core/shell nanofibers without any bacteria were also fabricated in a similar fashion.

Biotransformation of atrazine into hydroxyatrazine

Activity measurements of the optimized reactive membranes were conducted at room temperature. The reaction was initiated by exposing the optimized reactive membrane to 5 ml of 0.1 M potassium phosphate buffer (at pH 7.0) containing 150 μM (32.4 ppm) atrazine. The supernatant was sampled after 20 min and the concentrations of atrazine and its metabolite, hydroxyatrazine, were measured by high-performance liquid chromatography (HPLC) as previously described [52]. Activity measurements of the free bacteria were conducted in a similar fashion.

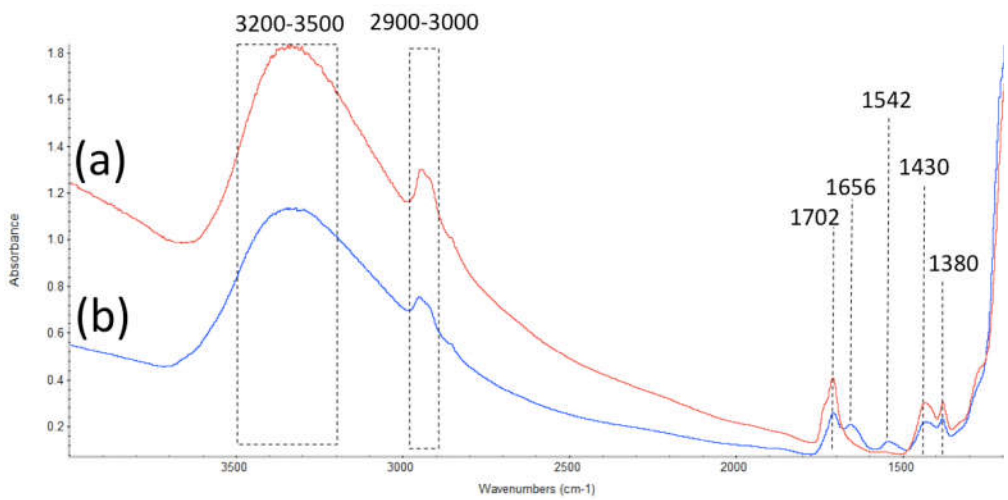

Figure 31 - FTIR spectra of the nanofibrous membranes fabricated via variable timing coaxial electrospinning technique developed here: (a) nanofibers comprising a PVA core and a silica/PVA composite shell surrounding the core; (b) nanofibers comprising an *E. coli*-containing PVA core and a silica/PVA composite shell surrounding the core.

5.3 Results and Discussion

5.3.1 Fabrication of silica-PVA-based core/shell encapsulating nanofibers

Silica is an excellent material for bioencapsulation because of its low cost, mechanical robustness, manufacturability, thermal and pH stability, and chemical inertness [28]. Unlike most electrospun fibers, especially those made of natural polymers such as gelatin or alginate, which are mechanically fragile and rapidly dissolve in water, silica fibers can maintain their morphology in water during continuous use. Nevertheless, the silica fibers are yet quite brittle. Fabrication of silica nanofibers via traditional electrospinning methods has previously been reported [119, 120]. For example, tetraethyl orthosilicate (TEOS) has widely been used for fabricating pure silica or silica-polymer nanofibers via sol-gel electrospinning [121, 122]. However, the sol-gel process unavoidably requires ethanol, which is not only released by the hydrolysis reaction but also is added to eliminate phase separation and to accelerate hydrolysis. However, ethanol is known to negatively affect the reactivity and the viability of the encapsulated bacteria. Therefore, to date there has been no report of successful encapsulation of reactive bacteria in electrospun silica nanofibers. A mixture of TEOS and aminopropyl triethoxysilane (APTES) [97] has also been used for forming silica nanofibers via sol-gel electrospinning but the process still requires ethanol.

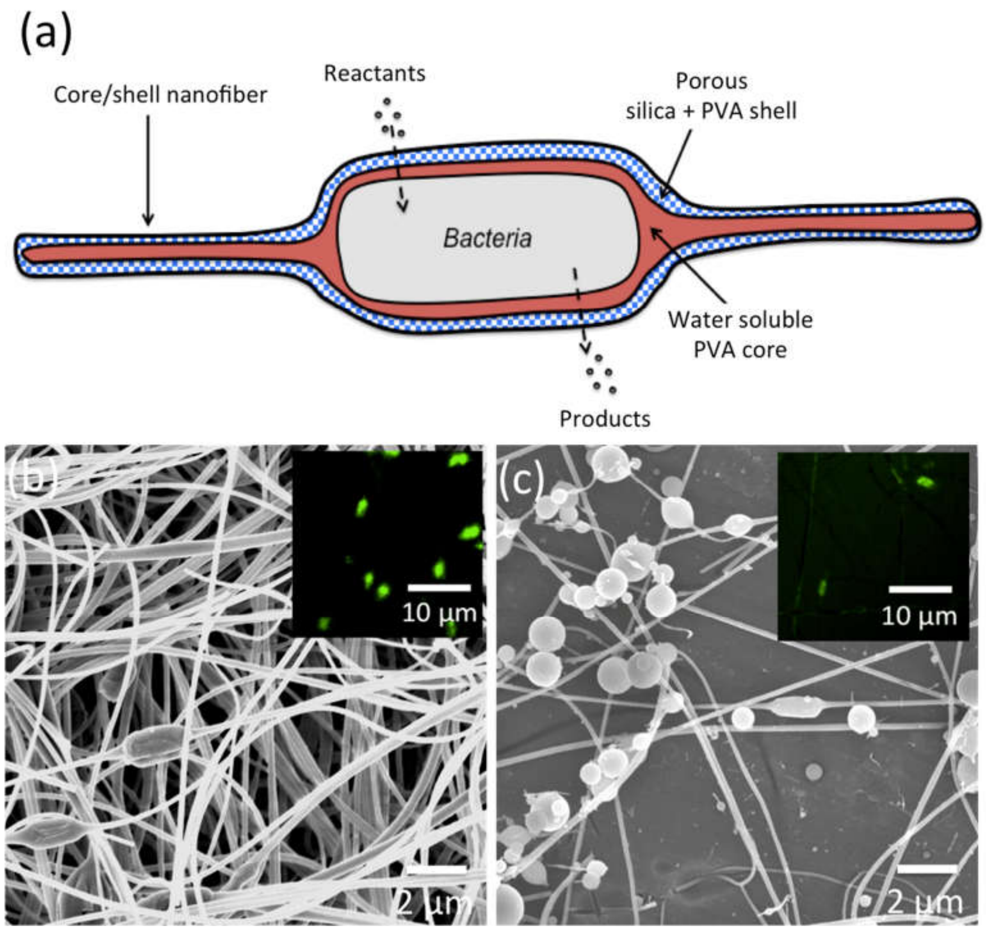

Figure 32 - (a) The nanofiber architecture comprised of a bacterium-containing water soluble PVA core and a silica porous shell surrounding the core. SEM micrographs and confocal microscopic images (insets) of the electrospun fibers with encapsulated *E. coli* expressing GFP: (b) Experiment #3; (c) Experiment #19.

In this communication, reactive membranes comprised of nanofibers made of silica and PVA were produced using a novel coaxial electrospinning process. The uniqueness of the approach presented here is that no extra ethanol needed to be added during the process, which maximized the biocompatibility of the produced material while enabling continuous production. Furthermore, the technology aims at encapsulation of intact bacteria, not purified enzymes. The advantage of encapsulating bacteria over enzymes is that it is easier and more economical to grow and use bacteria as the biodegradation agent since additional steps for enzyme purification are not required. Furthermore, in intact cell encapsulation, the enzymes are better protected against swings in temperature, pH and salinity since they reside in their native environment in the cytoplasm of the cells.

Polyvinyl Alcohol (PVA) used in the formulation served multiple purposes; 1) PVA acted as a thickener, helping to adjust the viscosity of the electrospinning solution, 2) enhanced biocompatibility of the bioencapsulation solution by enveloping and protecting the bacteria the geling silica precursors, 3) when mixed with the silica in the shell solution, decreased the brittleness of the shell and increased its flexibility, 4) Increased the porosity of the shell, and 5) dissolved away when the finished product was exposed to an aqueous solution, therefore increasing the permeability of the membrane (Figure 32a).

5.3.2 Optimization of electrospinning parameters

The quality of the electrospun reactive membrane (represented by the overall response, y) is a function of three parameters: cell loading density (represented by the response y1), defect formation (represented by the response y2), and uniformity of the produced fiber diameters (represented by the response y3). The value y was taken to be the average of y1, y2 and y3 and the lower the value of y, the higher the quality of the produced reactive membrane. The value y for each formulation was determined and is summarized in Table 7. It can be clearly seen that the overall response y reached the minimum at Experimental condition 3, corresponding to the optimum design conditions for manufacturing of the reactive membranes. On the contrary, the overall response y was the highest at Experimental condition 19, indicating that the combination of the design parameters resulted in a sub-standard membrane material.

Figure 32 shows the SEM micrographs of the reactive membranes that contain GFP expressing *E. coli* encapsulated at conditions corresponding to Exp. 3 (Figure 32b) and Exp. 19 (Figure 32c). The inserts show the confocal microscopic images of the same samples. It can be clearly seen that more cells were encapsulated in Exp. 3 compared to Exp. 19. This could be explained by rheological analysis: The viscosity of the core solution used in Exp. 3 was approximately 4000 cP while it was below 1000 cP in Exp. 19. The viscosity of the shell solution, identical in both cases, was measured to be 4173 ± 686 cP, a value very similar to the viscosity of the core solution in Exp. 3, but significantly higher than that in Exp 19. Therefore, it was easier for the core at Exp. 3 to be entrained by the shell solution and incorporated into the electrospun jet by the shear force generated at the core-shell interface, thus enhancing the cell encapsulation efficiency. Although the average diameter of the fibers fabricated at Exp. 19 was slightly smaller than that at Exp. 3, the membranes fabricated at Exp. 19 were not considered to be superior than those fabricated at Exp. 3 since the diffusional distance is independent of the fiber diameter when the fiber diameter is smaller than the width of the bacteria. The diameters of the fibers in both samples were smaller than the width of an *E. coli* cell (around 500 nm). Therefore, the thickness of the encapsulating shell produced in Exp. 19 should be similar to that of the encapsulating shell is Exp. 3, even though the average fiber diameter in Exp. 19 was smaller. The substantial number of droplets observed in Exp. 19 results in a lower quality of the manufactured membranes. In Exp. 19, the core solution flow rate was high but the core solution was poorly entrained into the jet. Therefore, it is highly likely that the excess core solution is drawn as a separate jet, which might be broken down into droplets by the electric forces.

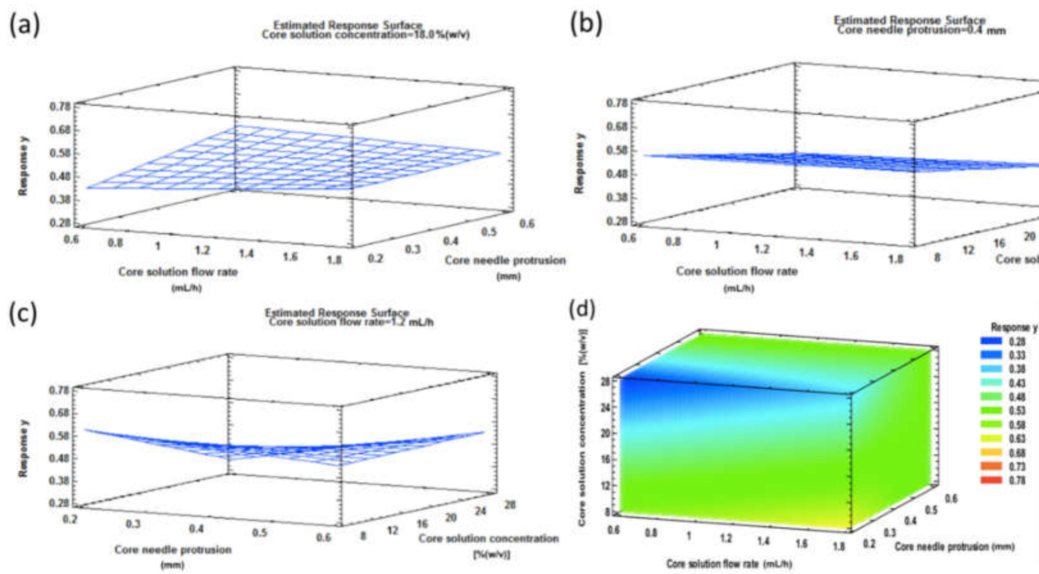

Figure 33 - Three-dimensional response surface plots for the interaction effects between: (a) core solution flow rate and core needle protrusion; (b) core solution flow rate and core solution concentration; (c) core needle protrusion and core solution concentration; (d) all three parameters.

The main effects of core solution flow rate, core needle protrusion and core solution concentration on the overall response y were investigated. Figure 33a shows the surface plot as a function of the core solution flow rate and the core needle protrusion distance when the core solution concentration is kept constant at the medium level of 18% (w/v). The minimal response for y was observed when the core solution flow rate and the core needle protrusion were low, indicating that a high quality membrane could be manufactured by reducing both the core solution flow rate and the core needle protrusion. Figure 33b shows the response surface as a function of the core solution flow rate and the core solution concentration, with the core needle protrusion kept constant at the medium level (0.4 mm). The response, y, in general decreased with increasing core solution concentration but the core solution flow rate did not play a significant role, implying that for this specific protrusion length, a higher core solution concentration would result in a higher quality membrane. Figure 33c shows the response surface as a function of the core needle protrusion distance and the core solution concentration, when the core solution flow rate was kept constant at the medium level (1.2 mL/h). The minimum response for y was observed when core needle protrusion was at the low level while the core solution concentration was at the high level, indicating that the quality of the membrane could be increased by reducing the core needle protrusion and increasing the core solution concentration. Figure 33d shows the response plot as a function of all three parameters and the plot clearly indicates that the minimum response of y (corresponding to the highest quality of the membrane) could be achieved when the core solution flow rate and core needle protrusion were set to low while the core solution concentration was set to high. Therefore, the optimum parameters were chosen as: Core solution flow rate = 0.6 mL/h; core needle protrusion = 0.2 mm; and core solution concentration = 28%(w/v) for the production of the membranes to be characterized and analyzed in detail as described below.

5.3.3 Characterizations of the optimized reactive membranes

E. coli-containing nanofibrous membranes fabricated under the optimized conditions were analyzed with FTIR spectroscopy. As shown in Figure 31, the silica/PVA matrix generated spectra with prominent peaks between 3200 and 3500 cm-1 originating from the -OH vibrations, the peaks between 2900 and 3000 cm-1 originating from the vibrations of the –CH2 groups, the peaks around 1430 cm-1 due to the scissoring motion of CH2, and the peaks around 1380 cm-1 due to the bending of CH2. Apart from the aforementioned common peaks, the FTIR spectrum for the *E. coli*-containing nanofibrous membrane exhibited additional peaks including the peak at 1656 cm-1 arising from the protein and water bending peaks generating the Amide I band and the peak at 1542 cm-1 due to the Amide II protein band. The amount of *E. coli* encapsulated in the electrospun nanofibrous membranes was measured using the ratio of the intensity of the Amide II peak to the intensity of the CH2 peak. In this analysis, the Amide II peak, instead of the Amide I peak, was used because the Amide II peak does not include spectral contributions from water bending peak located at 1650 cm-1 [123]. Table 8 shows the correlation between the Amide II-to-CH2 ratio (m) and the mass percentage of *E. coli* in fibers (n).

Table 8 - Relationship between the Amide II-to-CH_2 ratio (*m*) and the mass percentage of *E. coli* (*n*).

Mass percentage of *E. coli*, *n* (% g/g)	Amide II-to-CH_2 ratio, *m*
36	0.8405 ± 0.0871
44	1.2659 ± 0.1146
51	1.7051 ± 0.1131

The relationship between m and n was determined to be:

$$m = 0.1549e^{0.0473n} (5)$$

Using this equation, the mass ratio of the *E. coli* in the electrospun reactive membranes produced at the optimum condition (Exp. 3) was determined as approximately 40% g cells / g matrix. This is a very high level of loading that has not been reported elsewhere before.

SEM imaging was used to explore the ultrastructure of the core/shell nanofibers fabricated at the optimized conditions (i.e., the conditions that minimized y). Figure 34a shows the electrospun membrane comprising the core/shell nanofibers. When encapsulated, the bacteria were oriented along the longitudinal direction of the nanofiber without experiencing a significant morphological change due to encapsulation (Figure 34b). The surface of the nanofibers was smooth, indicating homogeneous mixing of the PVA with the silica. The average diameter of the AtzA expressing *E. coli*-containing nanofibers was 255 ± 19 nm, which was similar to that of the GFP expressing *E. coli*-containing nanofibers fabricated in Exp. 3 (263 ± 17 nm). The core/shell morphology of the nanofibers was confirmed by TEM imaging (Figure 34c), which showed that the thickness of the porous silica shell was approximately 20 nm.

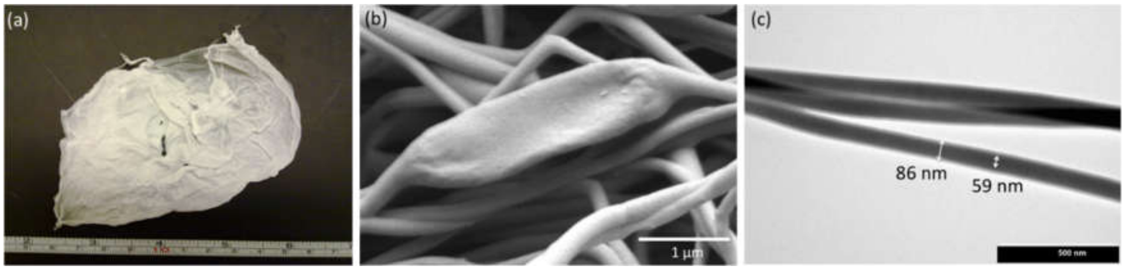

Figure 34 - (a) Core/shell nanofiber membrane produced by coaxial electrospinning with the optimized conditions, (b) SEM micrograph of the core/shell nanofibers showing an encapsulated *E. coli* (c) TEM image of the core/shell nanofibers showing the PVA core and a silica/PVA composite shell surrounding the PVA core (portion between encapsulated bacteria was selected).

5.3.4 Transformation of atrazine into hydroxyatrazine

Rietti-Shatti *et al*. immobilized Pseudomonas ADP using Ca-alginate encapsulation technique and found that the bacterium lost much of its atrazine degrading activity upon immobilization (50% reduction in atrazine concentration before immobilization versus 8% reduction in atrazine concentration after immobilization) [124]. Vancov *et al*. encapsulated Rhodococcus erythropolis cells in alginate-based spherical beads and demonstrated the ability of the encapsulated cells to degrade atrazine. However, with soft materials such as alginate, there is always the risk of releasing cells into the environment. Therefore, alginate gels are impractical for field applications due to their inferior mechanical properties, inability to stop cell leakage, and poor cell viability during storage [125]. A very recent study reported encapsulation of *Pseudomonas sp*. ADP cells into core/shell nanofibers for atrazine bioremediation [49]. The cell suspension was mixed with a core solution of polyethylene oxide dissolved in water, which was electrospun with a shell solution made of polycaprolactone and polyethylene glycol dissolved in chloroform and dimethylformamide. The atrazine degradation rate was reported as 0.0023 µmol / g of nanofibers / min following bioencapsulation. Although atrazine degradation was restored to 0.039 µmol / g of nanofibers / min by allowing the cells to grow in the nanofibers, the degradation rate of the encapsulated cells was still an order of magnitude less than the free cells. It is probable that the organic solvents involved in electrospinning had adverse effects on the enzymatic pathway for atrazine bioremediation.

In this study atrazine degradation activity of both free *E. coli* expressing AtzA and nanofiber encapsulated *E. coli* expressing AtzA were assessed using HPLC analysis. In order to measure the reaction rates and the bioremediation efficiency accurately, the measurements focused on production of hydroxyatrazine in order to eliminate the bias due to adsorption of atrazine by silica

[51]. Table 9 shows the quantities of atrazine degraded/adsorbed and hydroxyatrazine produced per unit gram of *E. coli* (or per gram of nanofibers) per minute for free and encapsulated *E. coli*. In both cases, the rate of atrazine degraded or adsorbed was comparable to that of hydroxyatrazine produced, implying that adsorption of atrazine into the silica-based nanofibers was negligible. The specific activity of the encapsulated *E. coli* was at the same order of magnitude as that of the free *E. coli*, indicating that the optimized reactive membranes did not present significant diffusional resistance.

Table 9 - Biotransformation of atrazine into hydroxyatrazine

	Free *E. coli* expressing AtzA	Encapsulated *E. coli* expressing AtzA
Mole of atrazine degraded or adsorbed (μmol / g of *E. coli* / min)	0.64	0.24
Mole of atrazine degraded or adsorbed (μmol / g of nanofibers / min)	N/A	0.10
Mole of hydroxyatrazine produced (μmol / g of *E. coli* / min)	0.61	0.23
Mole of hydroxyatrazine produced (μmol / g of nanofibers / min)	N/A	0.10

We showed that we could achieve high degradation activity levels in electrospun reactive filters that are comparable to free-cells. In a novel approach, a multilayer geometry was utilized and the bacterium-containing core was enveloped in a porous shell produced in a continuous fashion. This served the purpose of increasing the biocompatibility of the process, adding an extra layer of separation between the bacteria and the environment (to further protect against accidental release) and also enhanced the encapsulation efficiency while minimizing the diffusion length. This scalable technology can be used to manufacture bioreactive filters that can biodegrade chemicals at large throughput levels, replacing the traditional size exclusion-based filtration systems. This opens new avenues in industrial scale bioremediation of contaminated waters.

5.4 Conclusion

Reactive membranes comprising electrospun nanofibers composed of a PVA core that encapsulate reactive *E. coli* and a silica/PVA composite shell surrounding this core were fabricated by a novel coaxial electrospinning method. Using this method, a very high loading efficiency of up to 40 grams of *E. coli* in 100 grams of matrix material could be reached. The atrazine biodegradation rate achieved by the reactive membranes produced by this method was quite high at 0.24 μmol / g of *E. coli* / min, which is approximately 40% that of the free bacteria (0.64 μmol / g of *E. coli* / min).

Chapter 6: Silica gel co-encapsulation for synergistic bacterial biotransformation[5]

6.1 Introduction

Bacteria are used for chemical biotransformation (e.g. biosynthesis, biocatalysis, biodegradation, etc.) reactions at a commercial scale [126-129]. Applications of microbial biotransformation reactions extend to various sectors of the economy, including: renewable energy [130], healthcare [131], agriculture [132], and environmental remediation [133]. Traditionally, biotechnological processes have used pure cultures of specialized naturally-occurring or recombinant expression microorganisms. More recently, applications of mixed bacterial populations are being developed for commercial use, drawing on the ability of microbial consortia to perform a larger variety of more complicated tasks [134]. A major challenge in utilizing mixed bacterial species is to achieve population stability and control in an unstructured co-culture environment [135, 136], where species compete for resources leading to an unbalanced, suboptimal population ratio. These issues reduce the efficacy of the system, and can lead to complete process cessation if one of the species is eradicated.

Silica gel encapsulation is a simple and feasible method for utilizing synergistic bacteria for chemical biotransformation. Bioencapsulation (i.e. physical entrapment of whole-cells in a porous 3D matrix) enables precise control of individual bacterial populations by entrapping the bacteria in a restricted volume. Thus, populations of individual species in the matrix can be optimized to maximize the biotransformation efficiency. This method also facilitates transport of the substrates, since co-encapsulated bacteria are located within micron-scale proximity of each other in the matrix. Silica is a highly porous, mechanically strong and thermally/chemically stable material that can be synthesized via a cytocompatible sol-gel process using silicon alkoxides. Aqueous silica precursors such as silica nanoparticles (SNPs) and sodium silicate can also be incorporated into the gel, further improving its cytocompatibility [17, 51]. For biotransformation applications, silica gel also provides a robust mechanical structure, making the technology easier to integrate into existing chemical and physical process systems. Its optical transparency makes it an ideal candidate for encapsulation of phototrophs, as previously demonstrated [137]. As a result, silica gel encapsulation of cells (eukaryotes and prokaryotes) has been studied, as summarized in these review articles [14, 21].

[5] This chapter is part of a publication that is currently in preparation.

In this study, two different bacterial species: *Synechococcus elongatus* PCC 7942 (PCC 7942) and *Pseudomonas sp*. NCIB 9816 (NCIB 9816) were used for synergistic biotransformation. NCIB 9816 is a highly useful and extensively studied microorganism, which can aerobically transform over 100 aromatic hydrocarbons [138]. Aromatic hydrocarbons are an important subset of major industrial feedstock chemicals, which are oxidized to higher value products (e.g. phenols, benzoates, phthalates, quinones, hydroquinones, dyes, etc.). However, high oxygenation demand of biotransformation reactions makes them less economically feasible than chemical synthesis methods, despite their higher conversion efficiency. Some aromatic hydrocarbons, particularly those with polycyclic rings, are also prominent carcinogens and EPA priority pollutants [139]. Therefore, biotransformation reactions catalyzed by NCIB 9816 are also important for water bioremediation applications [140]. In water bioremediation, mechanical aeration systems are commonly used to provide the necessary oxygen for the biotransformation reactions. However, these systems come with a high monetary and energy cost, which can account for more than 50% of the overall energy consumption of the treatment process [141]. PCC 7942 is a cyanobacterium which can provide oxygen via photosynthetic oxygen evolution reactions, as an alternative to mechanical aeration systems. Photosynthetic oxygenation has been investigated in unstructured or partially structured environments, but these studies suffered from low biotransformation efficiencies due to lack of stabilization of the bacterial populations [142-144].

We developed a silica gel co-encapsulation matrix for NCIB 9816 and PCC 7942, for synergistic biotransformation of naphthalene (a model hydrocarbon) into CO_2 (Figure 35a). This was a self-sustained biotransformation system, which operated without external aeration. The proposed co-encapsulation system was designed such that NCIB 9816 and PCC 7942 preserved their biotransformation/oxygen generation activity after encapsulation, while the material exhibited high mechanical strength and optical transparency. Various silica gel compositions were tested, and an optimal silica gel matrix was selected for co-encapsulation of both bacterial species. In a silica gel cell encapsulation system, cells constitute the major proportion of the overall cost. Thus, encapsulated cell densities needed to be optimized to maximize the biotransformation efficiency. Light attenuation (due to absorption and scattering effects of the encapsulating gel and the cells within) in the silica gel matrix was modeled, and experimentally verified by oxygen generation rates of the encapsulated PCC 7942 at various cell densities. This model revealed a critical cell density parameter, which maximized the oxygen generation rate of encapsulated PCC 7942. Based on this rate, density of NCIB 9816 was optimized and the biotransformation performance of the system was experimentally measured. The developed co-encapsulation system was able to sustain biotransformation reactions after the oxygen was depleted. Furthermore, it was shown that photosynthetic oxygenation via co-encapsulated PCC 7942 was a more efficient method for providing oxygen than aeration through the headspace. We proposed that this was due to facilitated oxygen transport between the co-encapsulated bacteria in the gel. Confocal microscopy images verified that the cells were homogeneously distributed in the gel, and were within micron-scale proximity of each other. To the best of our knowledge, our study is the first to report co-encapsulation of different bacterial species in a non-proliferative matrix (silica) that demonstrates synergistic biotransformation.

6.2 Experimental

Materials

Reagent grade tetraethyl orthosilicate (TEOS, 98%) and Ludox HS-40/TM-40 colloidal silica nanoparticles (SNP) were purchased from Sigma-Aldrich (Sigma-Aldrich Corp. St. Louis, MO, USA.). NexSil 85-40/125-40 silica nanoparticles were purchased from Nyacol (Nyacol Nano Technologies Inc., Ashland, MA, USA). All chemicals were used without further purification. Ultrapure water (UPW) was used in all the experiments, which was prepared by filtering distilled water through a Milli-Q water purification system (Millipore, Billerica, MA, USA) to a final electrical resistance of > 18.2 MΩ/cm.

Bacterial strains and growth conditions

Synechococcus elongatus PCC 7942 was obtained from the Pasteur Culture Collection of Cyanobacteria, France. *S. elongatus* PCC 7942 was grown at 28 °C in BG-11 medium [145] and was contiguously bubbled with air. The cultures were incubated at light intensity of 50 ± 4 µmol photons m-2 s-1. Cell growth was monitored by measuring OD730 on a Beckman DU 640 spectrophotometer (Beckman Coulter, Fullerton, CA). When the culture reached OD730 of 0.8, it was harvested by centrifugation at 8,000 rpm for 20 min at 22 °C. Cultures of *Pseudomonas sp*. NCIB 9816-4 were grown on Luria Broth (LB) at 30°C for about 8 h and used to inoculate minimal salts buffer (MSB) at OD600 of 0.01. MSB was prepared following previously discussed methods [146], with the following substitutions (Hutner's Metals): 318 mg of Na2EDTA · 2H2O, 24 mg of CoSO4 · 7H2O, 17.7 mg of Na2B4O7 · 10H2O. The MSB was supplemented with 1 g naphthalene per 300 mL media. Cultures were grown in 2 L shake flasks (at 230 rpm) for 18 h at 25°C with vigorous aeration. Cultures that reached a final OD600 of 1.5–2.5 were filtered through glass wool to remove any naphthalene crystals remaining in the solution prior to harvest. Cells were harvested by centrifugation at 5,000g for 10 min. All cells were re-suspended at approximately 0.5 g wet mass/mL in phosphate buffered saline (PBS) for encapsulation. The OD730 of the cell suspensions were 1.2 after a 100-fold dilution.

Silica gel synthesis and encapsulation of bacteria

Tetraethyl orthosilicate (TEOS) was hydrolyzed by stirring 2 h at a 1:5.3:0.0013 molar ratio of TEOS:water:HCl. The pH of the SNPs was adjusted to 7.4 by adding 1M hydrochloric acid. After pH adjustment, PBS was added to further stabilize the pH of the SNPs and improve overall cytocompatibility of the solution. Bacteria suspension was added to SNP/PBS solution, and hydrolyzed TEOS was added to the SNP/PBS/bacteria solution by pipetting a few times to obtain a homogeneous sample. The final product was placed in glass vials or 96-well plates (depending upon the experiment) for gelation. Final volume of the gels consisted of 40% of silica precursors (TEOS + SNP) and 60% of (PBS + Bacteria suspension). Gels were named based on the volumetric ratio of TEOS to SNP in the gel formulation. For instance, SNP-3:1 gel with 10% [v/v] cells had 300 µL of SNP, 100 µL of hydrolyzed Si alkoxide, 100 µL of cell suspension and 500 µL of PBS per mL of gel.

Mechanical property measurement

Gels were synthesized in cylindrical molds (diameter = 12.5 mm, height = 12.5 mm). After gelation, samples were removed from the molds and placed briefly into PBS to keep them hydrated until testing. The samples were tested by axial compression until failure at a loading rate of 1 mm/min using an MTS QT10 mechanical testing machine (MTS Systems, Eden Prairie, MN). The stress at failure was reported as is, and elastic modulus was calculated from the linear-elastic region of the stress–strain curve using Matlab (Mathworks, Inc., Natick, MA).

Oxygen generation/consumption and biotransformation rate measurement

Oxygen generation and consumption rates of the silica gel encapsulated bacteria were measured by using an Oxygraph Oxytherm System (Hansatech Instruments Ltd., United Kingdom). Silica gels were made into cylindrical 200 µL test pieces by mixing the reagents and bacteria suspension in a 96-well plate. After gelation, a thin copper wire was used to extract the test pieces and suspend them in the reaction chamber during measurement. For oxygen production measurements with cyanobacteria containing gels, 3 mL of PBS was added to the chamber and the LED was turned on to provide light to the cyanobacteria. For oxygen consumption measurements with NCIB 9816 containing gels, 3 mL solution of PBS saturated with naphthalene was added to the chamber.

For biotransformation rate measurements, NCIB 9816 and PCC 7942 were mixed gently via vortexing prior to encapsulation. Silica gels with co-encapsulated cells were synthesized (500 µL volume) in septa sealed, glass vials. After gelation, 9 mL of saturated naphthalene + BG11 solution was added on top of the gel, ensuring that the vial was completely filled before sealing (except for the samples with additional 4 mL of headspace). Then, the samples were placed on a shaker setup and naphthalene concentrations in the solution were measured intermittently, as described in [147].

Confocal imaging of co-encapsulated cells

NCIB 9816 were incubated with BODIPY R6G fluorescent dye (ThermoFisher Scientific, MA, USA) before encapsulation. PCC 7942 were encapsulated without addition of a fluorescent dye because of their auto-fluorescence. Samples were prepared by pipetting 20 µL gel volume on a glass slide and were sealed using an adhesive spacer and a cover slip. Confocal images were taken using a Nikon A1Rsi inverted confocal microscope (Nikon Instruments Inc., Melville, NY), using a 488 nm laser.

6.3 Results and Discussion

6.3.1 Material design and characterization

Silica gels were synthesized using two different precursors: Tetraethyl orthosilicate (Si alkoxide) and aqueous silica nanoparticles (SNPs). The ratio of these two precursors, and the diameter of the SNPs were adjusted to modify the mechanical and optical properties of the gels. Optical properties of the gels exhibited a strong correlation with the diameter of the SNPs used. Gels made with HS40 (12 nm) and TM40 (22 nm) SNPs were visibly transparent, while NS85-40 (55 nm) and NS125-40 (85 nm) gels were white and opaque, independent of SNP to Si alkoxide ratio tested. Since optical transparency is crucial for efficient oxygen generation, NS85-40 and NS125-40 gels were not further investigated. Visibly transparent gels synthesized with HS40 and TM40 SNPs were further characterized using UV-Vis spectrophotometry (Figure 35b). 680 nm was selected as a representative wavelength based on the light absorption of Photosystem II (where oxygen evolving complex is located in cyanobacteria) being maximum. Nonetheless, in the entirety of the visible spectrum, light transmittance of the gels synthesized with smaller (HS40) SNPs was higher than that of gels synthesized with larger (TM40) SNPs (data not shown). It can be seen that transmittance of the TM40 gels decreased gradually as SNP to Si alkoxide ratio increased, but HS40 gels were unaffected (Figure 35b). It is proposed that this is due to formation of silica aggregates by the Si alkoxide during gel formation, as previously reported [68]. These aggregates are smaller than the TM40 SNPs but comparable in size to the HS40 SNPs, thus they do not affect the optical properties of the HS40 gels.

The gel with the best mechanical properties (HS40-1:1) had an elastic modulus of 8.79 ± 0.72 MPa and a stress at failure of 380 ± 34 kPa (Figure 35c-d). HS40 gels had higher mechanical properties as compared to the TM40 gels, for all the SNP to Si alkoxide ratios tested, which is due to the higher crosslinking density of the smaller nanoparticles. HS40 gels were also superior to TM40 gels in terms of optical transparency, thus TM40 gels were not further investigated. Mechanical properties (elastic modulus and stress at failure) of the gels declined as the SNP to Si alkoxide ratio of the matrix increased. This is in accordance with previously reported results that increasing Si alkoxide content of the gel improves its mechanical properties, albeit reducing the viability of the encapsulated biocatalytic bacteria [68]. In that system the encapsulated bacteria were recombinant *Escherichia coli* overexpressing a catalytic enzyme, and cell viability was not essential. However, in this system both NCIB 9816 and PCC 7942 cells must be in a viable state to carry out biotransformation and photosynthesis, respectively. Thus, we proceeded with measuring their post-encapsulation biological activity with respect to the SNP to Si alkoxide ratio of the gel.

Activity of encapsulated PCC 7942 was evaluated by measuring their oxygen generation rate. The rate increased significantly when the SNP to Si alkoxide ratio increased from 1:1 to 3:1, and plateaued around 4.4 ± 0.1 nmoles/min (Figure 35e). Conversely, activity of the silica gel encapsulated NCIB 9816 strain was evaluated by measuring oxygen uptake coupled to biotransformation of a saturated naphthalene solution. The naphthalene-dependent oxygen consumption rate of encapsulated NCIB 9816 increased significantly from 1:1 to 3:1, and a maximum of 45.3 ± 6.6 nmoles/min was achieved at 5:1 ratio (Figure 35e). These results verified that a compromise was necessary between the cytocompatibility and superior mechanical properties of the gel. HS40-3:1 gels had very small loss in oxygen generation (with PCC 7942) and biotransformation (with NCIB 9816) activity, while maintaining better mechanical properties as compared to the other cytocompatible (5:1 and 7:1) gels. Therefore, HS40-3:1 gels were selected as the optimal gel for modeling and optimization purposes.

6.3.2 Modeling of oxygen generation by silica gel encapsulated PCC 7942

Modeling was performed to obtain an analytical expression for the oxygen generation rate of silica gel encapsulated PCC 7942, as a function of cell density (ρ_c) and the light intensity (I) profile in the gel. Light intensity profile in the gel is non-uniform, as both the silica gel and bacteria contribute to light attenuation (At) via absorption and scattering effects. Thus, the oxygen generation rate is both implicitly and explicitly (via attenuation) correlated with encapsulated cell density. Light attenuation in photobioreactors (where bacteria are freely suspended in media) has been extensively studied [148], and typically modeled by the Beer-Lambert law:

$$At(\rho_C, x) = C_1\, \rho_C x \ (\mathbf{1a})$$

where attenuation coefficient **C_1** represents cells' contribution to light attenuation, ρ_c is the cell density (of PCC 7942), and x is the distance that the light travels in the cell suspension. This model can be modified for silica gel encapsulated cells as follows:

$$At(\rho_C, x) = (C_1\, \rho_C + C_0)x \ (\mathbf{1b})$$

where attenuation coefficient **C_0** represents silica gel's contribution to light attenuation, and x is the distance from the gel surface. Based on this model, it was hypothesized that when the cell density (ρ_c) is sufficiently high, cells that are farther from the light source receive very low intensity light and do not measurably contribute to the oxygen generation. Thus, the net oxygen generation rate of the encapsulated cells is expected to saturate beyond a specific ρ_c value.

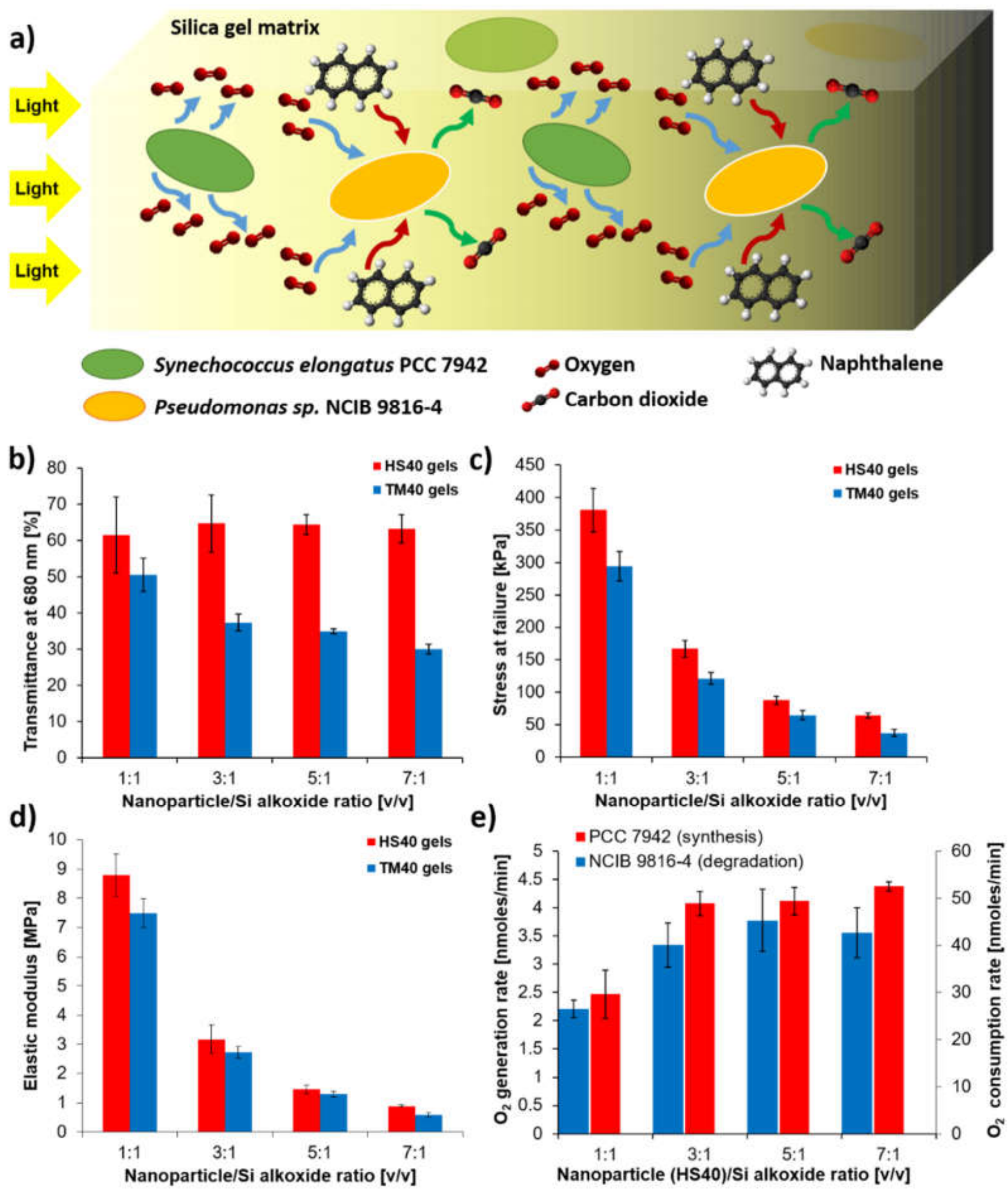

Figure 35 - Silica gel matrix characterization based on optical and mechanical properties of the material, and post-encapsulation activity of PCC 7942 and NCIB 9816. Four different nanoparticle to Si alkoxide ratios and two different nanoparticle sizes (HS40 – 12nm, TM40 – 22 nm) were tested. a) Schematic of the biotransformation system illustrating the silica gel encapsulated bacteria, and the transport of substrates between cells b) Optical transmittance of the gels at 680 nm and 1 cm path length, c) Stress at failure, d) Elastic modulus, e) Oxygen generation rate of encapsulated PCC 7942 (in PBS) and oxygen consumption rate of encapsulated NCIB 9816 during biotransformation (in saturated naphthalene solution) (All error bars indicate standard deviation, n ≥ 3).

To verify this hypothesis, coefficients of equation (1b) were experimentally determined by measuring light transmittance through silica gel encapsulated PCC 7942 at different cell densities, as well as free PCC 7942 in suspension (Figure 36a). It can be observed that the light attenuation through free and encapsulated cells are very similar, indicating that the optical transparency of the designed gel is sufficiently high and major contribution to light attenuation in the gel is due to the cells. Coefficients of equation (1b) were evaluated as $\mathbf{C_1}$ = 116.42 [mL/(mL cells-cm)] and $\mathbf{C_0}$ = 0.089 [1/cm] for encapsulated cells in HS40-3:1 gel, by fitting equation (1b) to the experimental data using least-squares regression. Using equation (1b), the light intensity (I) at a distance x from the gel surface for encapsulated PCC 7942 was determined as:

$$\frac{I(\rho_C, x)}{I_0} = T(\rho_C, x) = exp(-At) = exp(-(C_1\,\rho_C + C_0)x) \ (\mathbf{2})$$

Note that I0 is the light intensity on gel surface (which depends on the light source) and does not depend on ρ_c or x. Since the lighting configuration was consistent throughout the experiments, light transmittance profile (T) was used as the measure of light intensity in the gel instead.

An oxygen generation model was developed based on equation (2), for two different geometries based on the path of light being through: (Case I) a uniform cross-section box volume, (Case II) a non-uniform cross-section cylindrical volume, as shown in Figure 36b. For these two cases, the differential volumes were defined as:

$$dV = A\,dx \text{ (Case I)}$$

$$dV = R\,cos(\theta)\,h\,dx\,d\theta \text{ (Case II)}$$

where A is the cross-sectional area of the box volume (Case I), R is the radius and h is the height of the cylindrical volume (Case II). The oxygen generation rate of cyanobacteria is known to be linearly correlated with light intensity, up to a saturation limit where photo-inhibition effects start damaging the oxygen evolution complex [148]. The encapsulation system was designed for operation below the saturation limit, so the net oxygen generation rate in the differential volume can be defined as:

$$d\dot{q} = (k_{gen}\rho_C T(\rho_C, x) - k_{con}\rho_C)dV \ (\mathbf{3})$$

All the parameters used in the model are summarized in Table 10. The total net oxygen generation rate can be obtained by integrating the differential rate over the whole volume:

$$\dot{Q} = \int_{x=0}^{x=L} (k_{gen}\rho_C T(\rho, x) - k_{con}\rho_C)A\,dx \;\; \text{(Case I)}\,(\mathbf{4a})$$

$$\dot{Q} = 2\int_{\theta=0}^{\theta=\pi/2} \int_{x=0}^{x=2Rcos(\theta)} (k_{gen}\rho_C T(\rho, x) - k_{con}\rho_C)R\,cos(\theta)\,h\,dx\,d\theta \;\; \text{(Case II)}\,(\mathbf{4b})$$

Taking equation (4a-b)'s derivative with respect to ρ_c and finding its root reveals a critical cell density (ρ_{cr}) parameter, which yields a local extremum of the net oxygen generation rate. For the simple case of free cells in suspension and a box volume, ρ_{cr} is evaluated using equation (4a) as follows:

$$\dot{Q} = \frac{A(k_{gen} - exp(-\frac{C_1\rho_C V}{A})}{C_1} - k_{con}\rho_C V$$

Taking partial derivative with respect to ρ_c and solving for $\frac{\partial\dot{Q}}{\partial\rho_C} = 0$:

$$\frac{\partial\dot{Q}}{\partial\rho_C} = -k_{con}V + \; exp\left(-\frac{C_1\rho_C V}{A}\right)k_{gen}V \;(\mathbf{5a})$$

$$\rho_{cr} = \frac{A.\,ln\left(\frac{k_{gen}}{k_{con}}\right)}{C_1 V} = \frac{ln\left(\frac{k_{gen}}{k_{con}}\right)}{C_1 L} \;(\mathbf{5b})$$

It is trivial to perform a second derivative test using equation (5a) to show that ρ_{cr} yields a local maximum for $\dot{Q}$. This result is consistent with our hypothesis that there is a critical cell density that maximizes the net oxygen generation rate. Equation (5b) shows that ρ_{cr} is inversely proportional to the attenuation coefficient (**C_1**) and path length of the light (L). This means that more transparent and thinner (small **C_1** and L) materials have a larger ρ_{cr}, as expected. We propose that calculating ρ_{cr} during preliminary design stage of a biotransformation system is beneficial, since it yields an upper limit for the net oxygen generation rate of the system. If this limit is below the performance criterion, the system is considered to be unfeasible. While an analytical solution may not always be attainable for ρ_{cr}, it can still be numerically solved for more complicated cases (e.g. encapsulated cells in a cylindrical volume).

The modeling results were experimentally verified (See Table 11 for experimental parameters) using an oxygen electrode as shown in Figure 36c. Cell density (ρ_c) of the silica gel encapsulated PCC 7942 sample was varied from 1% to 30% [v/v] to determine how ρ_c affected oxygen generation rate of the gel. The net oxygen generation rate of the gel sample increased with an increasing amount of ρ_c up to a point, then slightly decreased (Figure 36d). The maximum oxygen generation rate of 3.7 ± 0.7 nmoles/min was achieved at ρ_c = 20% [v/v]. Base oxygen consumption rate constant of PCC 7942 ($\mathbf{k_{con}}$) was measured in the absence of light (to eliminate oxygen generation) as 22.1 ± 1.7 nmoles/(min.mL-cells). Incorporating $\mathbf{k_{con}}$ and other known experimental parameters for encapsulated cells into (4b), $\mathbf{k_{gen}}$ was evaluated by performing least-squares regression with the experimental data. This yielded a $\mathbf{k_{gen}}$ value of 1228.6 nmoles/(min.mL-cells) and a fit as shown in Figure 36d (blue). Then, finding local maximum of (4b) yielded a ρ_{cr} of 7.82% [v/v]. In (3), it is assumed that a differential volume receives only the transmitted light that passes through the cell volume, which is closer to the light source. However, it was shown in the literature that cells also receive some back-scattered light, which can also contribute to photosynthesis [149]. We addressed this issue by modifying the attenuation function with a coefficient CS, to account for the back-scattered light as follows:

$$At(\rho, x) = \frac{-(C_1\, \rho_C + C_0)}{C_S} x \; (\mathbf{6})$$

Then, we re-evaluated $\mathbf{k_{gen}}$ using (4b). This yielded a $\mathbf{k_{gen}}$ value of 721.74 nmoles/(min.mL-cells), and a Cs value of 1.88 and a fit as shown in Figure 36d (red). Finding local maximum of (4b) yielded a ρ_{cr} of 12.1% [v/v]. It is evident that the second model (which includes back-scattering effects) fit the data and captured the location of ρ_{cr} significantly better. This result suggests that the model underestimates the available light to a differential cell volume if it only accounts for the transmitted light and does not include the back-scattered light. This second model was then used to optimize the co-encapsulated cell densities for synergistic biotransformation study.

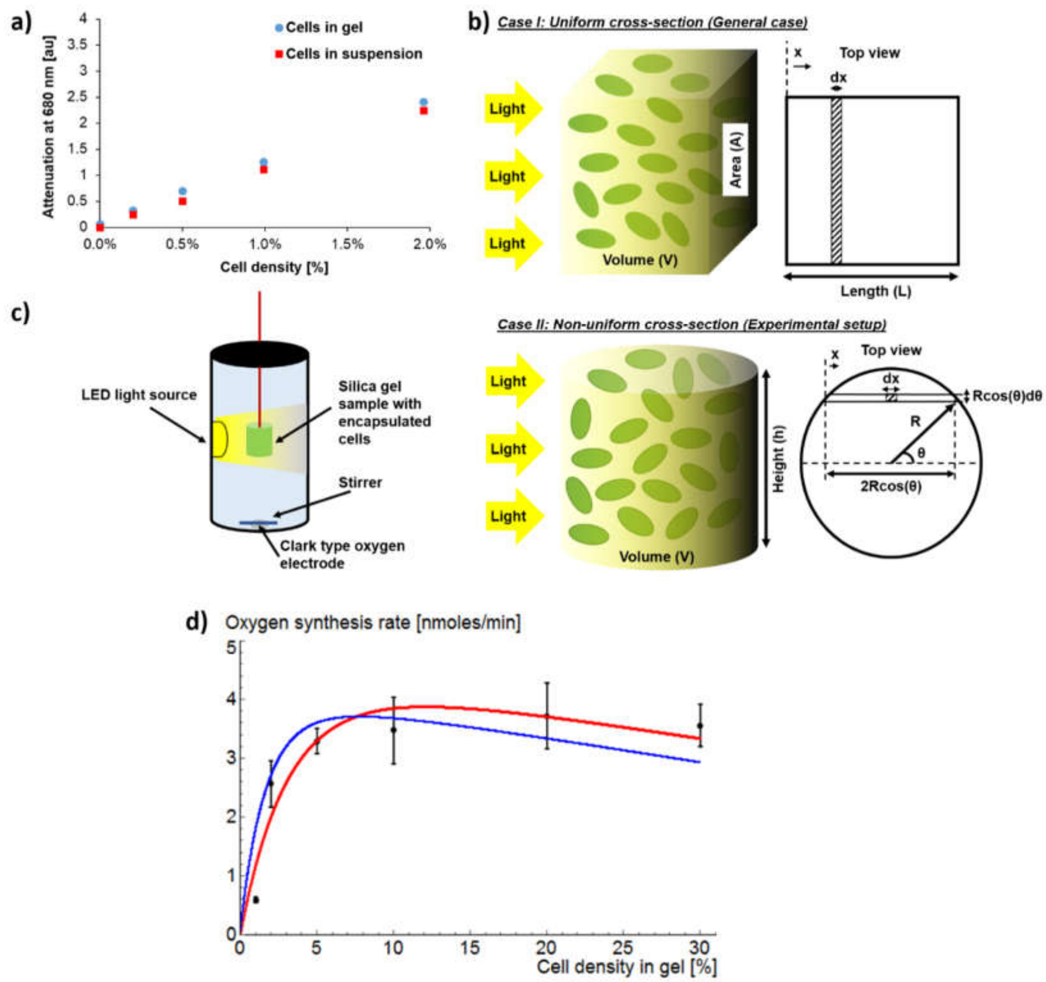

Figure 36 - Modeling the oxygen generation rate of the silica gel encapsulated PCC 7942. Light attenuation in the matrix by the silica gel material and encapsulated cells was characterized using UV-Vis spectroscopy. Modeling results were experimentally verified by measuring oxygen generation rate of encapsulated cells with varying cell density. a) Light attenuation in freely suspended in PBS (red) and silica gel encapsulated cells (blue), b) Model schematic illustrating the light attenuation in two different gel geometries with encapsulated cells, c) Experiment setup (Oxygraph) used for oxygen generation or consumption rate measurements with encapsulated cells, d) Experimental measurements of oxygen generation rate of silica gel encapsulated PCC 7942 (black diamonds), and model results with (red curve) and without (blue curve) light back-scattering effects (All error bars indicate standard deviation, n > 3).

6.3.3 Optimization of the co-encapsulation matrix

We initially hypothesized that oxygenation via co-encapsulated cyanobacterial cells (PCC 7942) is not only a sufficient, but also a more efficient way to provide oxygen for the biotransformation reactions. In mechanical aeration systems, oxygen needs to partition into water, diffuse in the bulk liquid, get into the encapsulation matrix and reach the biotransforming bacteria. We proposed that co-encapsulation with PCC 7942 enables oxygen generation in close vicinity of the biotransforming bacteria, eliminating this transport barrier. In order to illustrate the proximity of co-encapsulated cells in the gel matrix, confocal microscopy images were taken at two different ratios of PCC 7942 and NCIB 9816 (10%:10% [v/v] and 10%:1% [v/v]) (Figure 37a). These images show that after encapsulation, the bacterial cells were well distributed in the gel, and positioned within a few microns of each other. This result is due to rigorous mixing of the bacterial species prior to encapsulation, which is important for obtaining a homogeneous distribution.

The goal of the optimization study was to maximize the biotransformation of naphthalene to CO_2 using the silica gel co-encapsulation system (PCC 7942 and NCIB 9816). Modeling (in the previous section) showed that maximum oxygen generation rate was achieved at a critical PCC 7942 cell density: $\rho_c = \rho_{cr}$. In the case of a co-encapsulation system, bacterial species other than PCC 7942 also contribute to the light attenuation. Thus, the model developed in the previous section had to be modified to incorporate the cell density of NCIB 9816 (ρ_n). For simplicity, we assumed that both species have the same light attenuation characteristics based on their similar size and shape, as observed by confocal microscopy. Thus, ρ_c term in equation (6) was replaced by the total cell density $\boldsymbol{\rho_T}$, and then the total net oxygen generation rate for box and cylindrical volume cases were obtained by inserting into equation (4a-b):

$$\dot{Q} = \int_{x=0}^{x=L} (\underbrace{k_{gen}\rho_C exp\left(\frac{-(C_1\,\rho_T + C_0)}{C_S}x\right)}_{I} \underbrace{-k_{con}\rho_C}_{II} \underbrace{-k_{deg}\rho_N}_{III})A\,dx \quad (\mathbf{7a})$$

$$\dot{Q} = 2\int_{\theta=0}^{\theta=\pi/2}\int_{x=0}^{x=2Rcos(\theta)} (\underbrace{k_{gen}\rho_C exp\left(\frac{-(C_1\,\rho_T + C_0)}{C_S}x\right)}_{I} \underbrace{-k_{con}\rho_C}_{II} \underbrace{-k_{deg}\rho_N}_{III})R\,cos(\theta)\,h\,dx\,d\theta \quad (\mathbf{7b})$$

In equation (7a-b), (I), (II) and (III) represent the oxygen generation by PCC 7942, oxygen consumption by PCC 7942, and oxygen consumption during aerobic transformation by the NCIB 9816, respectively. We proposed that this system should be designed to have neither oxygen surplus (i.e. wasting oxygen that could be used for biotransformation) nor oxygen deficit (i.e. increasing the light attenuation in the gel and cost of the system by encapsulating more NCIB 9816 which cannot contribute to biotransformation). This design requirement was satisfied by solving equation (7a) for $\dot{Q} = 0$ (see Table 11 for experimental parameters), which yielded a non-linear ρ_c vs. ρ_n curve (Figure 37b). It can be seen that ρ_c increased with increasing ρ_n, up to ρ_n = 0.4% [v/v] where a ρ_{cr} value of 40% [v/v] was reached. If ρ_n is increased beyond this critical point, additional PCC 7942 cannot provide more oxygen for the biotransformation reactions, yielding an oxygen deficit ($\dot{Q} < 0$).

It is clear that in order to maximize the biotransformation rate of the system (which was the set optimization goal), the density of PCC 7942 should be set to ρ_{cr}, and the density of NCIB 9816 should be the corresponding ρ_n value which yields $\dot{Q} = 0$. It should be noted that the optimal solution is not the most cost-effective point to operate the system, due to non-linearity of the $\dot{Q} = 0$ curve. Thus, decreasing ρ_c and ρ_n respectively (i.e. moving left on the $\dot{Q} = 0$ curve) would increase the cost-effectiveness of the system. However, this also reduces the biotransformation rate, which may not satisfy the performance requirements.

Based on the experimental parameters selected (See Table 11), the optimal volumetric ratio of NCIB 9816 to PCC 7942 were approximately 1/100 = 0.01. We propose that the efficiency of oxygenation can be calculated by considering a hypothetical case with no light attenuation in the gel (either by the gel or cells), where all the PCC 7942 generate oxygen at the maximum rate ($\mathbf{k_{gen}}$). In such a case, the NCIB 9816 to PCC 7942 cell ratio would be equal to $\mathbf{k_{gen}}/\mathbf{k_{deg}}$ = 721.74/18000 = 0.04. Since 0.04 is the highest that this ratio can be, an efficiency factor (similar to the effectiveness factor in heterogeneous catalysts where the rate is governed by the coupled diffusion/reaction phenomenon) can be calculated as: η = 0.01/0.04 = 25%. This result means that if the cells were co-encapsulated in an extremely thin gel with a single cell layer, one fourth of the encapsulated PCC 7942 would be sufficient to supply the same amount of oxygen. In our experiment setup, the strong hydrophilic interactions between the gel and the glass surface made it difficult to obtain a very thin gel with uniform thickness. Thus, experimental parameters were kept constant despite the low efficiency factor.

Naphthalene biotransformation experiments with silica gel co-encapsulated cells were conducted as shown in Figure 37c. Four cases were tested: I) No cells: Silica gel without cells, II) NCIB 9816: Silica gel encapsulated NCIB 9816, III) NCIB 9816 with air: Silica gel encapsulated

NCIB 9816 with additional headspace which provides additional oxygen for biotransformation reactions and IV) NCIB 9816 with PCC 7942: Silica gel co-encapsulated NCIB 9816 and PCC 7942. Based on oxygen consumption experiments of a scaled-down system (data not shown), the point where the dissolved oxygen concentration in the solution was expected to be depleted was approximately 4 hours. Thus, the time points were selected as 4 and 24 hours for the naphthalene biotransformation experiment. In Case I, naphthalene concentration decreased only slightly over 24 hours (Figure 37d), verifying that the disappearance of naphthalene due to effects other than biotransformation was minimal. For cases II, III and IV, naphthalene concentrations were comparable after 4 hours at 52.3 ± 4.1%, 49.8 ± 10.9% and 43.9 ± 7.6% respectively. These values indicated that when a sufficient amount of dissolved oxygen was present in the solution, oxygen generation by encapsulated cyanobacteria did not make a difference. At 24 hours, the naphthalene concentrations in cases II and III were still comparable, whereas the naphthalene concentration for case IV was measured as 16.3 ± 2.3%, which was significantly lower than cases II and III. This indicated that dissolved oxygen was depleted in solution sometime between 4 and 24 hours, and after the depletion of dissolved oxygen, PCC 7942 provided oxygen to further drive the biotransformation reactions.

Experimental results also verified that oxygenation via co-encapsulated PCC 7942 (Case IV) was more efficient than providing oxygen via diffusion from a headspace (Case III). It is possible that an aeration system which provides air directly into the solution (e.g. bubbling) could perform better than Case III, since it eliminates the partitioning limitation of oxygen from air to solution. However, this condition was not tested since naphthalene is a very volatile chemical and ensuring that it would stay in the solution in an open system was not feasible. In our experiment, approximately 60% to 70% of the naphthalene was transformed with the amount of dissolved oxygen in water (Case II, Figure 37d). Dissolved oxygen in water at room temperature (260 µM) can be utilized to transform approximately 15% of a saturated (246 µM) naphthalene solution into CO_2 (based on 7.5 moles of O_2 per mole of naphthalene as previously reported [147]). This suggests that some partial transformation of naphthalene to intermediate species occurred without complete transformation.

Densities of PCC 7942 and NCIB 9816 were optimized based on their activity immediately after encapsulation, thus the biotransformation activity of the system was measured in a short time period (24 hours). It is known that the activity of encapsulated bacteria can vary over time, even when the cells' growth in the encapsulation matrix is restricted [28]. In addition, in our particular case a long term mutualistic relationship is expected to form between PCC 7942 and NCIB 9816, since CO_2 is essential for carbon fixation by PCC 7942. Thus, oxygen generation by PCC 7942 will be regulated by the biotransformation rate of NCIB 9816, and vice versa. While the long-term optimization problem was not explored in this study, a method to address this issue would be to encapsulate different species separately, measure their activity over time, and optimize the co-encapsulated cell densities based on the time average of individual species' activity. However, this method cannot account for any mutualistic relationship between the co-encapsulated species, as previously discussed.

6.4 Conclusion

In this study we demonstrated that silica gel co-encapsulation of different bacterial species is a feasible method for synergistic biotransformation. This technology has various immediate applications in chemical synthesis and environmental remediation, but could also be used for biosensing. The potential to use silica gel encapsulated bacteria as biosensors is reported in the literature [150, 151], and co-encapsulation of multiple species can amplify this potential. We expect that co-encapsulated species could either act as a supporting organism to the prime sensory species, or work successively to biotransform a sensory input (e.g. chemical) into a signal (e.g. light). This technology could also be utilized as a platform to study fundamental microbial behavior. It has been long known that bacteria can act as a community via quorum sensing, and more recently interspecies quorum sensing was reported [152]. Co-encapsulation could provide a unique method to study this communication by enabling precise adjustment of bacterial communities' volume and proximity.

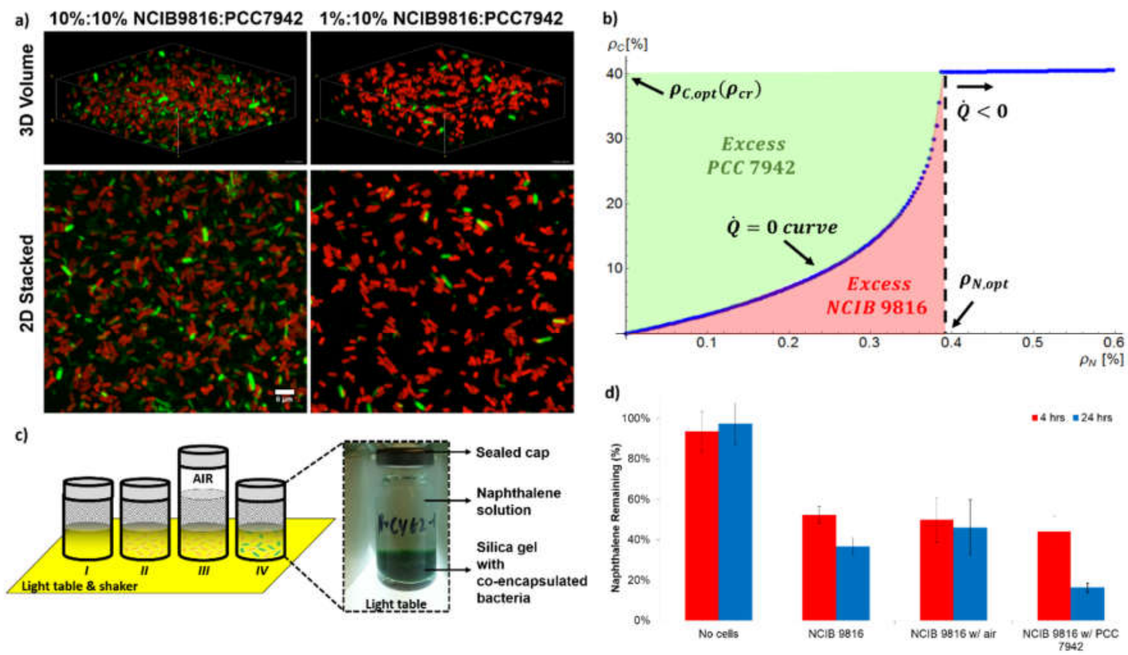

Figure 37 - Synergistic biotransformation by silica gel co-encapsulated NCIB 9816 and PCC 7942. a) Confocal images of silica gel co-encapsulated PCC 7942 (red) and NCIB 9816 (green) cells. Both species are homogeneously distributed in the silica gel matrix and positioned in micron-scale proximity. b) Cell densities of PCC 7942 (ρ_c) and NCIB 9816 (ρ_n) optimized for the experimental setup of the biotransformation experiment. $\dot{Q} = 0$ curve indicates the optimal operation conditions where the system has neither an oxygen deficit or surplus. The maximum biotransformation rate is achieved at $\rho_c = \rho_{cr}$ and corresponding ρ_n on the $\dot{Q} = 0$ curve c) Schematic of the experiment setup used for biotransformation of naphthalene. Four cases were tested: I) No cells (Negative control), II) NCIB 9816 (Oxygen is limited to the dissolved oxygen in solution) , III) NCIB 9816 with headspace (Additional oxygen is provided via the air in the headspace), IV) NCIB 9816 with PCC 7942 (Additional oxygen is provided by the co-encapsulated PCC 7942) d) Results of the naphthalene biotransformation experiment. NCIB 9816 with co-encapsulated PCC 7942 achieved the highest biotransformation ratio (All error bars indicate standard deviation, n = 3).

Table 10 – Oxygen generation rate model parameters

Symbol	Definition	Value	Units	Notes
$\mathbf{k_{gen}}$	O_2 generation rate constant per unit volume of PCC 7942 per s at 100% light intensity	721.74	nmoles/ (min-mL cells)	Evaluated by fitting experimental data into the developed model
$\mathbf{k_{con}}$	O_2 consumption rate constant per unit volume of PCC 7942 per s	22.1 ± 1.7	nmoles/ (min-mL cells)	Experimentally measured via Oxygraph
$\mathbf{k_{deg}}$	O_2 consumption rate constant during naphthalene transformation per unit volume of NCIB 9816 per s	~18,000	nmoles/ (min-mL cells)	Adapted from Sakkos *et al.* [147]
$\boldsymbol{\rho_T}$, ρ_c, ρ_n	Cell density (T: Total, C: PCC 7942, N: NCIB 9816)	Varies	mL cells/ (mL (gel) volume) % [v/v] *	ρ_c, ρ_n: Known $\boldsymbol{\rho_T} = \rho_c + \rho_n$
$\mathbf{C_0}$, $\mathbf{C_1}$, $\mathbf{C_s}$	Constants for contribution of cells ($\mathbf{C_0}$), silica gel ($\mathbf{C_1}$), and back-scattering effects (CS) to light attenuation	$\mathbf{C_0} = 0.089$, $\mathbf{C_1} = 116.42$, $C_s = 1.88$	[1/cm], [mL/(mL cells-cm], [dimensionless]	$\mathbf{C_0}$, $\mathbf{C_1}$: Experimentally measured via UV-Vis spectroscopy Cs: Evaluated using the model

*Cell volume (mL cells) was equal to the volume of PBS suspended cells. See methods for details of wet cell mass in a given cell volume.

Table 11 – Experimental parameters for: a) Oxygen generation and consumption (Oxygraph), and b) Naphthalene biotransformation

	Definition	Unit	Oxygen generation and consumption (Oxygraph)	Naphthalene biotransformation
V	Volume of sample(s)	mL	0.2	0.5
R	Radius of sample(s)	cm	0.32	-
H or L	Height or Length of sample(s)	cm	0.62	0.15
A	Cross-sectional area of samples(s)	cm2	-	3.46

Chapter 7: Research Summary

In this dissertation, studies were undertaken to develop a water bioremediation system which utilizes silica gel encapsulated biodegrading (biotransforming) bacteria. Various silica gels were developed, and evaluated in terms of the resulting materials' physicochemical properties, as well as commercial scalability of the approach and long term biotransformation activity. An optimization method based on biodegradation/transport modeling was proposed to determine the bacterial loading and size of the material based on the application. Long-term storage of the material was studied to improve the shelf life of the material and facilitate its use in real-world water treatment applications. Large-scale synthesis methods based on electrospinning were investigated to eliminate the diffusion barrier of substrates to cells and enable industry scale production of the material. A synergistic biotransformation system with multiple co-encapsulated bacterial species is also investigated. Significant results of this work are summarized in this chapter.

In Chapter 2, a method is presented for encapsulation of bacterial biocatalysts in silica gels formed by silica nanoparticles (SNP) and a silicon alkoxide crosslinker. Formulation of the gel was optimized by changing the SNP size, SNP to crosslinker ratio and crosslinker functionality. Hydrolysis and condensation reactions of silicon alkoxide were controlled by water to alkoxide ratio (r) and pH of the solution. FTIR analysis was used to verify that a reactive and temporally stable silicon alkoxide crosslinker was obtained. As a case study, recombinant *Escherichia coli* (*E. coli*) cells expressing atrazine dechlorinating enzyme AtzA were encapsulated. Synthesized bioreactive materials (silica gel encapsulated bacterial biocatalysts) were evaluated based on their gelation time, biocatalytic activity and mechanical strength. Diffusivity assays and SEM were used for characterization of the gel structure. It was found that SNP to crosslinker ratio affected all the evaluation features, whereas crosslinker functionality primarily affected gelation time and SNP size affected the mechanical strength and diffusivity. Based on systematic evaluation, three gel formulations were selected and subjected them to long-term activity assay in a continuous-flow bioreactor for removing trace levels of atrazine. The effluent atrazine concentration was sustained below 30% of the influent concentration, < 3 ppb, for 2 months.

In Chapter 3, a 3-step design and optimization method is presented for a bioremediation system utilizing silica gel encapsulated whole-cell biocatalyst. Characterization experiments were conducted to determine the parameters of a steady state reaction/diffusion model for encapsulated AtzA biocatalyst that was subsequently verified experimentally. Dimensionless numbers governing the reaction rate, the Thiele modulus (Φ) and effectiveness factor (η), were evaluated based on the design parameters of the material, ρ (cell loading density) and L_c (characteristic length). Mechanical properties of the gel were determined as a function of ρ. Optimal values for ρ and L_c were determined for a case study, based on biocatalytic performance, mechanical properties and cost. It was found that free biocatalyst reaction kinetics are first order with k'free = 7.38 x 10-2 s-1/(g cells/mL) and diffusivity of atrazine in the gel increases with ρ, from 3.51 x 10-4 mm2/s up to 6.93 x 10-4 mm2/s. Modeling results showed that ~20% of activity was lost during encapsulation. Diffusion limitations became significant ($\Phi > 1$) when L_c exceeded 0.1-0.3 mm. The optimal catalyst radius and cell loading density were determined to be $L_c = 0.2$ mm and $\rho = 0.11$ g cells/mL gel, for an atrazine bioremediation setup with a desired effluent < 3 ppb.

In Chapter 4, different drying conditions for a silica gel encapsulated bacterial biocatalyst (atrazine biodegrading *Escherichia coli*) were studied to enhance mechanical properties while sustaining long-term biocatalytic activity of the bacteria. Drying after encapsulation is desirable to enhance the strength of the gel and to make it lighter, facilitating its use, storage and transportation. However, preserving biological activity of the cells in a desiccated state remains a formidable challenge. Effects of lyoprotectant solutions containing 0.4M sucrose, 0.4M trehalose or 30% (wt/wt) glycerol on the activity of the encapsulated bacteria during drying were investigated. It was determined that two orders of magnitude increase in the elastic modulus (E) and the compressive stress at failure (σ) of the gel could be achieved by drying, independent of the drying rate. It was shown that partially desiccated silica gels preserved and enhanced the biocatalytic activity of the encapsulated bacteria up to a critical drying level. Atrazine biodegradation activity of encapsulated bacteria suspended with 0.4M sucrose and PBS increased with increasing water removal, reaching a maximum at 68% water loss. This enhanced activity was sustained for three months, when the gels were stored at 4°C.

In Chapter 5, an electrospinning method is discussed for manufacturing low cost, highly flexible and water insoluble bioreactive membranes. *E. coli* cells were encapsulated in reactive membranes comprised of electrospun nanofibers that have biocompatible polyvinyl alcohol (PVA)-based cores entrapping the *E. coli* and silica-based, mechanically sturdy porous shells. The reactive membranes were produced in a continuous fashion using a coaxial electrospinning system coupled to a microfluidic timer that mixed and regulated the reaction time of the silica precursor and the PVA solution streams. A factorial design method was employed to investigate the effects of the three critical design parameters of the system (the flow rate of the core solution, protrusion of the core needle, and the viscosity of the core solution) and to optimize these parameters for reproducibly and continuously producing high-quality core/shell nanofibers. The feasibility of using the reactive membranes manufactured in this fashion for bioremediation of atrazine, an herbicide, was also investigated. The atrazine degradation rate (0.24 µmol / g of *E. coli* / min) of the encapsulated *E. coli* cells expressing the atrazine-dechlorinating enzyme AtzA was measured to be relatively close to that measured with the free cells in solution (0.64 µmol / g of *E. coli* / min).

In Chapter 6, a co-encapsulation method is investigated for synergistically working bacterial populations in an optically transparent silica gel matrix. Bacterial species working synergistically can perform a larger variety of more complex chemical biotransformation reactions than a pure culture. Typically, bacteria are able to grow in bioreactors, which leads to an unbalanced, suboptimal population ratio with multiple species due to competition over resources, predation and *etc*. Two different species: *Pseudomonas sp.* NCIB 9816 and *Synechococcus elongatus* PCC 7942 were co-encapsulated. NCIB 9816 can aerobically transform over 100 aromatic hydrocarbons, which can be used for synthesis of commodity chemicals and environmental remediation of water and soil. In our system, NCIB 9816 was used for biotransformation of naphthalene (a model polycyclic aromatic hydrocarbon) into CO_2 and cyanobacterium PCC 7942 was used to provide the necessary oxygen for the biotransformation reactions via photosynthesis. The developed silica gel was a cytocompatible, mechanically robust (Elastic modulus > 8 MPa) and optically transparent (~4% transmittance loss per mm) material. The oxygen generation rate of encapsulated PCC 7942 cells was modeled, revealing a critical cell density parameter which maximized oxygen production. This model was then used to optimize the system and maximize biotransformation efficiency. Experimental results showed that the co-encapsulation system not only sustained the biotransformation reactions, but also performed better than oxygenation by external supplementation. It is proposed that this was due to micron-scale proximity of the co-encapsulated bacteria in the gel, which was verified by confocal microscopy.[153, 154]

Chapter 8: References

1. Walcarius, A.; Mercier, L., Mesoporous organosilica adsorbents: nanoengineered materials for removal of organic and inorganic pollutants. *Journal of Materials Chemistry* **2010,** *20* (22), 4478-4511. DOI: 10.1039/b924316j.

2. Macias-Flores, A.; Tafoya-Garnica, A.; Ruiz-Ordaz, N.; Salmeron-Alcocer, A.; Juarez-Ramirez, C.; Ahuatzi-Chacon, D.; Mondragon-Parada, M. E.; Galindez-Mayer, J., Atrazine biodegradation by a bacterial community immobilized in two types of packed-bed biofilm reactors. *World Journal of Microbiology & Biotechnology* **2009,** *25* (12), 2195-2204. DOI: 10.1007/s11274-009-0125-0.

3. Martín-Gullón, I.; Font, R., Dynamic pesticide removal with activated carbon fibers. *Water Research* **2001,** *35* (2), 516-520. DOI: 10.1016/s0043-1354(00)00262-1.

4. Fernandez, P.; Vilanova, R. M.; Martinez, C.; Appleby, P.; Grimalt, J. O., The historical record of atmospheric pyrolytic pollution over Europe registered in the sedimentary PAH from remote mountain lakes. *Environmental Science & Technology* **2000,** *34* (10), 1906-1913. DOI: 10.1021/es9912271.

5. Patel, A. C.; Li, S. X.; Yuan, J. M.; Wei, Y., In situ encapsulation of horseradish peroxidase in electrospun porous silica fibers for potential biosensor applications. *Nano Letters* **2006,** *6* (5), 1042-1046. DOI: 10.1021/nl0604560.

6. Wu, X. J.; Choi, M. M. F., An optical glucose biosensor based on entrapped-glucose oxidase in silicate xerogel hybridised with hydroxyethyl carboxymethyl cellulose. *Analytica Chimica Acta* **2004,** *514* (2), 219-226. DOI: 10.1016/j.aca.2004.03.052.

7. Dickson, D. J.; Page, C. J.; Ely, R. L., Photobiological hydrogen production from Synechocystis sp PCC 6803 encapsulated in silica sol-gel. *International Journal of Hydrogen Energy* **2009,** *34* (1), 204-215. DOI: 10.1016/j.ijhydene.2008.10.021.

8. Margaritis, A.; Kilonzo, P. M., Production of Ethanol Using Immobilised Cell Bioreactor Systems

Applications of Cell Immobilisation Biotechnology. Nedović, V.; Willaert, R., Eds. Springer Netherlands: 2005; Vol. 8B, pp 375-405. DOI: 10.1007/1-4020-3363-x_22.

9. Brinker, C. J.; Scherer, G. W., *Sol-gel science: the physics and chemistry of sol-gel processing*. Academic Press: 1990.

10. Kandimalla, V. B.; Tripathi, V. S.; Ju, H., Immobilization of biomolecules in sol-gels: Biological and analytical applications. *Critical Reviews in Analytical Chemistry* **2006,** *36* (2), 73-106. DOI: 10.1080/10408340600713652.

11. Shchipunov, Y. A.; Karpenko, T. Y.; Bakunina, L. Y.; Burtseva, Y. V.; Zvyagintseva, T. N., A new precursor for the immobilization of enzymes inside sol-gel-derived hybrid silica nanocomposites containing polysaccharides. *Journal of Biochemical and Biophysical Methods* **2004,** *58* (1), 25-38. DOI: 10.1016/s0165-022x(03)00108-8.

12. Ferrer, M. L.; Garcia-Carvajal, Z. Y.; Yuste, L.; Rojo, F.; del Monte, F., Bacteria viability in sol-gel materials revisited: Cryo-SEM as a suuitable tool to study the structural integrity of encapsulated bacteria. *Chemistry of Materials* **2006,** *18* (6), 1458-1463. DOI: 10.1021/cm0522275.

13. Rooke, J. C.; Leonard, A.; Su, B. L., Targeting photobioreactors: Immobilisation of cyanobacteria within porous silica gel using biocompatible methods. *Journal of Materials Chemistry* **2008,** *18* (12), 1333-1341. DOI: 10.1039/b717990a.

14. Avnir, D.; Coradin, T.; Lev, O.; Livage, J., Recent bio-applications of sol-gel materials. *Journal of Materials Chemistry* **2006,** *16* (11), 1013-1030. DOI: 10.1039/b512706h.

15. Nassif, N.; Roux, C.; Coradin, T.; Rager, M. N.; Bouvet, O. M. M.; Livage, J., A sol-gel matrix to preserve the viability of encapsulated bacteria. *Journal of Materials Chemistry* **2003,** *13* (2), 203-208. DOI: 10.1039/b210167j.

16. Lesot, P.; Chapuis, S.; Bayle, J. P.; Rault, J.; Lafontaine, E.; Campero, A.; Judeinstein, P., Structural-dynamical relationship in silica PEG hybrid gels. *Journal of Materials Chemistry* **1998,** *8* (1), 147-151. DOI: 10.1039/a704983h.

17. Coiffier, A.; Coradin, T.; Roux, C.; Bouvet, O. M. M.; Livage, J., Sol-gel encapsulation of bacteria: a comparison between alkoxide and aqueous routes. *Journal of Materials Chemistry* **2001,** *11* (8), 2039-2044. DOI: 10.1039/b101308o.

18. Nassif, N.; Coiffier, A.; Coradin, T.; Roux, C.; Livage, J.; Bouvet, O., Viability of bacteria in hybrid aqueous silica gels. *Journal of Sol-Gel Science and Technology* **2003,** *26* (1-3), 1141-1144. DOI: 10.1023/a:1020727311786.

19. Bhatia, S. R.; Khattak, S. F.; Roberts, S. C., Polyelectrolytes for cell encapsulation. *Current Opinion in Colloid & Interface Science* **2005,** *10* (1–2), 45-51. DOI: 10.1016/j.cocis.2005.05.004.

20. Orive, G.; Hernández, R. M.; Gascón, A. R.; Pedraz, J. L., Challenges in Cell Encapsulation

Applications of Cell Immobilisation Biotechnology. Nedović, V.; Willaert, R., Eds. Springer Netherlands: 2005; Vol. 8B, pp 185-196. DOI: 10.1007/1-4020-3363-x_10.

21. Meunier, C. F.; Dandoy, P.; Su, B.-L., Encapsulation of cells within silica matrixes: Towards a new advance in the conception of living hybrid materials. *Journal of Colloid and Interface Science* **2010,** *342* (2), 211-224. DOI: 10.1016/j.jcis.2009.10.050.

22. Muzzarelli, R.; Baldassarre, V.; Conti, F.; Ferrara, P.; Biagini, G.; Gazzanelli, G.; Vasi, V., BIOLOGICAL-ACTIVITY OF CHITOSAN - ULTRASTRUCTURAL-STUDY. *Biomaterials* **1988,** *9* (3), 247-252. DOI: 10.1016/0142-9612(88)90092-0.

23. White, I. D.; Mottershead, D. N.; Harrison, D. S. J., *Environmental Systems: An Introductory Text*. Thornes: 2004.

24. Perry, C. C.; Keeling-Tucker, T., Biosilicification: the role of the organic matrix in structure control. *Journal of Biological Inorganic Chemistry* **2000,** *5* (5), 537-550. DOI: 10.1007/s007750000130.

25. Snyder, M. A.; Demirgoz, D.; Kokkoli, E.; Tsapatsis, M., Benign, 3D encapsulation of sensitive mammalian cells in porous silica gels formed by Lys-Sil nanoparticle assembly. *Microporous and Mesoporous Materials* **2009,** *118* (1-3), 387-395. DOI: 10.1016/j.micromeso.2008.09.013.

26. Nieto, A.; Areva, S.; Wilson, T.; Viitala, R.; Vallet-Regi, M., Cell viability in a wet silica gel. *Acta Biomaterialia* **2009,** *5* (9), 3478-3487. DOI: 10.1016/j.actbio.2009.05.033.

27. Rooke, J. C.; Leonard, A.; Su, B.-L., Targeting photobioreactors: Immobilisation of cyanobacteria within porous silica gel using biocompatible methods. *Journal of Materials Chemistry* **2008,** *18* (12), 1333-1341. DOI: 10.1039/b717990a.

28. Nassif, N.; Bouvet, O.; Rager, M. N.; Roux, C.; Coradin, T.; Livage, J., Living bacteria in silica gels. *Nature Materials* **2002,** *1* (1), 42-44. DOI: 10.1038/nmat709.

29. Goldstein, D. B., EFFECT OF ALCOHOL ON CELLULAR MEMBRANES. *Annals of Emergency Medicine* **1986,** *15* (9), 1013-1018. DOI: 10.1016/s0196-0644(86)80120-2.

30. Ferrer, M. L.; Yuste, L.; Rojo, F.; del Monte, F., Biocompatible sol-gel route for encapsulation of living bacteria in organically modified silica matrixes. *Chemistry of Materials* **2003,** *15* (19), 3614-3618. DOI: 10.1021/cm034372t.

31. Conroy, J. F. T.; Power, M. E.; Martin, J.; Earp, B.; Hosticka, B.; Daitch, C. E.; Norris, P. M., Cells in Sol-Gels I: A Cytocompatible Route for the Production of Macroporous Silica Gels. *Journal of Sol-Gel Science and Technology* **2000,** *18* (3), 269-283. DOI: 10.1023/a:1008704208324.

32. Jaroch, D.; McLamore, E.; Zhang, W.; Shi, J.; Garland, J.; Banks, M. K.; Porterfield, D. M.; Rickus, J. L., Cell-Mediated Deposition of Porous Silica on Bacterial Biofilms. *Biotechnology and Bioengineering* **2011,** *108* (10), 2249-2260. DOI: 10.1002/bit.23195.

33. Reátegui, E.; Reynolds, E.; Kasinkas, L.; Aggarwal, A.; Sadowsky, M.; Aksan, A.; Wackett, L., Silica gel-encapsulated AtzA biocatalyst for atrazine biodegradation. *Applied Microbiology and Biotechnology*, 1-10. DOI: 10.1007/s00253-011-3821-2.

34. Fennouh, S.; Guyon, S.; Jourdat, C.; Livage, J.; Roux, C., Encapsulation of bacteria in silica gels. *Comptes Rendus De L Academie Des Sciences Serie Ii Fascicule C-Chimie* **1999,** *2* (11-13), 625-630. DOI: 10.1016/s1387-1609(00)88575-8.

35. Jang, E.; Park, S.; Park, S.; Lee, Y.; Kim, D.-N.; Kim, B.; Koh, W.-G., Fabrication of poly(ethylene glycol)-based hydrogels entrapping enzyme-immobilized silica nanoparticles. *Polymers for Advanced Technologies* **2010,** *21* (7), 476-482. DOI: 10.1002/pat.1455.

36. Perullini, M.; Rivero, M. M.; Jobbagy, M.; Mentaberry, A.; Blimes, S. A., Plant cell proliferation inside an inorganic host. *Journal of Biotechnology* **2007,** *127* (3), 542-548. DOI: 10.1016/j.jbiotec.2006.07.024.

37. Ralph, K. I., *The chemistry of silica: solubility, polymerization, colloid and surface properties, and biochemistry*. Wiley: 1979.

38. Chujo, Y.; Saegusa, T., Organic polymer hybrids with silica gel formed by means of the sol-gel method

Macromolecules: Synthesis, Order and Advanced Properties. Springer Berlin / Heidelberg: 1992; Vol. 100, pp 11-29. DOI: 10.1007/BFb0051634.

39. Leonard, A.; Rooke, J. C.; Meunier, C. F.; Sarmento, H.; Descy, J.-P.; Su, B.-L., Cyanobacteria immobilised in porous silica gels: exploring biocompatible synthesis routes for the development of photobioreactors. *Energy & Environmental Science* **2010,** *3* (3), 370-377. DOI: 10.1039/b923859j.

40. Nassif, N.; Livage, J., From diatoms to silica-based biohybrids. *Chemical Society Reviews* **2011,** *40* (2), 849-859. DOI: 10.1039/c0cs00122h.

41. Oh, C. Y.; Park, J. K., The characteristics of encapsulated whole cell beta-galactosidase. *Bioprocess Engineering* **1998,** *19* (6), 419-425. DOI: 10.1007/pl00009027.

42. Finnie, K. S.; Bartlett, J. R.; Woolfrey, J. L., Encapsulation of sulfate-reducing bacteria in a silica host. *Journal of Materials Chemistry* **2000,** *10* (5), 1099-1101. DOI: 10.1039/a909350h.

43. Perullini, M.; Amoura, M.; Roux, C.; Coradin, T.; Livage, J.; Laura Japas, M.; Jobbagy, M.; Bilmes, S. A., Improving silica matrices for encapsulation of *Escherichia coli* using osmoprotectors. *Journal of Materials Chemistry* **2011,** *21* (12), 4546-4552. DOI: 10.1039/c0jm03948a.

44. Organization, W. H. Atrazine and Its Metabolites in Drinking-water. http://www.who.int/water_sanitation_health/dwq/chemicals/dwq_background_20100701_en.pdf (accessed 6/3).

45. Agency, U. S. E. P. Interpreting the Atrazine Drinking Water Monitoring Data. http://www.epa.gov/oppsrrd1/reregistration/atrazine/atrazine_update.htm (accessed 6/3).

46. Zhu, L.; Ma, T.; Wang, J.; Xie, H.; Wang, J.; Xin, C.; Shao, B., Enhancement of Atrazine Removal by Free and Immobilized Arthrobacter Sp HB-5 in Soil and Wastewater. *Soil & Sediment Contamination* **2011,** *20* (1), 87-97. DOI: 10.1080/15320383.2011.528466.

47. Patricia Galindez-Najera, S.; Ramos-Monroy, O.; Ruiz-Ordaz, N.; Salmeron-Alcocer, A.; Juarez-Ramirez, C.; Ahuatzi-Chacon, D.; Curiel-Quesada, E.; Galindez-Mayer, J., Simultaneous degradation of atrazine and simazine by a binary culture of Stenotrophomonas maltophilia and Arthrobacter sp in a two-stage biofilm reactor. *Journal of Chemical Technology and Biotechnology* **2011,** *86* (4), 554-561. DOI: 10.1002/jctb.2550.

48. Liu, C.; Huang, X.; Wang, H., Start-up of a membrane bioreactor bioaugmented with genetically engineered microorganism for enhanced treatment of atrazine containing wastewater. *Desalination* **2008,** *231* (1-3), 12-19. DOI: 10.1016/j.desal.2007.11.034.

49. Klein, S.; Avrahami, R.; Zussman, E.; Beliavski, M.; Tarre, S.; Green, M., Encapsulation of *Pseudomonas sp* ADP cells in electrospun microtubes for atrazine bioremediation. *Journal of Industrial Microbiology & Biotechnology* **2012,** *39* (11), 1605-1613. DOI: 10.1007/s10295-012-1164-3.

50. Buttiglieri, G.; Migliorisi, L.; Malpei, F., Adsorption and removal at low atrazine concentration in an MBR pilot plant. *Water Science and Technology* **2011,** *63* (7), 1334-1340. DOI: 10.2166/wst.2011.130.

51. Reategui, E.; Reynolds, E.; Kasinkas, L.; Aggarwal, A.; Sadowsky, M. J.; Aksan, A.; Wackett, L. P., Silica gel-encapsulated AtzA biocatalyst for atrazine biodegradation. *Applied Microbiology and Biotechnology* **2012,** *96* (1), 231-240. DOI: 10.1007/s00253-011-3821-2.

52. deSouza, M. L.; Sadowsky, M. J.; Wackett, L. P., Atrazine chlorohydrolase from *Pseudomonas sp* strain ADP: Gene sequence, enzyme purification, and protein characterization. *Journal of Bacteriology* **1996,** *178* (16).

53. Brinker, C. J., HYDROLYSIS AND CONDENSATION OF SILICATES - EFFECTS ON STRUCTURE. *Journal of Non-Crystalline Solids* **1988,** *100* (1-3), 31-50. DOI: 10.1016/0022-3093(88)90005-1.

54. Siouffi, A. M., Silica gel-based monoliths prepared by the sol-gel method: facts and figures. *Journal of Chromatography A* **2003,** *1000* (1-2), 801-818. DOI: 10.1016/s0021-9673(03)00510-7.

55. Bird, R. B.; Stewart, W. E.; Lightfoot, E. N., *Transport Phenomena*. Wiley: 2007.

56. Innocenzi, P.; Abdirashid, M. O.; Guglielmi, M., Structure and properties of sol-gel coatings from methyltriethoxysilane and tetraethoxysilane. *Journal of Sol-Gel Science and Technology* **1994,** *3* (1), 47-55. DOI: 10.1007/BF00490148.

57. Snyder, S. A.; Westerhoff, P.; Yoon, Y.; Sedlak, D. L., Pharmaceuticals, personal care products, and endocrine disruptors in water: Implications for the water industry. *Environmental Engineering Science* **2003,** *20* (5), 449-469. DOI: 10.1089/109287503768335931.

58. Pierre, A. C., The Sol-Gel Encapsulation of Enzymes. *Biocatalysis & Biotransformation* **2004,** *22* (3), 145-170. DOI: 10.1080/10242420412331283314.

59. Perullini, M.; Jobbagy, M.; Mouso, N.; Forchiassin, F.; Bilmes, S. A., Silica-alginate-fungi biocomposites for remediation of polluted water. *Journal of Materials Chemistry* **2010,** *20* (31), 6479-6483. DOI: 10.1039/c0jm01144d.

60. Branyik, T.; Kuncova, G.; Paca, J.; Demnerova, K., Encapsulation of microbial cells into silica gel. *Journal of Sol-Gel Science and Technology* **1998,** *13* (1-3), 283-287. DOI: 10.1023/a:1008655623452.

61. Pannier, A.; Mkandawire, M.; Soltmann, U.; Pompe, W.; Bottcher, H., Biological activity and mechanical stability of sol-gel-based biofilters using the freeze-gelation technique for immobilization of Rhodococcus ruber. *Applied Microbiology and Biotechnology* **2012,** *93* (4), 1755-1767. DOI: 10.1007/s00253-011-3489-7.

62. Kaul, P.; Banerjee, A.; Banerjee, U. C., Stereoselective nitrile hydrolysis by immobilized whole-cell biocatalyst. *Biomacromolecules* **2006,** *7* (5), 1536-1541. DOI: 10.1021/bm0507913.

63. Aksu, Z.; Bulbul, G., Determination of the effective diffusion coefficient of phenol in Ca-alginate-immobilized P-putida beads. *Enzyme and Microbial Technology* **1999,** *25* (3-5), 344-348. DOI: 10.1016/s0141-0229(99)00051-4.

64. Chung, T. P.; Tseng, H. Y.; Juang, R. S., Mass transfer effect and intermediate detection for phenol degradation in immobilized Pseudomonas putida systems. *Process Biochemistry* **2003,** *38* (10), 1497-1507. DOI: 10.1016/s0032-9592(03)00038-4.

65. Laca, A.; Quiros, C.; Garcia, L. A.; Diaz, M., Modelling and description of internal profiles in immobilized cells systems. *Biochemical Engineering Journal* **1998,** *1* (3), 225-232. DOI: 10.1016/s1369-703x(98)00005-9.

66. Jablonowski, N. D.; Schaeffer, A.; Burauel, P., Still present after all these years: persistence plus potential toxicity raise questions about the use of atrazine. *Environmental Science and Pollution Research* **2011,** *18* (2), 328-331. DOI: 10.1007/s11356-010-0431-y.

67. Tong, H.-W.; Mutlu, B. R.; Wackett, L. P.; Aksan, A., Silica/PVA biocatalytic nanofibers. *Materials Letters* **2013,** *111*, 234-237. DOI: 10.1016/j.matlet.2013.08.102.

68. Mutlu, B. R.; Yeom, S.; Tong, H.-W.; Wackett, L. P.; Aksan, A., Silicon alkoxide cross-linked silica nanoparticle gels for encapsulation of bacterial biocatalysts. *Journal of Materials Chemistry A* **2013,** *1* (36), 11051-11060. DOI: 10.1039/C3TA12303K.

69. Davis, M. E.; Davis, R. J., *Fundamentals of Chemical Reaction Engineering*. Dover Publications: 2012.

70. Jones, J. R.; Rowlands, D. L. G.; Monk, C. B., Diffusion coefficient of water in water and in some alkaline earth chloride solutions at 25° C. *Transactions of the Faraday Society* **1965,** *61*, 1384-1388.

71. Harriott, P., *Chemical Reactor Design*. Taylor & Francis: 2002.

72. Fournier, R. L., *Basic Transport Phenomena in Biomedical Engineering*. Taylor and Francis: 2011.

73. Blondeau, M.; Coradin, T., Living materials from sol-gel chemistry: current challenges and perspectives. *Journal of Materials Chemistry* **2012,** *22* (42), 22335-22343. DOI: 10.1039/c2jm33647b.

74. Bartholomew, C. H., Mechanisms of catalyst deactivation. *Applied Catalysis a-General* **2001,** *212* (1-2), 17-60. DOI: 10.1016/s0926-860x(00)00843-7.

75. Wu, D.; Zhou, J.; Li, Y., Mechanical strength of solid catalysts: Recent developments and future prospects. *Aiche Journal* **2007,** *53* (10), 2618-2629. DOI: 10.1002/aic.11291.

76. Rabinovich, E. M.; Kurkjian, C. R.; Kopylov, N. A.; Fleming, D. A., MECHANICAL STRENGTH OF PARTICULATE SILICA-GELS. *Journal of Materials Science* **1991,** *26* (24), 6685-6692.

77. Mackenzie, J. D.; Huang, Q. X.; Iwamoto, T., Mechanical properties of ormosils. *Journal of Sol-Gel Science and Technology* **1996,** *7* (3), 151-161. DOI: 10.1007/bf00401034.

78. Potts, M., DESICCATION TOLERANCE OF PROKARYOTES. *Microbiological Reviews* **1994,** *58* (4), 755-805.

79. Leslie, S. B.; Israeli, E.; Lighthart, B.; Crowe, J. H.; Crowe, L. M., TREHALOSE AND SUCROSE PROTECT BOTH MEMBRANES AND PROTEINS IN INTACT BACTERIA DURING DRYING. *Applied and Environmental Microbiology* **1995,** *61* (10), 3592-3597.

80. Hubalek, Z., Protectants used in the cryopreservation of microorganisms. *Cryobiology* **2003,** *46* (3), 205-229. DOI: 10.1016/s0011-2240(03)00046-4.

81. Swift, H. F., PRESERVATION OF STOCK CULTURES OF BACTERIA BY FREEZING AND DRYING. *The Journal of experimental medicine* **1921,** *33* (1), 69-75.

82. Krupa, I.; Nedelcev, T.; Racko, D.; Lacik, I., Mechanical properties of silica hydrogels prepared and aged at physiological conditions: testing in the compression mode. *Journal of Sol-Gel Science and Technology* **2010,** *53* (1), 107-114. DOI: 10.1007/s10971-009-2064-5.

83. Sampedro, J. G.; Uribe, S., Trehalose-enzyme interactions result in structure stabilization and activity inhibition. The role of viscosity. *Molecular and Cellular Biochemistry* **2004,** *256* (1-2), 319-327. DOI: 10.1023/B:MCBI.0000009878.21929.eb.

84. Galmarini, M. V.; Baeza, R.; Sanchez, V.; Zamora, M. C.; Chirife, J., Comparison of the viscosity of trehalose and sucrose solutions at various temperatures: Effect of guar gum addition. *Lwt-Food Science and Technology* **2011,** *44* (1), 186-190. DOI: 10.1016/j.lwt.2010.04.021.

85. Luckey, M.; Nikaido, H., SPECIFICITY OF DIFFUSION CHANNELS PRODUCED BY LAMBDA-PHAGE RECEPTOR PROTEIN OF ESCHERICHIA-COLI. *Proceedings of the National Academy of Sciences of the United States of America-Biological Sciences* **1980,** *77* (1), 167-171. DOI: 10.1073/pnas.77.1.167.

86. Wang, Y. F.; Dutzler, R.; Rizkallah, P. J.; Rosenbusch, J. P.; Schirmer, T., Channel specificity: Structural basis for sugar discrimination and differential flux rates in maltoporin. *Journal of Molecular Biology* **1997,** *272* (1), 56-63. DOI: 10.1006/jmbi.1997.1224.

87. Mutlu, B. R.; Yeom, S.; Wackett, L. P.; Aksan, A., Modelling and optimization of a bioremediation system utilizing silica gel encapsulated whole-cell biocatalyst. *Chemical Engineering Journal* **2014**. DOI: http://dx.doi.org/10.1016/j.cej.2014.07.130.

88. de la Llave, E.; Molinero, V.; Scherlis, D. A., Water filling of hydrophilic nanopores. *Journal of Chemical Physics* **2010,** *133* (3). DOI: 10.1063/1.3462964.

89. Alvarez, G. S.; Desimone, M. F.; Diaz, L. E., Immobilization of bacteria in silica matrices using citric acid in the sol-gel process. *Applied Microbiology and Biotechnology* **2007,** *73* (5), 1059-1064. DOI: 10.1007/s00253-006-0580-6.

90. Guillette, L. J., Jr.; Iguchi, T., Life in a Contaminated World. *Science* **2012,** *337* (6102), 1614-1615. DOI: 10.1126/science.1226985.

91. Schwarzenbach, R. P.; Escher, B. I.; Fenner, K.; Hofstetter, T. B.; Johnson, C. A.; von Gunten, U.; Wehrli, B., The challenge of micropollutants in aquatic systems. *Science* **2006,** *313* (5790), 1072-1077. DOI: 10.1126/science.1127291.

92. Bhardwaj, N.; Kundu, S. C., Electrospinning: A fascinating fiber fabrication technique. *Biotechnology Advances* **2010,** *28* (3), 325-347. DOI: 10.1016/j.biotechadv.2010.01.004.

93. Lopez-Rubio, A.; Sanchez, E.; Wilkanowicz, S.; Sanz, Y.; Maria Lagaron, J., Electrospinning as a useful technique for the encapsulation of living bifidobacteria in food hydrocolloids. *Food Hydrocolloids* **2012,** *28* (1), 159-167. DOI: 10.1016/j.foodhyd.2011.12.008.

94. Miao, J.; Miyauchi, M.; Simmons, T. J.; Dordick, J. S.; Linhardt, R. J., Electrospinning of Nanomaterials and Applications in Electronic Components and Devices. *Journal of Nanoscience and Nanotechnology* **2010,** *10* (9), 5507-5519. DOI: 10.1166/jnn.2010.3073.

95. Zucchelli, A.; Focarete, M. L.; Gualandi, C.; Ramakrishna, S., Electrospun nanofibers for enhancing structural performance of composite materials. *Polymers for Advanced Technologies* **2011,** *22* (3), 339-349. DOI: 10.1002/pat.1837.

96. Abbasizadeh, S.; Keshtkar, A. R.; Mousavian, M. A., Preparation of a novel electrospun polyvinyl alcohol/titanium oxide nanofiber adsorbent modified with mercapto groups for uranium(VI) and thorium(IV) removal from aqueous solution. *Chemical Engineering Journal* **2013,** *220*, 161-171. DOI: 10.1016/j.cej.2013.01.029.

97. Irani, M.; Keshtkar, A. R.; Moosavian, M. A., Removal of cadmium from aqueous solution using mesoporous PVA/TEOS/APTES composite nanofiber prepared by sol-gel/electrospinning. *Chemical Engineering Journal* **2012,** *200*, 192-201. DOI: 10.1016/j.cej.2012.06.054.

98. Li, S.; Yue, X.; Jing, Y.; Bai, S.; Dai, Z., Fabrication of zonal thiol-functionalized silica nanofibers for removal of heavy metal ions from wastewater. *Colloids and Surfaces a-Physicochemical and Engineering Aspects* **2011,** *380* (1-3), 229-233. DOI: 10.1016/j.colsurfa.2011.02.027.

99. Ma, Z.; Ji, H.; Teng, Y.; Dong, G.; Zhou, J.; Tan, D.; Qiu, J., Engineering and optimization of nano- and mesoporous silica fibers using sol-gel and electrospinning techniques for sorption of heavy metal ions. *Journal of Colloid and Interface Science* **2011,** *358* (2), 547-553. DOI: 10.1016/j.jcis.2011.02.066.

100. Mahapatra, A.; Mishra, B. G.; Hota, G., Studies on Electrospun Alumina Nanofibers for the Removal of Chromium(VI) and Fluoride Toxic Ions from an Aqueous System. *Industrial & Engineering Chemistry Research* **2013,** *52* (4), 1554-1561. DOI: 10.1021/ie301586j.

101. Wang, F.; Ge, M., Fibrous mat of chitosan/polyvinyl alcohol/containing cerium(III) for the removal of chromium(VI) from aqueous solution. *Textile Research Journal* **2013,** *83* (6), 628-637. DOI: 10.1177/0040517512454188.

102. Wang, Z.-G.; Wan, L.-S.; Liu, Z.-M.; Huang, X.-J.; Xu, Z.-K., Enzyme immobilization on electrospun polymer nanofibers: An overview. *Journal of Molecular Catalysis B-Enzymatic* **2009,** *56* (4), 189-195. DOI: 10.1016/j.molcatb.2008.05.005.

103. Zussman, E., Encapsulation of cells within electrospun fibers. *Polymers for Advanced Technologies* **2011,** *22* (3), 366-371. DOI: 10.1002/pat.1812.

104. Dai, Y.; Niu, J.; Yin, L.; Xu, J.; Xu, J., Laccase-carrying electrospun fibrous membrane for the removal of polycyclic aromatic hydrocarbons from contaminated water. *Separation and Purification Technology* **2013,** *104*, 1-8. DOI: 10.1016/j.seppur.2012.11.013.

105. Niu, J.; Dai, Y.; Guo, H.; Xu, J.; Shen, Z., Adsorption and transformation of PAHs from water by a laccase-loading spider-type reactor. *Journal of Hazardous Materials* **2013,** *248*, 254-260. DOI: 10.1016/j.jhazmat.2013.01.017.

106. Niu, J.; Xu, J.; Dai, Y.; Xu, J.; Guo, H.; Sun, K.; Liu, R., Immobilization of horseradish peroxidase by electrospun fibrous membranes for adsorption and degradation of pentachlorophenol in water. *Journal of Hazardous Materials* **2013,** *246*, 119-125. DOI: 10.1016/j.jhazmat.2012.12.023.

107. Singh, P.; Mondal, K.; Sharma, A., Reusable electrospun mesoporous ZnO nanofiber mats for photocatalytic degradation of polycyclic aromatic hydrocarbon dyes in wastewater. *Journal of Colloid and Interface Science* **2013,** *394*, 208-215. DOI: 10.1016/j.jcis.2012.12.006.

108. Klein, S.; Kuhn, J.; Avrahami, R.; Tarre, S.; Beliavski, M.; Green, M.; Zussman, E., Encapsulation of Bacterial Cells in Electrospun Microtubes. *Biomacromolecules* **2009,** *10* (7), 1751-1756. DOI: 10.1021/bm900168v.

109. Liu, Y.; Rafailovich, M. H.; Malal, R.; Cohn, D.; Chidambaram, D., Engineering of bio-hybrid materials by electrospinning polymer-microbe fibers. *Proceedings of the National Academy of Sciences of the United States of America* **2009,** *106* (34), 14201-14206. DOI: 10.1073/pnas.0903238106.

110. Fung, W.-Y.; Yuen, K.-H.; Liong, M.-T., Agrowaste-Based Nanofibers as a Probiotic Encapsulant: Fabrication and Characterization. *Journal of Agricultural and Food Chemistry* **2011,** *59* (15), 8140-8147. DOI: 10.1021/jf2009342.

111. Gensheimer, M.; Becker, M.; Brandis-Heep, A.; Wendorff, J. H.; Thauer, R. K.; Greiner, A., Novel biohybrid materials by electrospinning: Nanofibers of poly(ethylene oxide) and living bacteria. *Advanced Materials* **2007,** *19* (18), 2480-+. DOI: 10.1002/adma.200602936.

112. Lopez-Rubio, A.; Sanchez, E.; Sanz, Y.; Lagaron, J. M., Encapsulation of Living Bifidobacteria in Ultrathin PVOH Electrospun Fibers. *Biomacromolecules* **2009,** *10* (10), 2823-2829. DOI: 10.1021/bm900660b.

113. Salalha, W.; Kuhn, J.; Dror, Y.; Zussman, E., Encapsulation of bacteria and viruses in electrospun nanofibres. *Nanotechnology* **2006,** *17* (18), 4675-4681. DOI: 10.1088/0957-4484/17/18/025.

114. Kim, Y.-J.; Ahn, C. H.; Choi, M. O., Effect of thermal treatment on the characteristics of electrospun PVDF-silica composite nanofibrous membrane. *European Polymer Journal* **2010,** *46* (10), 1957-1965. DOI: 10.1016/j.eurpolymj.2010.08.009.

115. Ponton, A.; Warlus, S.; Griesmar, P., Rheological study of the sol-gel transition in silica alkoxides. *Journal of Colloid and Interface Science* **2002,** *249* (1), 209-216. DOI: 10.1006/jcis.2002.8227.

116. Strong, L. C.; McTavish, H.; Sadowsky, M. J.; Wackett, L. P., Field-scale remediation of atrazine-contaminated soil using recombinant *Escherichia coli* expressing atrazine chlorohydrolase. *Environmental Microbiology* **2000,** *2* (1), 91-98. DOI: 10.1046/j.1462-2920.2000.00079.x.

117. Reznik, S. N.; Yarin, A. L.; Zussman, E.; Bercovici, L., Evolution of a compound droplet attached to a core-shell nozzle under the action of a strong electric field. *Physics of Fluids* **2006,** *18* (6). DOI: 10.1063/1.2206747.

118. Moghe, A. K.; Gupta, B. S., Co-axial electrospinning for nanofiber structures: Preparation and applications. *Polymer Reviews* **2008,** *48* (2), 353-377. DOI: 10.1080/15583720802022257.

119. Shin, K.-H.; Sung, J.-H.; Koh, Y.-H.; Lee, J.-H.; Choi, W.-Y.; Kim, H.-E., Direct coating of bioactive sol-gel derived silica on poly(epsilon-caprolactone) nanofibrous

scaffold using co-electrospinning. *Materials Letters* **2010,** *64* (13), 1539-1542. DOI: 10.1016/j.matlet.2010.04.014.

120. Tsou, P. H.; Chou, C. K.; Saldana, S. M.; Hung, M. C.; Kameoka, J., The fabrication and testing of electrospun silica nanofiber membranes for the detection of proteins. *Nanotechnology* **2008,** *19* (44). DOI: 10.1088/0957-4484/19/44/445714.

121. Katoch, A.; Kim, S. S., Synthesis of Hollow Silica Fibers with Porous Walls by Coaxial Electrospinning Method. *Journal of the American Ceramic Society* **2012,** *95* (2), 553-556. DOI: 10.1111/j.1551-2916.2011.04923.x.

122. Pirzada, T.; Arvidson, S. A.; Saquing, C. D.; Shah, S. S.; Khan, S. A., Hybrid Silica-PVA Nanofibers via Sol-Gel Electrospinning. *Langmuir* **2012,** *28* (13), 5834-5844. DOI: 10.1021/la300049j.

123. Pelton, J. T.; McLean, L. R., Spectroscopic methods for analysis of protein secondary structure. *Analytical Biochemistry* **2000,** *277* (2), 167-176. DOI: 10.1006/abio.1999.4320.

124. RiettiShati, M.; Ronen, D.; Mandelbaum, R. T., Atrazine degradation by Pseudomonas strain ADP entrapped in sol-gel glass. *Journal of Sol-Gel Science and Technology* **1996,** *7* (1-2), 77-79. DOI: 10.1007/bf00401886.

125. Vancov, T.; Jury, K.; Van Zwieten, L., Atrazine degradation by encapsulated Rhodococcus erythropolis NI86/21. *Journal of Applied Microbiology* **2005,** *99* (4), 767-775. DOI: 10.1111/j.1365-2672.2005.02679.x.

126. Chance, R. E.; Frank, B. H., RESEARCH, DEVELOPMENT, PRODUCTION, AND SAFETY OF BIOSYNTHETIC HUMAN INSULIN. *Diabetes Care* **1993,** *16*, 133-142.

127. Martens, J. H.; Barg, H.; Warren, M. J.; Jahn, D., Microbial production of vitamin B-12. *Applied Microbiology and Biotechnology* **2002,** *58* (3), 275-285. DOI: 10.1007/s00253-001-0902-7.

128. Desai, J. D.; Banat, I. M., Microbial production of surfactants and their commercial potential. *Microbiology and Molecular Biology Reviews* **1997,** *61* (1), 47-&.

129. Biebl, H.; Menzel, K.; Zeng, A. P.; Deckwer, W. D., Microbial production of 1,3-propanediol. *Applied Microbiology and Biotechnology* **1999,** *52* (3), 289-297.

130. Du, J.; Shao, Z.; Zhao, H., Engineering microbial factories for synthesis of value-added products. *Journal of Industrial Microbiology & Biotechnology* **2011,** *38* (8), 873-890. DOI: 10.1007/s10295-011-0970-3.

131. Ferrer-Miralles, N.; Domingo-Espin, J.; Corchero, J. L.; Vazquez, E.; Villaverde, A., Microbial factories for recombinant pharmaceuticals. *Microbial Cell Factories* **2009,** *8*. DOI: 10.1186/1475-2859-8-17.

132. Amarger, N., Genetically modified bacteria in agriculture. *Biochimie* **2002,** *84* (11), 1061-1072. DOI: 10.1016/s0300-9084(02)00035-4.

133. Pieper, D. H.; Reineke, W., Engineering bacteria for bioremediation. *Current Opinion in Biotechnology* **2000,** *11* (3), 262-270. DOI: 10.1016/s0958-1669(00)00094-x.

134. Brenner, K.; You, L.; Arnold, F. H., Engineering microbial consortia: a new frontier in synthetic biology. *Trends in Biotechnology* **2008,** *26* (9), 483-489. DOI: 10.1016/j.tibtech.2008.05.004.

135. Minty, J. J.; Singer, M. E.; Scholz, S. A.; Bae, C.-H.; Ahn, J.-H.; Foster, C. E.; Liao, J. C.; Lin, X. N., Design and characterization of synthetic fungal-bacterial consortia for direct production of isobutanol from cellulosic biomass. *Proceedings of the National Academy of Sciences of the United States of America* **2013,** *110* (36), 14592-14597. DOI: 10.1073/pnas.1218447110.

136. Shong, J.; Diaz, M. R. J.; Collins, C. H., Towards synthetic microbial consortia for bioprocessing. *Current Opinion in Biotechnology* **2012,** *23* (5), 798-802. DOI: 10.1016/j.copbio.2012.02.001.

137. Dickson, D. J.; Ely, R. L., Silica sol-gel encapsulation of cyanobacteria: lessons for academic and applied research. *Applied Microbiology and Biotechnology* **2013,** *97* (5), 1809-1819. DOI: 10.1007/s00253-012-4686-8.

138. Resnick, S. M.; Lee, K.; Gibson, D. T., Diverse reactions catalyzed by naphthalene dioxygenase from *Pseudomonas sp* strain NCIB 9816. *Journal of Industrial Microbiology & Biotechnology* **1996,** *17* (5-6), 438-457. DOI: 10.1007/bf01574775.

139. Pashin, Y. V.; Bakhitova, L. M., MUTAGENIC AND CARCINOGENIC PROPERTIES OF POLYCYCLIC AROMATIC-HYDROCARBONS. *Environmental Health Perspectives* **1979,** *30* (JUN), 185-189. DOI: 10.2307/3429123.

140. Aukema, K. G.; Kasinkas, L.; Aksan, A.; Wackett, L. P., Use of Silica-Encapsulated *Pseudomonas sp* Strain NCIB 9816-4 in Biodegradation of Novel Hydrocarbon Ring Structures Found in Hydraulic Fracturing Waters. *Applied and Environmental Microbiology* **2014,** *80* (16), 4968-4976. DOI: 10.1128/aem.01100-14.

141. Tchobanoglous, G.; Burton, F. L.; Stensel, H. D.; Metcalf; Eddy, *Wastewater Engineering: Treatment and Reuse*. McGraw-Hill Education: 2003.

142. Borde, X.; Guieysse, B.; Delgado, O.; Munoz, R.; Hatti-Kaul, R.; Nugier-Chauvin, C.; Patin, H.; Mattiasson, B., Synergistic relationships in algal-bacterial microcosms for the treatment of aromatic pollutants. *Bioresource Technology* **2003,** *86* (3), 293-300. DOI: 10.1016/s0960-8524(02)00074-3.

143. Munoz, R.; Guieysse, B.; Mattiasson, B., Phenanthrene biodegradation by an algal-bacterial consortium in two-phase partitioning bioreactors. *Applied Microbiology and Biotechnology* **2003,** *61* (3), 261-267. DOI: 10.1007/s00253-003-1231-9.

144. Praveen, P.; Loh, K.-C., Photosynthetic aeration in biological wastewater treatment using immobilized microalgae-bacteria symbiosis. *Applied Microbiology and Biotechnology* **2015**, 1-10. DOI: 10.1007/s00253-015-6896-3.

145. Rippka, R.; Deruelles, J.; Waterbury, J. B.; Herdman, M.; Stanier, R. Y., GENERIC ASSIGNMENTS, STRAIN HISTORIES AND PROPERTIES OF PURE CULTURES OF CYANOBACTERIA. *Journal of General Microbiology* **1979,** *111* (MAR), 1-61.

146. Turner, K.; Xu, S.; Pasini, P.; Deo, S.; Bachas, L.; Daunert, S., Hydroxylated polychlorinated biphenyl detection based on a genetically engineered bioluminescent

whole-cell sensing system. *Analytical Chemistry* **2007,** *79* (15), 5740-5745. DOI: 10.1021/ac0705162.

147. Sakkos, J. K.; Kieffer, D. P.; Mutlu, B. R.; Wackett, L. P.; Aksan, A., Engineering of a silica encapsulation platform for hydrocarbon degradation using *Pseudomonas sp*. NCIB 9816-4. *Biotechnology and bioengineering* **2015**.

148. Bechet, Q.; Shilton, A.; Guieysse, B., Modeling the effects of light and temperature on algae growth: State of the art and critical assessment for productivity prediction during outdoor cultivation. *Biotechnology Advances* **2013,** *31* (8), 1648-1663. DOI: 10.1016/j.biotechadv.2013.08.014.

149. Pottier, L.; Pruvost, J.; Derernetz, J.; Cornet, J. F.; Legrand, J.; Dussap, C. G., A fully predictive model for one-dimensional light attenuation by Chlamydomonas reinhardtii in a torus photobioreactor. *Biotechnology and Bioengineering* **2005,** *91* (5), 569-582. DOI: 10.1002/bit.20475.

150. Premkumar, J. R.; Rosen, R.; Belkin, S.; Lev, O., Sol-gel luminescence biosensors: Encapsulation of recombinant E-coli reporters in thick silicate films. *Analytica Chimica Acta* **2002,** *462* (1), 11-23.

151. Depagne, C.; Roux, C.; Coradin, T., How to design cell-based biosensors using the sol-gel process. *Analytical and Bioanalytical Chemistry* **2011,** *400* (4), 965-976. DOI: 10.1007/s00216-010-4351-y.

152. Federle, M. J.; Bassler, B. L., Interspecies communication in bacteria. *Journal of Clinical Investigation* **2003,** *112* (9), 1291-1299. DOI: 10.1172/jci200320195.

153. Mutlu, B. R.; Hirschey, K.; Wackett, L. P.; Aksan, A., Long-term preservation of silica gel-encapsulated bacterial biocatalysts by desiccation. *Journal of Sol-Gel Science and Technology* **2015,** *74* (3), 823-833. DOI: 10.1007/s10971-015-3690-8.

154. Tong, H.-W.; Mutlu, B. R.; Wackett, L. P.; Aksan, A., Manufacturing of Bioreactive Nanofibers for Bioremediation. *Biotechnology and Bioengineering* **2014,** *111* (8), 1483-1493. DOI: 10.1002/bit.25208.